DISSERTATION

MODELING NONPOINT-SOURCE URANIUM POLLUTION IN AN IRRIGATED STREAM-AQUIFER SYSTEM: CALIBRATION AND SIMULATION

Submitted by

Ibraheem A. Qurban

Department of Civil and Environmental Engineering

In partial fulfillment of the requirements

For the Degree of Doctor of Philosophy

Colorado State University

Fort Collins, Colorado

Summer 2024

Doctoral Committee:

Advisor: Timothy K. Gates

Ryan T. Bailey
Neil S. Grigg
James A. Ippolito

Copyright by Ibraheem A. Qurban 2024

All Rights Reserved

ABSTRACT

MODELING NONPOINT-SOURCE URANIUM POLLUTION IN AN IRRIGATED STREAM-AQUIFER SYSTEM: CALIBRATION AND SIMULATION

The Lower Arkansas River Valley (LARV) in southeastern Colorado has been a source of significant agricultural productivity for well over a century, primarily due to extensive irrigation practices. Mirroring trends seen in other semi-arid irrigated areas globally, however, irrigated agriculture in the LARV has resulted in several challenges for the region. In addition to the emergence of waterlogging and soil salinization, leading to decreased crop yields, elevated levels of nutrients and trace elements have appeared in the soil and water. Among these constituents, uranium (U), along with co-contaminants selenium (Se) and nitrate (NO_3), has shown particularly high concentrations in groundwater, surface water, and soils. These heightened concentrations pose environmental concerns, impacting human health and the well-being of aquatic life such as fish and waterfowl. Careful monitoring and management practices are crucial to prevent potential harm to water resources.

The main goal of this research is to develop a comprehensive numerical model for assessing U pollution in a stream-aquifer system within a large irrigated area. To achieve this, a computational model is built and tested that can predict with reasonable accuracy how U, along with Se and NO_3, are mobilized and move within a coupled system of streams and groundwater. The approach combines two key modeling components: a MODFLOW package, which handles the simulation of groundwater and stream flow dynamics, and an RT3D package, which addresses the reactive transport of U, Se, and nitrogen (N) species in both groundwater and interconnected streams. RT3D relies on the simulated flows generated by MODFLOW to track the movement of

U, Se, and N species between streams and the aquifer in the irrigated landscape, updating daily to adequately capture changes over time. This integrated model provides an understanding of how these contaminants behave and interact within the stream-aquifer system, aiding in effective pollution assessment and providing insights valuable to the planning of management strategies.

The coupled MODFLOW-RT3D flow and reactive transport model is applied to a 550 km² area within the LARV, stretching from Lamar, Colorado, to the Colorado-Kansas border and spanning a period of 14 years. The flow package is compared with observations of groundwater hydraulic head and stream flow, along with estimates of return flow along the Arkansas River. The reactive transport package is assessed by comparing predicted U, Se, and NO_3 concentrations against data collected from groundwater monitoring wells and stream sampling sites along with estimates of solute mass loads to the river. To calibrate and refine the model, the PESTPP-iES iterative ensemble smoother (iES) software is employed. This calibration process is dedicated to enhancing the model's accuracy in predicting both flow and transport dynamics. PESTPP-iES addresses calibration uncertainty by establishing prior frequency distributions for key model parameters based on data and expertise, then iteratively adjusts these parameters during calibration to align model predictions with observed data. Post-calibration, posterior distributions reflect updated parameter values and reduced uncertainties.

Demonstrating a strong alignment with concentrations of C_{NO_3}, C_{Se}, and C_U values found in groundwater, streams, and the mass loading entering the Arkansas River, outcomes of the model-based simulations reveal a substantial violation of the Colorado chronic standard (85th percentile = 30 µg/L) for C_U throughout the study region. On average, simulated C_{NO_3}, C_{Se}, and C_U values for groundwater in non-riparian areas in the region are 3.6 mg/L, 41 µg/L, and 126 µg/L, compared to respective averages of 4 mg/L, 53 µg/L, and 112 µg/L observed in monitoring wells. When

considering the 85th percentile of simulated C_{NO_3}, C_{Se}, and C_U values, the figures for non-riparian groundwater are 6 mg/L, 50 µg/L, and 218 µg/L, respectively. Groundwater in riparian areas shows lower average simulated C_{NO_3}, C_{Se}, and C_U values of 3 mg/L, 26 µg/L, and 72 µg/L, respectively, and 85th percentile values of 5 mg/L, 41 µg/L, and 152 µg/L. Additionally, simulated average mass loading rates for NO_3, Se, and U along the river are 8.8 kg/day per km, 0.05 kg/day per km, and 0.27 kg/day/km respectively, compared to stochastic mass balance estimates of 9.2 kg/day per km , 0.06 kg/day per km , and 0.23 kg/day per km. The simulated 85th percentile C_{NO_3}, C_{Se}, and C_U values in the Arkansas River are 1 mg/L, 11 µg/L, and 87 µg/L, respectively. Notably, the simulated U levels in groundwater exceed the chronic standard across 44% of the region. Along the Arkansas River, concentrations consistently surpass the chronic standard, averaging 2.9 times higher. Predicted Se concentrations also show significant exceedances of the chronic standard, while NO_3 violations are slight to moderate. The varying pollutant levels across the region highlight specific areas of concern that require targeted attention, indicating potential contributing factors to these hotspots. Findings outline how serious and widespread the problem is in the LARV, providing a starting point for comparing potential pollution reduction from alternative water and land best management strategies (BMPs) to be explored in future applications of the calibrated model.

ACKNOWLEDGMENTS

I would like to express my gratitude to all the people who helped me complete this dissertation. I express my deep appreciation to Dr. Timothy K. Gates, my advisor, for his constant guidance, encouragement, and support throughout this project. Without his invaluable mentorship, this work could not have reached completion, particularly in the context of the Lower Arkansas River Valley. Dr. Gates has been instrumental in shaping my academic and personal development, providing constant assistance, encouragement, and motivation. Also, I thank my committee members, Dr. Ryan T. Bailey, Dr. Neil S. Grigg, and Dr. James A. Ippolito for their assistance, encouragement, and advice. I extend my sincere appreciation to Dr. Eric D. Morway for his invaluable support and guidance in completing essential aspects of the research. Special thanks to Dr. Jeremy T. White and Dr. Michael N. Fienen for their expert guidance regarding model calibration, including allowing me to utilize some of their computational facilities. Gratitude is also extended to John T. Cox and to Erin Underwood for their helpful assistance with the extension of the flow model and the building of the U reactions into the solute transport model, as well as to my other fellow graduate students and colleagues over the past years.

I offer heartfelt gratefulness to my mother, brothers, sisters, and family members for their unwavering support throughout my journey. Their constant encouragement has increased my strength. A deep debt of gratitude is owed to my beloved wife Ghofran Hamoh, whose constant patience, selflessness, and unwavering support have been my pillars. To my sons, Abdulaziz and Nawaf, your love, encouragement, and understanding have fueled my determination every step of the way.

Finally, it is a pleasure to acknowledge my thanks to the Saudi government and King Abdulaziz University for their financial support and cooperation for affording me the privilege of

pursuing a Doctor of Philosophy degree in the Civil and Environmental Engineering Department at Colorado State University. Financial grants, especially in support of field data used in this study, from the National Integrated Water Quality Program of the USDA National Institute of Food and Agriculture, the Colorado Department of Public Health and Environment, the Colorado Geological Survey, the Colorado Agricultural Experiment Station, the Southeastern Colorado Water Conservancy District, the Lower Arkansas Valley Water Conservancy District, and the United States Bureau of Reclamation are gratefully acknowledged. The views and conclusions contained in this document are those of the authors and should not be interpreted as representing the opinions or policies of the government of Saudi Arabia, Colorado, or the US.

TABLE OF CONTENTS

LIST OF TABLES

LIST OF FIGURES

CHAPTER 1: INTRODUCTION

1.1.Overview

Heavy metals and trace elements are considered sources of water contamination in irrigated regions (Hoffman et al. 2007). The high concentrations of trace elements often found in these regions relate to different factors, such as arid and semi-arid climates, open basins versus closed topography, and the presence of geological sources (Presser et al. 1994). An essential trace element recently documented with high concentration in irrigated stream-aquifer systems is uranium (U). The mobilization and movement of U in water traversing and beneath irrigated lands have resulted in toxic contamination of aquifers and receiving streams that can become harmful to humans, livestock, and aquatic life. The presence of U in irrigated regions has resulted in concern for future water quality and food chain demands with concentrations exceeding the maximum contaminant levels (85^{th} percentile = 30 μg/L) set by the World Health Organization (WHO) and the United States Environmental Protection Agency (USEPA).

U is present in soils and sediments at concentrations ranging from 2 to 4 mg/kg (Fayek et al. 2011, Westrop et al. 2022). It is found in all kinds of rock, with particularly high concentrations in marine shale deposited during the Cretaceous period. The incompatible heavy metals in the magmatic differentiation increase the U concentration in felsic igneous rock, such as pegmatites, granites, and aluminous metamorphic host rocks (Finch and Murakami 1999, Prakash et al. 2020). Sandstone is considered a source of U since it contains around a third of the world's U and more than 95% of the U.S. reserves (Adler 1974). Most of the U in marine shale, soils, and sediments is an insolubly reduced form known as uraninite. Uraninite minerals exposed to an oxidizing

environment will produce dissolved and mobile U, known as uranyl. Also, U originates from the process of oxidative weathering occurring in bedrock and exposed shale regions facilitated by constituents like dissolved oxygen (O_2) and nitrate (NO_3) linked to irrigation and fertilization of agricultural land. These oxidation reactions within geological formations, and soil minerals weathered from them, lead to the mobilization of U into groundwater, thereby influencing concentrations within the aquifer systems (Langmuir 1978, Abdelouas et al. 1999, Large et al. 2014).

In addition to being mobilized by inefficient irrigation (e.g. losses in excess of crop evapotranspiration, such canal seepage, and deep percolation and surface runoff from fields) , U can be released due to other human activities such as mining, millings, fertilizers, U energy production, and coal combustion (Gavrilescu et al. 2009, WHO 2012). Long-time use of U in producing energy worldwide has led to severe groundwater contamination due to U leaching from mill tailings (Abdelouas 2006). Numerous aquifers across the United States have detected chemical pollutants like U, along with arsenic, radon, manganese, selenium (Se), and NO_3 (DeSimone et al. 2009). In recent times, elevated levels of U have become prevalent, causing water contamination and significant concerns regarding water quality. U chemical and radiological toxicity can seriously damage communities' water resources (Brugge et al. 2005).

In the western United States, Cretaceous sedimentary rock is considered the primary source of salts and trace metals mobilized by irrigation (Bern and Stogner 2017). Several conditions that are more common in the western United States than in the east lead to high concentrations of U, such as arid and semi-arid climates in conjunction with areas having shallow groundwater, the nature of the spatial distribution of U in soils and gravel aquifers, and the presence of granitic crystalline rocks (DeSimone et al. 2009, Burow et al. 2017). The Pierre shale and Niobrara

formation have been determined to be geological sources of radioactive U (Landis 1959, Ivahnenko et al. 2012). Due to geochemical processes, U is discharged into groundwater from rocks and sediments through dissolution and adsorption from the surfaces of minerals (Jerden and Sinha 2006). Other factors that lead to U and its mobility in groundwater are the oxidation state; the soluble aqueous complex; soil and crop type; and interactions between water, soil, and rocks (Coyte et al. 2018). Moreover, elevated U concentrations exceeding the WHO standard have been reported in both the High Plains and Central Valley aquifers (see Fig. 1) (Nolan and Weber 2015). These two aquifers are considered the world's largest and most productive crop aquifers (Scanlon et al. 2012). They are also considered to be the primary aquifers containing dissolved U in groundwater (Nolan and Weber 2015). Also, in eastern San Joaquin Valley, California, high U concentrations have been reported over time (Thiros et al. 2015).

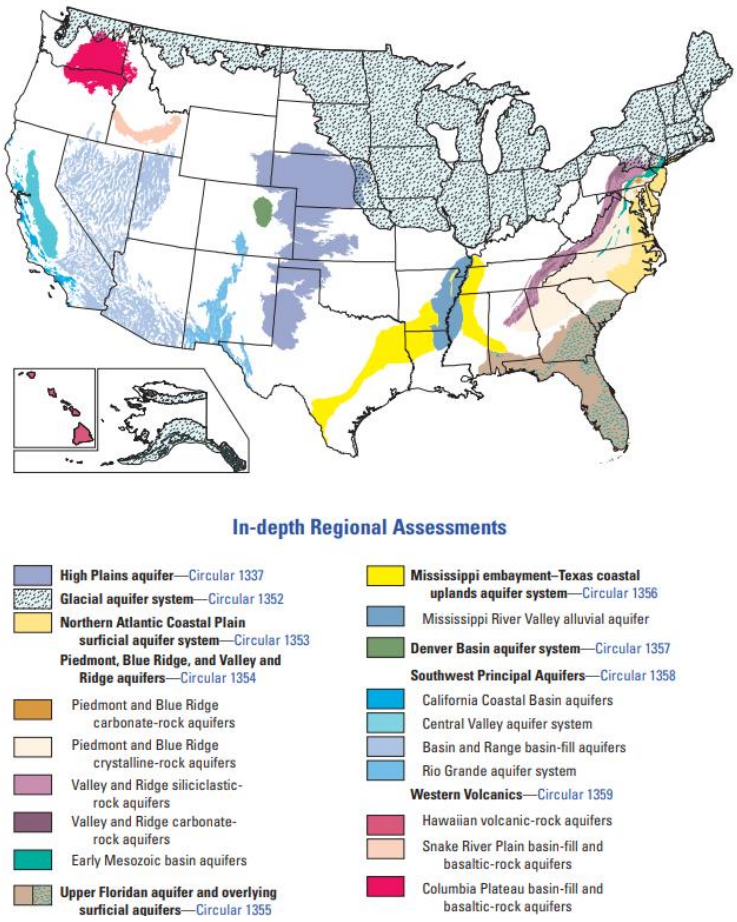

Figure 1**. Major groundwater aquifers location in the United States (DeSimone et al. 2009)**

The Lower Arkansas River Valley (LARV) in southeastern Colorado has faced a challenge for water quality since reported in an early study by Gilbert (1896). The LARV is an important agricultural region (Fig. 2) in the High Plains area of the United States that is stricken by U pollution. Situated in a semi-arid climate, it is overlain by Cretaceous marine and Tertiary sedimentary rocks that include Pierre shale, Niobrara formation, and Benton group rocks.

Bern and Stogner (2017) found that concentrations of total dissolved solids and U are significantly high in the Niobrara formation along the Arkansas River during both irrigation and non-irrigation periods. They noted that U concentrations were significantly elevated in water inflows. Given that the LARV is recognized as one of Colorado's most productive agricultural regions, concerns about water quality degradation are paramount.

Total dissolved solids (TDS), nutrients (especially NO_3 and phosphorus), and trace elements such as Se and U, have been found in high concentrations in both groundwater and surface water in the stream–aquifer system. Oxic return flows from intensive and long-term agricultural irrigation in the LARV have contributed to these high concentrations which not only threaten crop productivity but routinely violate the chronic standards set by the Colorado Department of Public Health and Environment (CDPHE) over broad expanses.

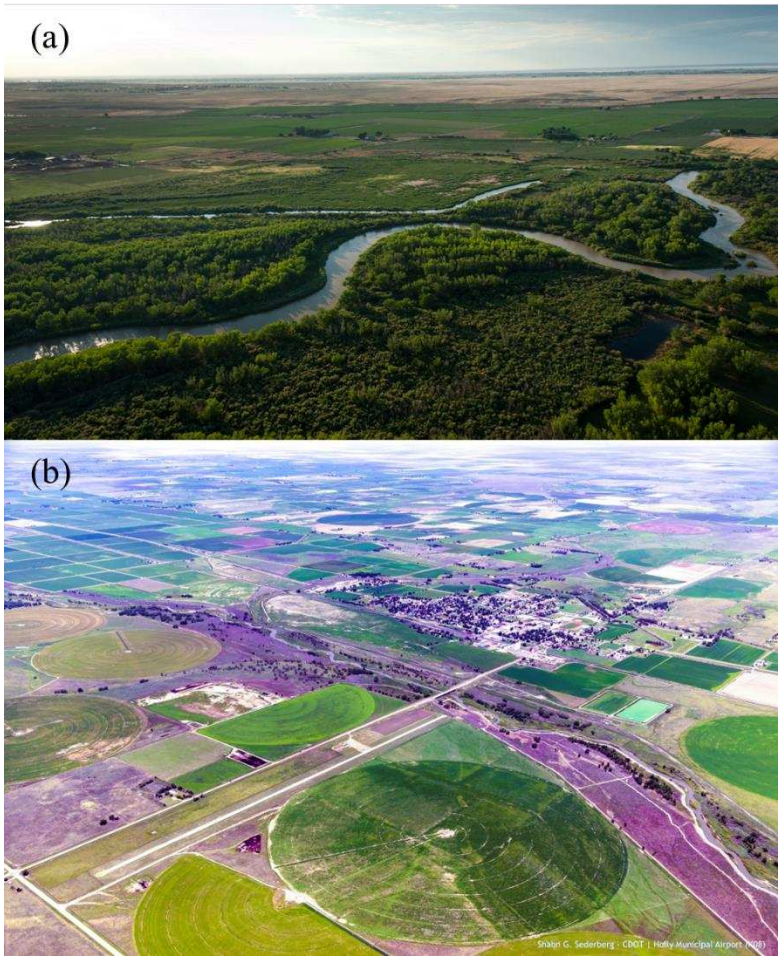

Figure 2. The Lower Arkansas River Valley showing (a) vista of the Arkansas River near Las Animas, Colorado, and (b) irrigated fields along the downstream reach of the Arkansas River near Holly, Colorado.

1.2.Research Objectives

The overall goal of this research is to employ calibrated computational modeling to assess the contamination of U in the stream–aquifer system for both groundwater and surface water in a region of the Lower Arkansas River Valley (LARV), a representative irrigated stream-aquifer system. The region extends along the lower reach of the Arkansas River from Lamar, Colorado to the Colorado-Kansas border, as described in detail in Section 3.8. The coupled flow and reactive transport model will be calibrated against a broad array of field data over a multi-year period, with consideration of calibration uncertainty. Tasks related to the following objectives are followed to achieve this goal:

1. Construct a physically-based distributed parameter model of flow in the stream-aquifer system, as affected by irrigation, for the period from 2007 to 2016 using a finite-difference approximation. The model accounts for groundwater flow in the saturated and unsaturated zones, interacting with flow in the river network.
2. Evaluate water quality and contamination related to U in the Downstream Study Region (DSR) from previously collected water samples from observation wells and the Arkansas River network, including a determination of the water and solute mass exchange of the stream-aquifer system.
3. Construct a physically-based distributed parameter model of the fate and transport of U, Se, and NO_3, as affected by O_2, in the irrigated stream–aquifer system. The finite-difference model links to the flow model to solve the advection-diffusion-reaction equations in the saturated and unsaturated subsurface and in the stream network.
4. Calibrate parameters of the coupled flow and reactive transport model against data on groundwater hydraulic head, groundwater return flows, and stream flows, as well as on

NO_3, Se, and U concentrations in the groundwater, mass loading to the river, and concentrations in streams. Uncertainty in the calibration process will be addressed by providing comparison of prior and posterior frequency distributions of parameters and calibration targets.

5. Apply the calibrated coupled model to provide a baseline description of the nature, severity, and patterns of U, along with Se and NO_3, pollution across the region over the study period, with a view toward future use in exploring the potential impact of alternative land and water best management practices (BMP) in relation to the baseline.

1.3. Dissertation Organization

This dissertation includes 5 chapters. In addition to this Introduction, Chapter 2 presents a literature review of previous studies of U in stream-aquifer systems, Chapter 3 contains a paper submitted for possible publication in the Journal of Hydrology that describes the methodology and results, Chapter 4 provides discussion and major conclusions, including a description of modeling challenges and limitations, and Chapter 5 provides proposed directions for future work. Also included are References and an Appendix containing a variety of details.

1.4. References

Abdelouas, A., Lutze, W., and Nuttall, H. E., 1999. Oxidative dissolution of uraninite precipitated on Navajo sandstone. Journal of Contaminant Hydrology, 36(3–4), 353–375. https://doi.org/10.1016/S0169-7722(98)00151-X

Abdelouas, A., 2006. Uranium mill tailings: Geochemistry, mineralogy, and environmental impact. Elements, 2(6), 335–341. https://doi.org/10.2113/gselements.2.6.335

Adler, H. H., 1974. Concepts of uranium--ore formation in reducing environments in sandstones and other sediments. International Atomic Energy Agency, Vienna.

Bern, C. R., and Stogner, R. W., 2017. The Niobrara Formation as a challenge to water quality in the Arkansas River, Colorado, USA. Journal of Hydrology: Regional Studies, 12(April), 181–195. https://doi.org/10.1016/j.ejrh.2017.05.001

Brugge, D., De Lemos, J. L., and Oldmixon, B., 2005. Exposure pathways and health effects associated with chemical and radiological toxicity of natural uranium: A review. In Reviews on Environmental Health (Vol. 20, Issue 3, pp. 177–193). Freund Publishing House Ltd. https://doi.org/10.1515/REVEH.2005.20.3.177

Burow, K. R., Belitz, K., Dubrovsky, N. M., and Jurgens, B. C., 2017. Large decadal-scale changes in uranium and bicarbonate in groundwater of the irrigated western U.S. Science of the Total Environment, 586, 87–95. https://doi.org/10.1016/j.scitotenv.2017.01.220

Coyte, R. M., Jain, R. C., Srivastava, S. K., Sharma, K. C., Khalil, A., Ma, L., and Vengosh, A., 2018. Large-scale uranium contamination of groundwater resources in India. Environmental Science and Technology Letters, 5(6), 341–347. https://doi.org/10.1021/acs.estlett.8b00215

DeSimone, L. A., McMahon, P. B., and Rosen, M. R., 2009. The quality of our Nation's waters: Water quality in principal aquifers of the United States, 1991-2010. In Circular. https://doi.org/10.3133/cir1360

Fayek, M., Horita, J., and Ripley, E. M., 2011. The oxygen isotopic composition of uranium minerals: A review. Ore Geology Reviews, 41(1), 1–21. https://doi.org/10.1016/j.oregeorev.2011.06.005

Finch, R., and Murakami, T., 1999. Systematics and paragenesis of uranium minerals, in: P.C. Burns, R. Finch (Eds.), Uranium: Mineralogy, Geochemistry and the Environment. Reviews in Mineralogy, vol. 38, Mineralogical Society of America, Washington, DC, 1999, pp. 91–179.

Gavrilescu, M., Pavel, L. V., and Cretescu, I., 2009. Characterization and remediation of soils contaminated with uranium. Journal of Hazardous Materials, 163(2–3), 475–510. https://doi.org/10.1016/j.jhazmat.2008.07.103

Hoffman, G. J., Evans, R. G., Jensen, M. E., Martin, D. L., and Elliott, R. L., 2007. Design and operation of farm irrigation systems 2nd edition. http://irrigationtoolbox.com/IrrigationToolBox/Section 2 - Irrigation System Planning/ASABE DesignandOperationofFarmIrrigationSystems/Preface.pdf

Ivahnenko, T., Ortiz, R. F., and Robert W. Stogner, S., 2012. Characterization of streamflow, water quality, and instantaneous dissolved solids, selenium, and uranium loads in selected reaches of the Arkansas River, southeastern Colorado, 2009-2010. In Scientific Investigations Report.

Jerden, J. L., and Sinha, A. K., 2006. Geochemical coupling of uranium and phosphorous in soils overlying an unmined uranium deposit: Coles Hill, Virginia. Journal of Geochemical Exploration, 91(1–3), 56–70. https://doi.org/10.1016/j.gexplo.2005.12.003

Landis, E. R., 1959. Radioacti'vity and uranium content of the Sharon Springs member of the Pierre shale and associated rocks in western Kansas and eastern Colorado Trace Elements Investigations Report 573.

Langmuir, D., 1978. Uranium solution-mineral equilibria at low temperatures with applications to sedimentary ore deposits. Geochimica et Cosmochimica Acta, 42(6 PART A), 547–569. https://doi.org/10.1016/0016-7037(78)90001-7

Large, R. R., Halpin, J. A., Danyushevsky, L. V., Maslennikov, V. V., Bull, S. W., Long, J. A., Gregory, D. D., Lounejeva, E., Lyons, T. W., Sack, P. J., McGoldrick, P. J., and Calver, C. R., 2014. Trace element content of sedimentary pyrite as a new proxy for deep-time ocean-atmosphere evolution. Earth and Planetary Science Letters, 389, 209–220. https://doi.org/10.1016/j.epsl.2013.12.020

Nolan, J., and Weber, K. A., 2015. Natural uranium contamination in major U.S. aquifers linked to nitrate. Environmental Science and Technology Letters, 2(8), 215–220. https://doi.org/10.1021/acs.estlett.5b00174

Prakash, R., Bhartariya, K. G., Singh, S., Singh, K., Rajak, M., and Kaushik, Y. B., 2020. Uranium and its correlation with other geogenic contaminants in ground water of Ganga Yamuna Doab, Fatehpur District, Uttar Pradesh, India. Journal of the Geological Society of India, 95(4), 359–365. https://doi.org/10.1007/s12594-020-1444-x

Presser, T. S., Sylvester, M. A., and Low, W. H., 1994. Bioaccumulation of selenium from natural geologic sources in western states and its potential consequences. Environmental Management, 18(3), 423–436. https://doi.org/10.1007/BF02393871

Scanlon, B. R., Faunt, C. C., Longuevergne, L., Reedy, R. C., Alley, W. M., McGuire, V. L., and McMahon, P. B., 2012. Groundwater depletion and sustainability of irrigation in the US High Plains and Central Valley. Proceedings of the National Academy of Sciences of the United States of America, 109(24), 9320–9325. https://doi.org/10.1073/pnas.1200311109

Thiros, S. A., Paul, A. P., Bexfield, L. M., and Anning, D. W., 2015. The quality of our Nation's waters: Water quality in basin-fill aquifers of the southwestern United States: Arizona, California, Colorado, Nevada, New Mexico, and Utah, 1993-2009. In Circular. https://doi.org/10.3133/cir1358

Westrop, J. P., Snow, D. D., and Weber, K. A., 2022. Mobilization of naturally occurring uranium in groundwater under intensely managed farmland. Food, Energy, and Water Nexus: A Consideration for the 21st Century, 215–232. https://doi.org/10.1007/978-3-030-85728-8_12

World Health Organization., 2001. Depleted uranium: Sources, exposure and health effects. April, 1–195.

http://apps.who.int/iris/bitstream/handle/10665/66930/WHO_SDE_PHE_01.1.pdf;jsessionid=E2B432AE38E0F2FD0A66B98AECDB1864?sequence=1

CHAPTER 2: LITERATURE REVIEW

Preface

Chapter 3 provides a detailed account of U geochemistry and its transformations. In this chapter, we present a broad overview of how U appears and the extent of its contamination worldwide.

2.1.Uranium in The World

Worldwide, U contamination of groundwater and surface water has been investigated in locations that exceed the WHO standard for U concentration in drinking water (30 µg/L) (World Health Organization 2011a, 2011b). Studies have investigated high U concentrations in groundwater and surface water that have been released from U mining tailing or U nuclear power waste. Kazakhstan, Canada, and Australia have the highest levels of production of U from mines, providing 43%, 13%, and 12% of the world's supply, respectively (World Nuclear Association 2020). Therefore, high concentrations of U have been reported at Kazakhstan mining sites in both groundwater and surface water, leading to risks and prompting local authorities to look for new remediation methods (Zoriy et al. 2010, Uralbekov et al. 2011). In addition, Canada has reported U contamination in the aqueous environment resulting from the activities at mining and milling sites (Donahue and Hendry 2003). In Portugal, radioactive U has been found in groundwater from old mining sites (Neves and Matias 2007). The U contamination could enter the irrigated aquifer system, migrate to crops, and then enter the human body during consumption, thus posing an environmental and human health risk.

In addition to human activities and nuclear power fuel, irrigated stream-aquifer systems have been affected by high U contamination. The quaternary aquifer of the Datong Basin in China has been found to have a high concentration of U in the groundwater. An investigation concluded that the shallow groundwater of that aquifer may not be useable for drinking water and irrigation due to U contamination (Wu et al. 2019). India, one of the countries that relies most on groundwater as a primary source for drinking water and irrigation purposes, has extracted more than a third of the world's groundwater (Dalin et al. 2017). Along with arsenic and fluoride contamination, the elevated concentration of U that migrate into groundwater aquifers has become a serious health risk, since it exceeds 30 µg/L (Coyte et al. 2018), leading the Indian authorities to start applying remediation strategies. In addition, Nalgonda district, in South India, also investigated and reported high U concentrations. Most agricultural land areas using drip irrigation methods have high crop production, such as paddy, sweet lime, castor, cotton, and groundnut. This area is located under granitic rocks and has a semi-arid climate, which is the typical setting for irrigated areas affected by high U concentrations. Reported concentrations of U exceeded the WHO limit for groundwater, creating a serious problem for the Indian authorities as irrigated areas rely on groundwater. The U content in groundwater is caused by the recharge and discharge that resulted in dissolved U, or it is leached from watershed soil into the groundwater zone (Brindha et al. 2011). In Saudi Arabia, high U concentrations have been found in the topsoil released from the earth's crust, leading to a possible risk of groundwater contamination (Alshahri 2019).

Further, U has been found at concentrations > 30 µg/L in various aquifers in Norway. One investigation showed that among all the trace elements that have been measured in the Norwegian bedrock, U had become the most problematic element in the groundwater (Frengstad et al. 2000). Pakistan found excessive U concentrations in drinking water samples, exceeding the WHO limit

(Ullah et al. 2013). In addition, studies have shown that the P and N applied in agriculture worldwide as a fertilizer to achieve improved crop growth and quality could lead to the accumulation of heavy metals, including perhaps U, in groundwater and topsoil; thus, elevated phosphate and N mineral fertilizer can result in a risk for both humans and the environment (Kratz et al. 2016). However, as discussed in the following, heavy metals derived from fertilizers can be negligible compared to that derived from other sources.

2.2.Uranium in The United States

High concentrations of U have become widespread in recent years, leading to water contamination and water quality issues. The mining boom that started in 1948 in the United States, particularly in Colorado, Utah, Arizona, and the Colorado Plateau in New Mexico, concentrated on radium and vanadium found in the soft sandstone ore (Brugge and Goble 2002). Most of the U mining in the US has been contained to the Navajo Nation territory, and due to a lack of knowledge and equipment, mining employees were exposed to U radiation, which leads to health risks such as lung cancer (Sethi et al. 2012, Gajski et al. 2014). Most of these sites have been abandoned, and the mining has stopped (Brugge and Goble 2002). However, U contamination has leached into the surface water at high concentrations that affect the quality of the water supply (Gajski et al. 2014). Tuba City, Arizona, a Navajo area, reported high U concentrations that exceed the WHO drinking water standard by 550 µg/L; this has also been reported as a long-term health risk (Abdelouas et al. 1999, Gajski et al. 2014). The Naturita, Colorado, mining site has also reported high U concentrations. Further, several U mill tailing areas have been investigated due to high U radionuclide contamination, such as Hanford, Washington State, Savannah River Plant, Georgia, and Oak Ridge National Laboratory, Tennessee (Riley and Zachara 1992).

Other studies have shown high concentrations of U in the irrigated stream–aquifer systems, where there is high groundwater-surface water interaction. In western Nebraska and the North Platte River, high concentrations of NO_3 and U that exceed the allowable contamination level set by WHO has been reported in several locations with wide temporal and spatial variations. Several sources of high U concentration in the area were investigated, such as the alluvium aquifer that underlies the Chadron and Lance Formations, the use of phosphate fertilizer, and the dissolution of volcanic ash in the bedrock under oxidizing conditions (Verstraeten et al. 2000, Böhlke et al. 2007). In addition, the Snake River Plain Aquifer in Idaho is considered one of the largest aquifers in the US that people rely on for drinking water and agricultural purposes. After a long history of storing and disposing of radioactive U, this aquifer experienced high U concentrations in the groundwater and the surface water, affecting both the water quality and crop production (Roback et al. 2001).

Finally, in the Rio Grande Valley in Colorado, New Mexico, and Texas, trace elements and isotopic data have been reported in both groundwater and surface water. The agricultural crops in this aquifer are irrigated mainly from surface water diverted from the Rio Grande River. Elevated concentrations of U that exceed 30 µg/L have been reported in both groundwater and surface water, resulting in groundwater/surface water contamination (Bexfield and Anderholm 1997).

2.3.Uranium in The Environment

U is very dense and is a radioactive element of the actinide series. The concentration of U on the earth's surface has increased not only due to natural forces such as erosion, but also due to human activities such as mining, fertilizer use, U energy production, and coal combustion (Gavrilescu et al. 2009, WHO 2012). The geochemistry of U, including its various solid and

dissolved species, is discussed in Section 3.3. Although U is a chemical that is naturally present in groundwater and surface water, it can be lethal if it occurs at an excessive concentration (Waseem et al. 2015). The elevated levels of U exceeding the WHO standard have occurred in several locations (Levander and Burk 2006), such as the United States, the Middle East, Asia, and Europe (Frengstad et al. 2000, Orloff et al. 2004, Gates et al. 2009, Ullah et al. 2013, Wu et al. 2014). These toxic levels can lead to several serious diseases. In humans, consuming drinking water with a concentration of U > 30 µg/L can cause kidney damage (Zamora et al. 1998). Also, U is considered a naturally radioactive element in that the U nucleus is not stable and will undergo decay processes until it reaches a stable state. However, U has not been considered one of the highest radioactive elements since its decay rates are slow. Three U isotopes occur naturally ^{238}U, ^{235}U, and ^{234}U, and the half-life of ^{238}U is 4.5 billion years, where ^{234}U is considered the most radioactive isotope (Skeppström and Olofsson 2007, Keith et al. 2013) . The radioactivity that occurs in groundwater with high U concentrations is highly toxic and can lead to DNA damage, chromosomal aberrations, and carcinogenicity (Asic et al. 2017, Bjørklund et al. 2017).

In addition, U dioxide (UO_2) often occurs in sandstone due to the presence of anaerobic bacteria, which leads to an accumulation of insoluble U and the formation of U ore deposits; these have proven economically beneficial, especially in Wyoming, New Mexico, and Colorado (Adler 1974, Wall and Krumholz 2006). This insoluble U can be mobilized in a rich oxygen environment through autotrophic reduction of receptors like NO_3 and O_2. Soluble U can be reduced by entering a rich organic region, where the organic materials act as a source of electrons for localized chemical reduction of U that results in a deposit (Wall and Krumholz 2006).

In the United States, several groundwater aquifers have been discovered to have high concentrations of U at a toxic level, leading to severe water quality problems. These are mainly in

the western United States, due to geological factors such as Cretaceous sedimentary rocks, low humidity, and low recharge rates (DeSimone et al., 2009, Nolan and Weber 2015, Bern and Stogner 2017, Burow et al. 2017). North Dakota, Nebraska, California, Wyoming, and Colorado, among other areas, were reported to have elevated U levels over the last decade, as illustrated in Fig. 3.

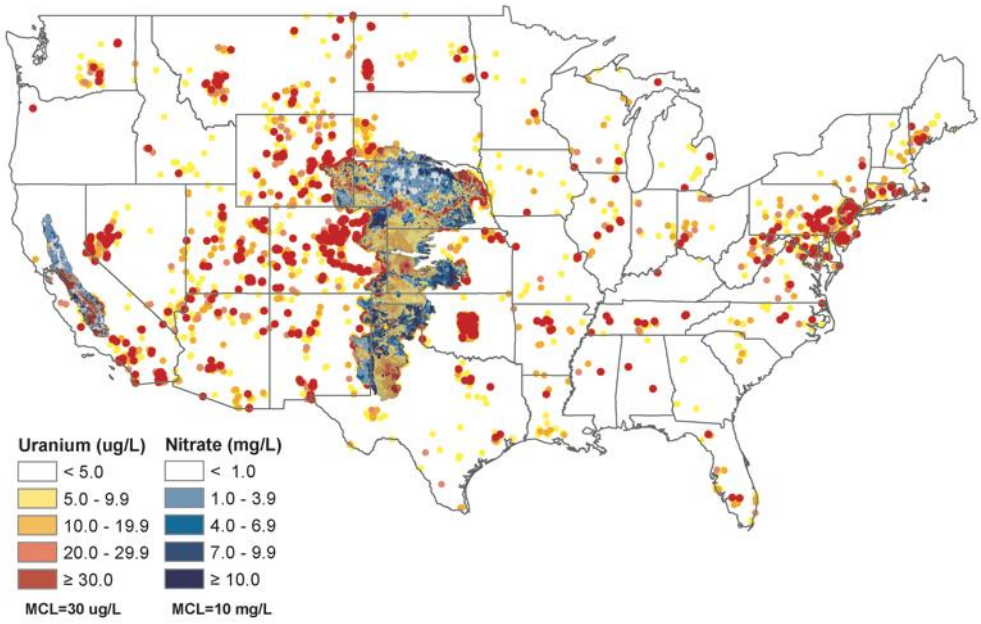

Figure 3. Groundwater concentrations for U and NO_3 (Nolan and Weber 2015).

Areas with a high evaporative index (e.g., arid to semi-arid environments such as those found in the western US), which thus use irrigation for crop production, and with a landscape underlain by Cretaceous marine sedimentary rock, commonly have U contamination (Bern and Stogner 2017). Notice that the LARV in southeastern Colorado has a high evaporation index and is underlain by Cretaceous marine sedimentary rock, as highlighted in Fig. 4.

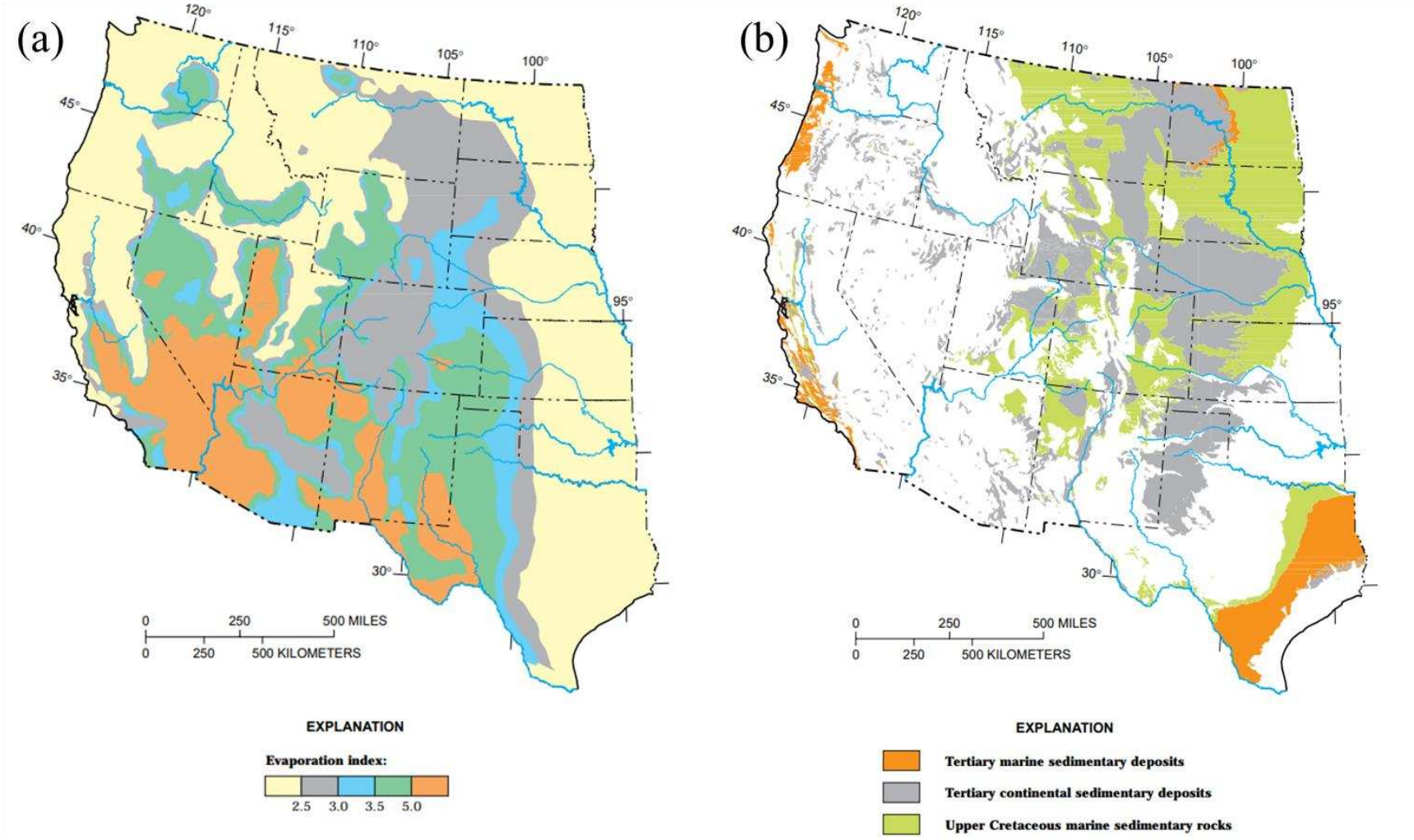

Figure 4. (A) Locations of regions in the western United States with high evaporation index and (B) location of the Upper Cretaceous marine sedimentary rocks (green) (Seiler et al. 1999).

Some N and P fertilizers, nuclear plant emissions, mining sites, radioactive waste, and fossil fuels are sources of anthropogenic U contamination (WHO 2012). However, the most significant volume of U waste comes from mine and mill tailings that include all the natural radioactive elements found in U ore (Abdelouas 2006). Worldwide, U stockpile waste from tailings is estimated to weigh 20 billion tons, while U waste rocks are estimated to weigh more than 40 billion tons. It has been shown that it is difficult to isolate tailings from the environment (Ma et al. 2020). U from mill tailings piles infiltrate the ground surface, leading to the contamination of shallow water table aquifers (Narasimhan et al. 1986). The radionuclides and radioactivity are released from the mill tailings. U infiltrates the soils and groundwater through different processes, such as weathering, the erosion of meteoric water, denudation, suspension, and percolation (Ma et al. 2020). Most of this mill tailings waste leaches into the ground surface, landfills, ponds, basins, and pits, leading to considerable damage to the ecological environment (Riley and Zachara 1992, Teixeira et al. 2015). The Hanford site, the Savannah River Plant, and Oak Ridge National Laboratory are historical examples of intensive chemical waste disposal in the United States (Riley and Zachara 1992). The United States, China, the Russian Federation, Australia, the Czech Republic, Canada, and Kazakhstan have produced the most U from mining and milling. Two-thirds of the world's produced U from mining comes from Australia, Canada, and Kazakhstan. U has been found in high concentrations in other countries as well; for example, it has appeared in agricultural soil after a long period of fertilizer use in Japan (Takeda et al. 2006), rocks have produced U naturally, affecting groundwater aquifers in Finland and India (Salonen 1994, Coyte et al. 2018), and it has been found in gold mine tailings in South Africa (Kamunda et al. 2016).

Fig. 5 illustrates the general sources of U contamination. U can be leached from nuclear power plants and/or U mill tailings. It has been found as insoluble U(IV), and by leaching into the

ground, it is oxidized by O_2 and other oxidants to produces soluble U(VI). Also, U has leached following commercial fertilizer applications (such as phosphate (PO_4) and ammonium (NH_4)). P fertilizers, commonly used in agriculture, can inadvertently increase the availability of U in soils. This occurs because U, an impurity in phosphate rock, is transferred to fertilizers during production, leading to its gradual accumulation in agricultural land with repeated fertilizer applications. In some cases, this process can potentially impact soil quality and contribute to U uptake by plants, raising concerns about environmental and health implications (Mwalongo et al. 2024). NH_4 undergoes nitrification in the soil, converting NH_4 into NO_3 with the help of specialized bacteria and O_2, or adsorbed to the soil matrix. This process occurs before water reaches the groundwater. U(IV) can also be oxidized to U(VI) through various processes, including reactions with O_2 in geologic formations like bedrock and weathered soils, contributing to the overall Oxidation-reduction (redox) reactions that impact U behavior are described in more detail in Section 3.6. Water leached from an unlined surface irrigation canal can percolate deeply to the aquifer, leading to Se and U mobility derived from shale and weathered materials. Mobile U and Se in the sub-surface can eventually rejoin the river as a return flow (Bern et al. 2020).

In the LARV, high concentrations of NO_3, Se, U, and salts have been discovered and investigated (Gates et al. 2009, Bailey et al. 2014, Qurban et al. 2018, Shultz et al. 2018, Javed et al., 2019) . The LARV is recognized as a source of geogenic contaminants because it sits above geological formations like marine shale. The interaction between these formations and groundwater results in the release of U into surface water. These source led to the groundwater contamination reported in the LARV as TDS, Fe, U, NH_4, and Se. NH_4 has been widely used in the LARV as a fertilizer, and this produces high concentrations of NO_3 that is highly correlated with U. The presence of NO_3 along with various electron acceptors and bacterial respiration will

accelerate the oxidation process that can result in selenate (SeO_4), U(VI), and other solute ions under appropriate redox conditions (Gates et al. 2009). Thus, U can oxidize from the solid mineral U(IV) located in the shale and other bedrocks by the autotrophic reduction of O_2, NO_3, and other oxidants. This results in a high concentration of dissolved U, leading to groundwater and surface water contamination.

Finally, at the DSR, NH_4 applied as fertilizer is applied in greater amounts and used more widely as compared with phosphate fertilizer. Thus, in the irrigated stream–aquifer system, when applying (N) fertilizers, U in the groundwater will remain mobile. Once U in applied irrigation water leaches (from canals and pumping wells) through the system and is released in the form of a solution in the vadose zone, advection and dispersion processes will transport U through the aquifer. Then, due to the upward flow, U can re-enter the vadose zone and pass through the surface water.

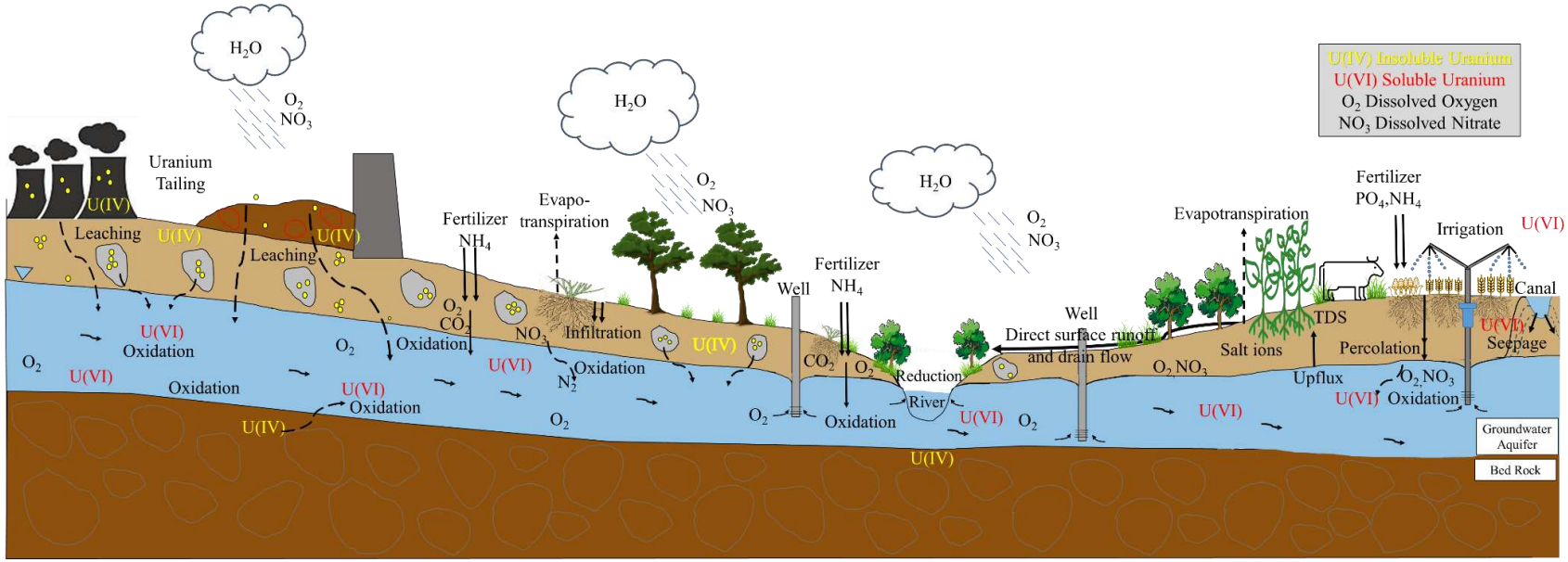

Figure 5. General U contamination sources in the environment.

2.4.Biological and Non-Biological Mediation of U(VI) and U(IV)

The most dangerous species of U is U in the mobile hexavalent (VI) oxidation state. Converting this form of U to an insoluble form can help reduce environmental risk. Several laboratory and in situ studies show that microorganisms and their processes (e.g., biological reduction, respiration), biogeochemical processes, and physico-chemical processes can remediate and reduce the soluble and dissolved U(VI) to insoluble U(IV) and prevent U migration through groundwater (Lovley and Phillips 1992, Senko et al. 2005, Gavrilescu et al. 2009, Lakaniemi et al. 2019). Wersin et al. (1994) show that the sulfide minerals can efficiently reduce U to the insoluble form of U(IV). Its immobilization occurs through the adsorption of U(VI), autotrophic reduction of sorbed U(VI) and U(VI) in the presence of rocks containing sulfide (like pyrite), and precipitation of a mixed U(VI)-U(IV) oxide. Understanding these processes in natural water conditions is facilitated by employing suitable spectroscopic methods. XPS analysis provides valuable insights into the redox process by identifying surface reaction products such as U(VI), U(IV), and polysulfide (Wersin et al. 1994). Also, at low pH and low bicarbonate concentrations, the aqueous sulfide plays a significant role in reducing the U(VI) to microcrystalline uraninite (Hua et al. 2006, Ginder-Vogel and Fendorf 2007). Several studies show how the bioremediation of U can be affected in situ, and bacteria enzymatically linked with an electron donor and U-phosphate biomineralization show promising results for reducing U from U(VI) to U(IV) (Newsome et al. 2014). In situ treatment has the ability to reduce the mobility of U in groundwater instead of removing it from the subsurface, and this is considered an effective way to contain the contamination because the conditions are still reduced (Lakaniemi et al. 2019). Furthermore, the enzymatic desulfovibrio desulfuricans and dissimilatory metal-reducing bacteria (DMRB) can reduce U(VI) to U(VI) much faster than nonenzymatic sulfide (Gorby and Lovley 1992, Lovley

and Phillips 1992). In addition, in a bicarbonate buffer, sulfate-reducing bacteria (genus desulfovibrio) play the role of the biotransferring the U(VI) to U(IV) (Lovley and Phillips 1992). All these methods have shown relatively good reduction of U; however, they do not include the complexity of the highly reactive properties and the U transport pathways that are considered effective for the reduction of U concentrations in solution (Jemison et al. 2020)

2.5.Impact of Uranium on Human Health and Environment

U is a human health concern as it contains chemical toxicity that is lower than radiological toxicity (WHO 2012, Kurttio et al. 2002). U can enter the human body by ingestion through drinking water, food, or by inhalation of airborne U contaminated dust particles (Saini et al. 2016). Most of the U that enters the human body through food, drinking water, or cooking water can be removed and eliminated by the body; however, small particles can remain and absorb into the digestive system and enter the blood (Eggers et al. 2015). The remaining particles of U that enter the bloodstream are not removed by urine but concentrated in the skeleton and kidneys (Wrenn et al. 1983). Also, cumulative concentrations of U can increase the possibility of cancer and liver damage (U.S. Environmental Protection Agency 2012). In addition, depleted U has been found to be a possible cause of DNA damage, DNA breaks, and chromosomal aberrations (Asic et al. 2017). Exposure to U in infants has a more significant effect on their growth and health than in adults (EFSA 2009). These U contaminations are mainly found in the environment, crops, soil, surface water, and groundwater wells. Mining and mill tailing sites are other sources of health concerns for local communities, due to U ore migration through communities and radioactive waste (Brugge and Buchner 2011), leading to dust and contaminated water (Neves and Matias 2007). Workers in mines are at risk of lung cancer and silicosis by inhalation of radon gas and radiation of chemical toxicity (Brugge and Buchner 2011). At the same time, hydrosystems including natural water

bodies such as rivers, lakes, and oceans, as well as artificial structures like reservoirs, irrigation networks, and drainage systems can be exposed to contamination via trace metals from U mining sites, impacting aquatic organisms (Fleeger et al. 2003). U occurring in lakes and streams leads to acute renal failure, liver dysfunction and paralytic ileum in mammals and fish (Cooley et al. 2000). In animals, toxic levels of U affect the tubular epithelium in the kidney (Craft et al. 2004), and glomerular changes with huge decreases in renal insulin levels have been found in animals exposed to U (Stopps and Todd 1982).

2.6.Modeling of U Transport in Stream-Aquifer Systems

Several studies have presented analyses and results of U in soils and groundwater using numerical models. Yabusaki et al. (2008) developed a conceptual process model for U reactive transport in vadose zone–aquifer–river systems that occur due to large diurnal and seasonal fluctuations in the river stage. The researchers then applied both 1D and 2D simulations on an extent of 0.4 km by 1 km in order to study the U transportation in the vadose zone–aquifer–river system. The Subsurface Transport Over Multiple Phases, STOMP, has been coupled with a multicomponent reactive transport simulation. The STOMP model is a finite-difference that has 26,268 grid cells and a nonuniform grid spacing ranging from 2 to 50 m in the horizontal plane and 0.5 to 2 m in the vertical plane. The flow model was tested against three monitoring wells from March 1992 to February 1993. The authors assumed constant distribution coefficient, K_d, U sorption, and a rate of mass transfer and surface complexation compared with the flow model coupled with the reactive transport simulation. Their results indicated that the U mobility is affected by the spatially and temporally variable chemistry that comes from the river and groundwater exchange in the aquifer. Ultimately, they suggested to fill knowledge gaps in U migration by developing mechanistic models that consider spatial variations in hydrologic

properties and reactive surfaces. This work includes determining existing U concentrations in the subsurface to better understand potential enhanced U mobility and its impact on reactive transport modeling.

Yabusaki et al. (2011) developed a 3D model that integrates flow dynamics and biogeochemical reactions to analyze a U bioremediation experiment in Rifle, Colorado. The goal was to gain a better understanding of how transport processes and biogeochemical reactions interact to control U behavior under specific conditions such as pulsed acetate injection, seasonal water table variations, and spatially variable material properties.

Jemison et al. (2020) developed a U isotope model that simulated the geochemical reactions and transport process in the area of a former U mill in Rifle, Colorado. The numerical reactive transport model applied by the researchers shows the chemical reactions of the $^{238}U/^{235}U$ ratio and the U mobility in the groundwater and its distribution in the subsurface. In addition, they used an isotope-enabled reactive transport model to understand the complex formation of U, artificial tracer concentrations, $^{238}U/^{235}U$ ratio measurements, and the concentrations of the other species relevant to U over two years of field experiments. They used the 1D CrunchTope reactive transport model with 2 meters span in length that discretized into 40 grid cells, a grid size of 0.05 m. The model was calibrated using PEST against the observed data to determine the cation exchange equilibrium, the intrinsic reduction rate of SO_4, U(VI) and Fe (III) oxides, and the surface area of quartz. Their results showed that the δ^{238} U can reduce the mobility of U(VI) and transfer it to the insoluble form U(IV); also, since acetate as an electron donor has the ability to reduce U concentration through injection, low δ^{238} U can reduce the U(VI) mobility in an aquifer.

Kent et al. (2024) applied numerical simulations of U transport and uncertainty analysis at a former U mill site in the southwestern United States. The MODFLOW-USG model, coupled

with the first-order residual source decay model, was utilized for this purpose and was calibrated using PESTPP-iES, with 500 realizations applied. They found that residual vadose zone sources of U significantly impact the time frame required for groundwater remediation at legacy U processing sites. Despite achieving a 99% mass removal during mill tailings disposal, the presence of residual U in vadose zone sediments, particularly in semiarid climates, sustains dissolved plumes for thousands of years. This prolonged persistence of U contamination poses challenges for achieving groundwater remediation goals through monitored natural attenuation or traditional treatment methods. The findings underscore the need for revised forecasted cleanup times and the consideration of alternative remedial strategies to effectively manage and mitigate U contamination at such sites. Multiple other groundwater aquifer models have been applied for U solute transfer at mill sites (Curtis et al. 2006, Fox et al. 2012). Curtis et al. (2006) coupled MODFLOW-RIV for a shallow aquifer with the nonreactive transport model (MT3DMS) at Naturita, CO, for a 3 km span. MODFLOW-RIV was calibrated using UCODE against the available hydraulic conductivity and Cl concentrations. Also, they simulated reactive transport of U(VI) using the SCM model. 66 monitoring wells from DOE and USGS have been used between 1986 to 2001 to collect samples of alkalinity, pH, U(VI) and Cl concentrations from the groundwater. This model has been tested against the observed data, and they found that the simulated U(VI) concentrations sensitive to the recharge flux due to the higher influx of U(VI) into the aquifer. The geochemical response of U(VI) was most affected by alkalinity and showed less sensitivity to variations in pH.

Fox et al. (2012) applied a 1D SCM small-scale tracer model for U(VI) reactive transport in PHREEQC, calibrated with UCODE. The tracer test at the Rifle Integrated Field Research Challenge site revealed that adding bicarbonate increased dissolved U(VI) concentrations by 1.2–2.6 times due to higher bicarbonate alkalinity and Ca concentrations, with more U(VI) mobilized in shallower aquifer zones containing finer-grained sediments. An equilibrium-based model overestimated U(VI) concentrations, while a multirate mass transfer model accurately simulated the nonequilibrium desorption behavior, highlighting the importance of incorporating heterogeneous sediment properties for accurate predictions.

Ma et al. (2014) constructed a 3D multi-model analysis on a field scale to control the U(VI) reactive transport during the tracer test. Also, they applied for a tracer test in order to assess the in-situ desorption kinetics of U(VI). The researchers used a MODFLOW code with 3D groundwater flow, an hourly time step, an assumption of no recharge, and a model domain of 120 m x 122 m. PHT3D coupled with MT3DMS and PHREEQC was used for the reactive transport simulations. They also considered the multi-rate surface complexation model (SCM). They conduct their analysis at the IFRC site located in southeastern Washington State, which contains 36 monitoring wells to monitor the U(VI) concentrations in groundwater. Also, seven wells monitor the river stage and the flow rates. The model showed a good match between the U(VI) model and the observed U(VI) concentrations from the monitoring wells, with the model accounting for the complexity of the heterogeneous aquifer and the dynamic flow condition. Most of these studies have been conducted under limited conditions such as steady-state and/or 1D flow. Also, most of these models have been applied on a relatively small scale, that is, between 1 and 10 ha, and in areas affected by mining operations. They do not conclude the hydrology of U reactivity due to the lack of constraints, and they measure the concentration only. Also, numerous laboratory-

scale models have been developed and applied to simulate U - sediment interactions, leading to reactive transport under limited conditions (Davis et al. 2004, Hay et al. 2011, Stoliker et al. 2013). No studies of U occurrence, mobilization, and reactive transport, including the coupling of groundwater and surface water interaction, are known to have been conducted at a regional scale in irrigated agricultural regions.

Water resources and irrigation in the LARV have been studied by Colorado State University (CSU) for over 22 years with a focus on two study regions, the DSR and an Upstream Study Region (USR), described in Section 3.8. Numerical models that simulate the spatial and temporal distribution of salt ions, NO_3, Se in groundwater and surface water have been calibrated, tested, and applied in the LARV. The groundwater flow component of the model (MODFLOW) has been used to simulate the groundwater flow and groundwater head, which accounts for both recharge and discharge from the aquifer. Morway et al. (2013) constructed and calibrated the model MODFLOW-UZF-RIV. Bailey et al. (2013a) constructed a 3D reactive transport model (RT3D) that is based on a mass balance approach that solves advection, diffusion-dispersion, sorption, and chemical reaction and is linked with the unsaturated zone (UZF1) and MODFLOW, which is known as UZF-RT3D. The UZF-RT3D model included Se and N cycling due to agriculture practices in the soil crop–water system, and oxidation-reduction reactions for application to the USR (Bailey et al. 2013b). The UZF-RT3D model was coupled to OTIS by Bailey and Ahmadi (2014) and by Shultz et al. (2018) to solve the 1D chemical transport of species in streamflow with terms for transient storage, lateral inflow, first-order decay and sorption (Runkel 1998). The original OTIS code was modified to include QUAL2E chemical reactions for O_2 and N cycling. In addition, Qurban et al. (2018) used the MODFLOW output to drive the numerical model of the UZF-RT3D coupled with OTIS and QUAL2E models to solve the reactive

transport of NO_3 and Se in DSR. The model solves different redox reactions between DO and NO_3, along with organic material, humus, and manure. These models form a foundation on which models of U mobilization and reactive transport that applied for the DSR in the LARV.

U is transported in the aqueous environment through advection, dispersion, and diffusion. Furthermore, the abiotic and bio-reduction process, adsorption, and aqueous complexation, known as chemical alterations, play a role in transporting U in the environment (Jemison et al., 2020). Here, we are applying a similar procedure for the U concentrations by constructing a groundwater flow model (MODFLOW) and linking it with the RT3D-OTIS to account for the oxidation of U(IV) from shale bedrock, the heterotrophic reduction of U(VI), heterotrophic and autotrophic denitrification, and nitrification.

2.7.Novelty of This Research

Elevated U concentrations in mine tailings and nuclear power waste sites have been modeled in laboratory soil columns and at limited field scales. However, no physically-based distributed-parameter models of U in the waters of irrigated stream-aquifer systems are known to have been developed to date. The research herein constructs, calibrates, and applies such a model to a representative system of this type in Colorado's LARV.

In the LARV, high concentrations of U, Se, NO_3, and TDS have been found in the groundwater, soils, and streams. Several modeling studies have been carried out in the LARV to investigate Se, NO_3, and TDS as summarized in Table 1. Three of these studies were conducted in the USR of the LARV and have been published in refereed literature. Three MS theses describe analyses in the DSR, but none address U reactive transport. The present research forges a new path of investigation by engaging in the objectives described in Section 1.2 to build and apply a

computational model to gain insights about the spatio-temporal patterns of U pollution in a large expanse of an irrigated stream-aquifer system supported by extensive field data.

Table 1. Flow and solute transport models studies applied to Colorado's LARV.

Study	Period	Area	Flow and Solute Transport Models	Chemical Species
Bailey et al. 2014, 2015a, 2015b	1999–2009	USR	MODFLOW -RIV and RT3D-OTIS	Se and NO_3
Shultz et al. 2018a, 2018b	1999–2009	USR	MODFLOW -SFR and RT3D-OTIS	Se and NO_3
Tavakoli et al. 2019	1999–2009	USR	MODFLOW - RIV and RT3D	TDS
Wei and Bailey 2021	1999–2016	USR	SWAT-MODFLOW and RT3D	NO_3 and P
Hosseini and Bailey 2022, Bailey and Hosseini 2023	1999–2009	USR	SWAT-MODFLOW-salt	TDS
Tummalapenta et al. 2015 (MS Thesis)	2002-2007	DSR	MODFLOW -RIV and RT3D	Se and NO_3
Qurban et al. 2018 (MS Thesis)	2002–2007	DSR	MODFLOW -SFR and RT3D-OTIS	Se and NO_3

Javed et al. 2019 (MS Thesis)	2002–2007	DSR	MODFLOW -SFR and RT3D-OTIS	TDS

2.8.References

Abdelouas, A., Lutze, W., and Nuttall, H. E., 1999. Oxidative dissolution of uraninite precipitated on Navajo sandstone. Journal of Contaminant Hydrology, 36(3–4), 353–375. https://doi.org/10.1016/S0169-7722(98)00151-X

Abdelouas, A., 2006. Uranium mill tailings: Geochemistry, mineralogy, and environmental impact. Elements, 2(6), 335–341. https://doi.org/10.2113/gselements.2.6.335

Adler, H. H., 1974. Concepts of uranium--ore formation in reducing environments in sandstones and other sediments. International Atomic Energy Agency, Vienna.

Alshahri, F., 2019,. Uranium and trace metals contamination in topsoil from different zones around Industrial City, Al Jubail, Saudi Arabia. Archives of Environmental Contamination and Toxicology, 77, 308–319. https://doi.org/10.1007/s00244-019-00642-9

Asic, A., Kurtovic-Kozaric, A., Besic, L., Mehinovic, L., Hasic, A., Kozaric, M., Hukic, M., and Marjanovic, D., 2017. Chemical toxicity and radioactivity of depleted uranium: The evidence from in vivo and in vitro studies. Environmental Research, 156(December 2016), 665–673. https://doi.org/10.1016/j.envres.2017.04.032

Bailey, R. T., Gates, T. K., and Halvorson, A. D., 2013a. Simulating variably-saturated reactive transport of selenium and nitrogen in agricultural groundwater systems. Journal of Contaminant Hydrology, 149, 27–45. https://doi.org/10.1016/j.jconhyd.2013.03.001

Bailey, R. T., and Ahmadi, M., 2014. Spatial and temporal variability of in-stream water quality parameter influence on dissolved oxygen and nitrate within a regional stream network. Ecological Modelling, 277, 87–96. https://doi.org/10.1016/j.ecolmodel.2014.01.015

Bailey, R. T., Gates, T. K., and Ahmadi, M., 2014. Simulating reactive transport of selenium coupled with nitrogen in a regional-scale irrigated groundwater system. Journal of Hydrology, 515, 29–46. https://doi.org/10.1016/j.jhydrol.2014.04.039

Bern, C. R., and Stogner, R. W., 2017. The Niobrara Formation as a challenge to water quality in the Arkansas River, Colorado, USA. Journal of Hydrology: Regional Studies, 12(April), 181–195. https://doi.org/10.1016/j.ejrh.2017.05.001

Bern, C. R., Holmberg, M. J., and Kisfalusi, Z. D.,2020. Salt flushing, salt storage, and controls on selenium and uranium: A 31-year mass-balance analysis of an irrigated, semiarid Valley. JAWRA Journal of the American Water Resources Association, 56(4), 647–668. https://doi.org/10.1111/1752-1688.12841

Bexfield, L. M., and Anderholm, S. K., 1997. Water-quality assessment of the Rio Grande Valley, Colorado, New Mexico and Texas; ground-water quality in the Rio Grande flood plain, Cochiti Lake, New Mexico, to El Paso, Texas, 1995. In Water-Resources Investigations Report. https://doi.org/10.3133/wri964249

Bigalke, M., Ulrich, A., Rehmus, A., and Keller, A., 2017. Accumulation of cadmium and uranium in arable soils in Switzerland. Environmental Pollution, 221, 85–93. https://doi.org/10.1016/j.envpol.2016.11.035

Bjørklund, G., Albert Christophersen, O., Chirumbolo, S., Selinus, O., and Aaseth, J., 2017. Recent aspects of uranium toxicology in medical geology. Environmental Research, 156(March), 526–533. https://doi.org/10.1016/j.envres.2017.04.010

Böhlke, J. K., Verstraeten, I. M., and Kraemer, T. F., 2007. Effects of surface-water irrigation on sources, fluxes, and residence times of water, nitrate, and uranium in an alluvial aquifer. Applied Geochemistry, 22(1), 152–174. https://doi.org/10.1016/j.apgeochem.2006.08.019

Brindha, K., Elango, L., and Nair, R. N., 2011. Spatial and temporal variation of uranium in a shallow weathered rock aquifer in southern India. Journal of Earth System Science, 120(5), 911–920. https://doi.org/10.1007/s12040-011-0117-y

Brugge, D., and Goble, R., 2002. The history of uranium mining and the Navajo people. In American Journal of Public Health (Vol. 92, Issue 9, pp. 1410–1419). American Public Health Association Inc. https://doi.org/10.2105/AJPH.92.9.1410

Brugge, D., De Lemos, J. L., and Oldmixon, B., 2005. Exposure pathways and health effects associated with chemical and radiological toxicity of natural uranium: A review. In Reviews on Environmental Health (Vol. 20, Issue 3, pp. 177–193). Freund Publishing House Ltd. https://doi.org/10.1515/REVEH.2005.20.3.177

Brugge, D., and Buchner, V., 2011. Health effects of uranium: New research findings. Reviews on Environmental Health, 26(4), 231–249. https://doi.org/10.1515/REVEH.2011.032

Burow, K. R., Belitz, K., Dubrovsky, N. M., and Jurgens, B. C., 2017. Large decadal-scale changes in uranium and bicarbonate in groundwater of the irrigated western U.S. Science of the Total Environment, 586, 87–95. https://doi.org/10.1016/j.scitotenv.2017.01.220

Cooley, H. M., Evans, R. E., and Klaverkamp, J. F., 2000. Toxicology of dietary uranium in lake whitefish (Coregonus clupeaformis). Aquatic Toxicology, 48(4), 495–515. https://doi.org/10.1016/S0166-445X(99)00057-0

Coyte, R. M., Jain, R. C., Srivastava, S. K., Sharma, K. C., Khalil, A., Ma, L., and Vengosh, A., 2018. Large-scale uranium contamination of groundwater resources in India. Environmental Science and Technology Letters, 5(6), 341–347. https://doi.org/10.1021/acs.estlett.8b00215

Curtis, G. P., Davis, J. A., and Naftz, D. L., 2006. Simulation of reactive transport of uranium(VI) in groundwater with variable chemical conditions. Water Resources Research, 42(4), 1–15. https://doi.org/10.1029/2005WR003979

Dalin, C., Wada, Y., Kastner, T., and Puma, M. J., 2017. Groundwater depletion embedded in international food trade. Nature, 543(7647), 700–704. https://doi.org/10.1038/nature21403

Davis, J. A., Meece, D. E., Kohler, M., and Curtis, G. P., 2004. Approaches to surface complexation modeling of Uranium(VI) adsorption on aquifer sediments. Geochimica et Cosmochimica Acta, 68(18), 3621–3641. https://doi.org/10.1016/j.gca.2004.03.003

DeSimone, L. A., McMahon, P. B., and Rosen, M. R., 2009. The quality of our Nation's waters: Water quality in principal aquifers of the United States, 1991-2010. In Circular. https://doi.org/10.3133/cir1360

Donahue, R., and Hendry, M. J., 2003. Geochemistry of arsenic in uranium mine mill tailings, Saskatchewan, Canada. Applied Geochemistry, 18(11), 1733–1750. https://doi.org/10.1016/S0883-2927(03)00106-9

EFSA., 2009. Uranium in foodstuffs, in particular mineral water. EFSA Journal, 7(4). https://doi.org/10.2903/j.efsa.2009.1018

Eggers, M., Moore-Nall, A., Doyle, J., Lefthand, M., Young, S., Bends, A., Committee, C., and Camper, A., 2015. Potential health risks from uranium in home well water: An investigation by the Apsaalooke (Crow) Tribal Research Group. Geosciences, 5(1), 67–94. https://doi.org/10.3390/geosciences5010067

Fayek, M., Horita, J., and Ripley, E. M., 2011. The oxygen isotopic composition of uranium minerals: A review. Ore Geology Reviews, 41(1), 1–21. https://doi.org/10.1016/j.oregeorev.2011.06.005

Finch, R., and Murakami, T., 1999. Systematics and paragenesis of uranium minerals, in: P.C. Burns, R. Finch (Eds.), Uranium: Mineralogy, Geochemistry and the Environment. Reviews in Mineralogy, vol. 38, Mineralogical Society of America, Washington, DC, 1999, pp. 91–179.

Fleeger, J. W., Carman, K. R., and Nisbet, R. M., 2003. Indirect effects of contaminants in aquatic ecosystems. In Science of the Total Environment (Vol. 317, Issues 1–3, pp. 207–233). Elsevier. https://doi.org/10.1016/S0048-9697(03)00141-4

Fox, P. M., Davis, J. A., Hay, M. B., Conrad, M. E., Campbell, K. M., Williams, K. H., and Long, P. E., 2012. Rate-limited U(VI) desorption during a small-scale tracer test in a heterogeneous uranium-contaminated aquifer. Water Resources Research, 48(5), 1–18. https://doi.org/10.1029/2011WR011472

Frengstad, B., Midtgård Skrede, A. K., Banks, D., Reidar Krog, J., and Siewers, U., 2000. The chemistry of Norwegian groundwaters: III. The distribution of trace elements in 476 crystalline bedrock groundwaters, as analysed by ICP-MS techniques. Science of the Total Environment, 246(1), 21–40. https://doi.org/10.1016/S0048-9697(99)00413-1

Gajski, G., Oreščanin, V., Gerić, M., Kollar, R., Lovrenčić Mikelić, I., and Garaj-Vrhovac, V., 2014. Toxicity assessment of the water used for human consumption from the Cameron/Tuba City abandoned uranium mining area prior/after the combined electrochemical treatment/advanced oxidation. https://doi.org/10.1007/s11356-014-3376-8

Gates, T. K., Cody, B. M., Donnelly, J. P., Herting, A. W., Bailey, R. T., and Mueller Price, J., 2009. Assessing selenium contamination in the irrigated stream–aquifer system of the Arkansas River, Colorado. Journal of Environment Quality, 38(6), 2344. https://doi.org/10.2134/jeq2008.0499

Gavrilescu, M., Pavel, L. V., and Cretescu, I., 2009. Characterization and remediation of soils contaminated with uranium. Journal of Hazardous Materials, 163(2–3), 475–510. https://doi.org/10.1016/j.jhazmat.2008.07.103

Ginder-Vogel, M., and Fendorf, S., 2007. Chapter 11 Biogeochemical uranium redox transformations: Potential oxidants of uraninite. Developments in Earth and Environmental Sciences, 7(07), 293–319. https://doi.org/10.1016/S1571-9197(07)07011-5

Gorby, Y. A., and Lovley, D. R., 1992. Enzymatic uranium precipitation. In Environ. Sci. TechnoI (Vol. 26). https://pubs.acs.org/sharingguidelines

Hay, M. B., Stoliker, D. L., Davis, J. A., and Zachara, J. M., 2011. Characterization of the intragranular water regime within subsurface sediments: Pore volume, surface area, and mass transfer limitations. Water Resources Research, 47(10). https://doi.org/10.1029/2010WR010303

Hoffman, G. J., Evans, R. G., Jensen, M. E., Martin, D. L., and Elliott, R. L., 2007. Design and operation of farm irrigation systems 2nd edition. http://irrigationtoolbox.com/IrrigationToolBox/Section 2 - Irrigation System Planning/ASABE DesignandOperationofFarmIrrigationSystems/Preface.pdf

Hua, B., Xu, H., Terry, J., and Deng, B., 2006. Kinetics of uranium(VI) reduction by hydrogen sulfide in anoxic aqueous systems. Environmental Science and Technology, 40(15), 4666–4671. https://doi.org/10.1021/es051804n

Ivahnenko, T., Ortiz, R. F., and Robert W. Stogner, S., 2012. Characterization of streamflow, water quality, and instantaneous dissolved solids, selenium, and uranium loads in selected reaches of the Arkansas River, southeastern Colorado, 2009-2010. In Scientific Investigations Report.

Javed, A. B., Gates, T. K., Bailey, R. T., and Ronayn, M. J., 2019. Thesis modeling the distribution of major salt ions in regional agricultural groundwater and surface water systems: model calibration and application submitted by. Colorado State University. libraries.

Jemison, N. E., Bizjack, M. T., Johnson, T. M., and Druhan, J. L., 2020. Influence of physical and chemical hydrology on bioremediation of a U-contaminated aquifer informed by reactive transport modeling incorporating 238U/235U ratios. Geochimica et Cosmochimica Acta, 269, 303–328. https://doi.org/10.1016/j.gca.2019.10.031

Jerden, J. L., and Sinha, A. K., 2006. Geochemical coupling of uranium and phosphorous in soils overlying an unmined uranium deposit: Coles Hill, Virginia. Journal of Geochemical Exploration, 91(1–3), 56–70. https://doi.org/10.1016/j.gexplo.2005.12.003

Kamunda, C., Mathuthu, M., and Madhuku, M., 2016. An assessment of radiological hazards from gold mine tailings in the Province of Gauteng in South Africa. International Journal of Environmental Research and Public Health, 13(1), 138. https://doi.org/10.3390/ijerph13010138

Keith, S., Faroon, O., Roney, N., Scinicariello, F., Wilbur, S., Ingerman, L., Llados, F., Plewak, D., Wohlers, D., and Diamond, G., 2013. Toxicological profile for uranium. Agency for Toxic Substances and Disease Registry (US), Atlanta (GA). http://europepmc.org/books/NBK158802

Kratz, S., Schick, J., and Schnug, E., 2016. Trace elements in rock phosphates and P containing mineral and organo-mineral fertilizers sold in Germany. Science of the Total Environment, 542, 1013–1019. https://doi.org/10.1016/j.scitotenv.2015.08.046

Kurttio, P., Auvinen, A., Salonen, L., Saha, H., Pekkanen, J., Mäkeläinen, I., Väisänen, S. B., Penttilä, I. M., and Komulainen, H., 2002. Renal effects of uranium in drinking water. In Environmental Health Perspectives • VOLUME (Vol. 110, Issue 4). http://ehpnet1.niehs.nih.gov/docs/2002/110p337-342kurttio/abstract.html

Lakaniemi, A. M., Douglas, G. B., and Kaksonen, A. H., 2019. Engineering and kinetic aspects of bacterial uranium reduction for the remediation of uranium contaminated environments. Journal of Hazardous Materials, 371(January), 198–212. https://doi.org/10.1016/j.jhazmat.2019.02.074

Landis, E. R., 1959. Radioacti'vity and uranium content of the Sharon Springs member of the Pierre shale and associated rocks in western Kansas and eastern Colorado Trace Elements Investigations Report 573.

Langmuir, D., 1978. Uranium solution-mineral equilibria at low temperatures with applications to sedimentary ore deposits. Geochimica et Cosmochimica Acta, 42(6 PART A), 547–569. https://doi.org/10.1016/0016-7037(78)90001-7

Large, R. R., Halpin, J. A., Danyushevsky, L. V., Maslennikov, V. V., Bull, S. W., Long, J. A., Gregory, D. D., Lounejeva, E., Lyons, T. W., Sack, P. J., McGoldrick, P. J., and Calver, C. R., 2014. Trace element content of sedimentary pyrite as a new proxy for deep-time ocean-atmosphere evolution. Earth and Planetary Science Letters, 389, 209–220. https://doi.org/10.1016/j.epsl.2013.12.020

Levander, O. A., and Burk, R. F., 2006. Update of human dietary standards for selenium. In D. L. Hatfield, M. J. Berry, and V. N. Gladyshev (Eds.), Selenium: Its Molecular Biology and Role in Human Health (pp. 399–410). Springer US. https://doi.org/10.1007/0-387-33827-6_35

Zamora, M., Tracy, B. L., Zielinski, J. M., Meyerhof, D. P., and Moss, M. A., 1998. Chronic ingestion of uranium in drinking water: A study of kidney bioeffects in humans. Toxicological Sciences, 43(1), 68–77. https://doi.org/10.1006/toxs.1998.2426

Liu, C., Zachara, J. M., Qafoku, N. P., and Wang, Z., 2008. Scale-dependent desorption of uranium from contaminated subsurface sediments. Water Resources Research, 44(8). https://doi.org/10.1029/2007WR006478

Lovley, D. R., and Phillips, E. J. P.. 1992. Reduction of uranium by desulfovibrio desulfuricans. In Applied And Environmental Microbiology (Vol. 58, Issue 3).

Ma, R., Zheng, C., Liu, C., Greskowiak, J., Prommer, H., and Zachara, J. M., 2014. Assessment of controlling processes for field-scale uranium reactive transport under highly transient flow conditions. Water Resources Research, 50(2), 1006–1024. https://doi.org/10.1002/2013WR013835

Ma, W., Gao, B., Guo, Y., Sun, Z., Zhang, Y., Chen, G., Zhu, X., and Zhang, C., 2020. Occurrence and distribution of uranium in a hydrological cycle around a uranium mill tailings pond, Southern China. International Journal of Environmental Research and Public Health, 17(3), 773. https://doi.org/10.3390/ijerph17030773

Mar, S. S., and Okazaki, M., 2012. Investigation of Cd contents in several phosphate rocks used for the production of fertilizer. Microchemical Journal, 104, 17–21. https://doi.org/10.1016/j.microc.2012.03.020

Morway, E. D., Gates, T. K., and Niswonger, R. G., 2013. Morway, E. D., Gates, T. K., and Niswonger, R. G., 2013. Appraising options to reduce shallow groundwater tables and enhance flow conditions over regional scales in an irrigated alluvial aquifer system. Journal of Hydrology, 495, 216–237. https://doi.org/1. Journal of Hydrology, 495, 216–237. https://doi.org/10.1016/j.jhydrol.2013.04.047

Mwalongo, D. A., Haneklaus, N. H., Lisuma, J. B., Mpumi, N., Amasi, A. I., Mwimanzi, J. M., Chuma, F. M., Kivevele, T. T., and Mtei, K. M., 2024. Uranium Dissemination with Phosphate Fertilizers Globally: A Systematic Review with Focus on East Africa. In Sustainability (Vol. 16, Issue 4). https://doi.org/10.3390/su16041496

Narasimhan, T. N., White, A. F., and Tokunaga, T., 1986. Groundwater contamination from an inactive uranium mill tailings pile: 2. Application of a dynamic mixing model. Water Resources Research, 22(13), 1820–1834. https://doi.org/10.1029/WR022i013p01820

Neves, O., and Matias, A. M. J., 2007. Assessment of groundwater quality and contamination problems ascribed to an abandoned uranium mine (Cunha Baixa region, Central Portugal). https://doi.org/10.1007/s00254-007-0785-8

Newsome, L., Morris, K., and Lloyd, J. R., 2014. The biogeochemistry and bioremediation of uranium and other priority radionuclides. In Chemical Geology (Vol. 363, pp. 164–184). Elsevier. https://doi.org/10.1016/j.chemgeo.2013.10.034

Nolan, J., and Weber, K. A., 2015. Natural uranium contamination in major U.S. aquifers linked to nitrate. Environmental Science and Technology Letters, 2(8), 215–220. https://doi.org/10.1021/acs.estlett.5b00174

Orloff, K., Mistry, K., Charp, P., Metcalf, S., Marino, R., Shelly, T., Melaro, E., Donohoe, A., and Jones, R., 2004. Human exposure to uranium in groundwater. Environmental Research, 94, 319–326. https://doi.org/10.1016/S0013-9351(03)00115-4

Prakash, R., Bhartariya, K. G., Singh, S., Singh, K., Rajak, M., and Kaushik, Y. B., 2020. Uranium and its correlation with other geogenic contaminants in ground water of Ganga Yamuna Doab, Fatehpur District, Uttar Pradesh, India. Journal of the Geological Society of India, 95(4), 359–365. https://doi.org/10.1007/s12594-020-1444-x

Presser, T. S., Sylvester, M. A., and Low, W. H., 1994. Bioaccumulation of selenium from natural geologic sources in western states and its potential consequences. Environmental Management, 18(3), 423–436. https://doi.org/10.1007/BF02393871

Qurban, I. A., Bailey, R. T., Gates, T. K., and Suter, J. F., 2018. Thesis finding water management practices to reduce selenium and nitrate concentrations in the irrigated stream-aquifer system along the Lower reach of Colorado's Arkansas River Valley submitted by. Colorado State University. libraries.

Riley, R. G., and Zachara, J. M., 1992. Chemical contaminants on DOE lands and selection of contaminant mixtures for subsurface science research. https://doi.org/10.2172/10147081

Roback, R. C., Johnson, T. M., McLing, T. L., Murrell, M. T., Luo, S., and Ku, T. L., 2001. Uranium isotopic evidence for groundwater chemical evolution and flow patterns in the Eastern Snake River Plain aquifer, Idaho. Bulletin of the Geological Society of America, 113(9), 1133–1141. https://doi.org/10.1130/0016-7606(2001)113<1133:UIEFGC>2.0.CO;2

Runkel, R. L., 1998. One-dimensional transport with inflow and storage (otis): a solute transport model for streams and rivers. Water-Resources Investigations Report 98-4018, 0–80. https://doi.org/Cited By (since 1996) 47\nExport Date 4 April 2012

Saini, K., Singh, P., and Bajwa, B. S., 2016. Comparative statistical analysis of carcinogenic and non-carcinogenic effects of uranium in groundwater samples from different regions of Punjab, India. Applied Radiation and Isotopes, 118, 196–202. https://doi.org/10.1016/j.apradiso.2016.09.014

Salonen, L., 1994. 238 U series radionuclides as a source of increased radioactivity in groundwater originating from Finnish bedrock (Issue 222).

Scanlon, B. R., Faunt, C. C., Longuevergne, L., Reedy, R. C., Alley, W. M., McGuire, V. L., and McMahon, P. B., 2012. Groundwater depletion and sustainability of irrigation in the US High Plains and Central Valley. Proceedings of the National Academy of Sciences of the United States of America, 109(24), 9320–9325. https://doi.org/10.1073/pnas.1200311109

Seiler, R., Skorupa, J., and Peltz, L., 1999. Areas susceptible to irrigation-induced selenium contamination of water and biota in the Western United States. US Geological Survey, 1180. http://minerals.er.usgs.gov/minerals/

Senko, J. M., Mohamed, Y., Dewers, T. A., and Krumholz, L. R., 2005. Role for Fe(III) minerals in nitrate-dependent microbial U(IV) oxidation. Environmental Science and Technology, 39(8), 2529–2536. https://doi.org/10.1021/es048906i

Sethi, T. K., El-Ghamry, M. N., and Kloecker, G. H., 2012. Radon and lung cancer. Clinical Advances in Hematology and Oncology : HandO, 10(3), 157–164.

Shultz, C. D., Bailey, R. T., Gates, T. K., Heesemann, B. E., and Morway, E. D., 2018. Simulating selenium and nitrogen fate and transport in coupled stream-aquifer systems of irrigated regions. Journal of Hydrology. https://doi.org/10.1016/j.jhydrol.2018.02.027

Shultz, C. D., Gates, T. K., and Bailey, R. T., 2018b. Evaluating best management practices to lower selenium and nitrate in groundwater and streams in an irrigated river valley using a calibrated fate and reactive transport model. Journal of Hydrology, 566, 299–312. https://doi.org/10.1016/J.JHYDROL.2018.09.005

Skeppström, K., and Olofsson, B., 2007. Uranium and radon in groundwater - An overview of the problem. European Water, 17, 51–62.

Stoliker, D. L., Liu, C., Kent, D. B., and Zachara, J. M., 2013. Characterizing particle-scale equilibrium adsorption and kinetics of uranium(VI) desorption from U-contaminated sediments. Water Resources Research, 49(2), 1163–1177. https://doi.org/10.1002/wrcr.20104

Stopps, G. J., and Todd, M., 1982. The chemical toxicity of uranium with special reference to effects on the kidney and the use of urine for biological monitoring. http://inis.iaea.org/search/search.aspx?orig_q=RN:15006066

Takeda, A., Tsukada, H., Takaku, Y., Hisamatsu, S., and Nanzyo, M., 2006. Accumulation of uranium derived from long-term fertilizer applications in a cultivated Andisol. Science of the Total Environment, 367(2–3), 924–931. https://doi.org/10.1016/j.scitotenv.2006.01.006

Tavakoli, S., Bailey, R., and Gates, T., 2019. A salinity reactive transport and equilibrium chemistry model for regional-scale agricultural groundwater systems. Journal of Hydrology, 572. https://doi.org/10.1016/j.jhydrol.2019.02.040

Teixeira, J., Chaminé, H. I., Espinha Marques, J., Carvalho, J. M., Pereira, A. J. S. C., Carvalho, M. R., Fonseca, P. E., Pérez-Alberti, A., and Rocha, F., 2015. A comprehensive analysis of groundwater resources using GIS and multicriteria tools (Caldas da Cavaca, Central Portugal): environmental issues. Environmental Earth Sciences, 73(6), 2699–2715. https://doi.org/10.1007/s12665-014-3602-1

Thiros, S. A., Paul, A. P., Bexfield, L. M., and Anning, D. W., 2015. The quality of our Nation's waters: Water quality in basin-fill aquifers of the southwestern United States: Arizona, California, Colorado, Nevada, New Mexico, and Utah, 1993-2009. In Circular. https://doi.org/10.3133/cir1358

Tummalapenta, R. K. T., 2015. Investigating best management practices to reduce selenium and nitrate contamination in a regional scale irrigated agricultural groundwater system: Lower Arkansas River Valley, Southeastern Colorado.

U.S. Environmental Protection Agency., 2012. U.S. Environmental Protection Agency. https://www.epa.gov/radiation/radiation-health-effects

Ullah, H., Rehman, A., Ahmad, I., Khattak, N. U., Fozia, A., Ali, N., and Wasim, A., 2013. Estimation of uranium concentration in drinking water sources of tehsil takht-e-nasrati, district karak, khyber pakhtunkhwa, pakistan using fission track technique. Journal of the Chemical Society of Pakistan, 35(3), 1000–1004.

Uralbekov, B. M., Smodis, B, and Burkitbayev, M.,2011. Uranium in natural waters sampled within former uranium mining sites in Kazakhstan and Kyrgyzstan. https://doi.org/10.1007/s10967-011-1154-3

Verstraeten, I. M., Bohlke, J. K., and Kraemer, T. F., 2000. Groundwater/surface-water interactions and sources of nitrogen and uranium in an irrigated area of Nebraska, USA. IAHS-AISH Publication, 262, 525–531.

Wall, J. D., and Krumholz, L. R., 2006. Uranium reduction. annual review of microbiology, 60(1), 149–166. https://doi.org/10.1146/annurev.micro.59.030804.121357

Wei, X., and Bailey, R. T., 2021. Evaluating nitrate and phosphorus remediation in intensively irrigated stream-aquifer systems using a coupled flow and reactive transport model. Journal of Hydrology, 598(April), 126304. https://doi.org/10.1016/j.jhydrol.2021.126304

Waseem, A., Ullah, H., Rauf, M. K., and Ahmad, I., 2015. Distribution of natural uranium in surface and groundwater resources: A review. Critical Reviews in Environmental Science and Technology, 45(22), 2391–2423. https://doi.org/10.1080/10643389.2015.1025642

Wersin, P., Hochella, M. F., Per Persson, J. R., Redden, G., Leckie, J. 0, and Harris, D. W., 1994. Interaction between aqueous uranium (VI) and sulfide minerals: Spectroscopic evidence for sorption and reduction. In Geofhimica et Cosmochimica Acta (Vol. 58, Issue 13).

Westrop, J. P., Snow, D. D., and Weber, K. A., 2022. Mobilization of naturally occurring uranium in groundwater under intensely managed farmland. Food, Energy, and Water Nexus: A Consideration for the 21st Century, 215–232. https://doi.org/10.1007/978-3-030-85728-8_12

World Health Organization., 2001. Depleted uranium: Sources, exposure and health effects. April, 1–195. http://apps.who.int/iris/bitstream/handle/10665/66930/WHO_SDE_PHE_01.1.pdf;jsessionid=E2B432AE38E0F2FD0A66B98AECDB1864?sequence=1

World Health Organization., 2011a. Guidelines for drinking-water quality. Geneva. :pp. 472–475. http://apps.who.int/iris/bitstream/10665/44584/1/9789241548151_eng.pdf

World Health Organization., 2011b. Uranium in drinking-water. WHO/SDE/WSSH/03.04/118/Rev/1: Geneva. 21 pp. http://www.who.int/water_sanitation_health/dwq/%0Achemicals/uranium_forcomment_20110211_en.pdf

World Nuclear Association., 2020. World uranium mining - World Nuclear Association. https://www.world-nuclear.org/information-library/nuclear-fuel-cycle/mining-of-uranium/world-uranium-mining-production.aspx

Wrenn, M. D., Durbin, P. W., Howard, B., Lipsztein, J., Rundo, J., Still, E. T., and Willis, D. L., 1983. Metabolism of ingested uranium and radium. http://inis.iaea.org/search/search.aspx?orig_q=RN:17002385\

Wu, Y., Wang, Y., and Xie, X., 2014. Occurrence, behavior and distribution of high levels of uranium in shallow groundwater at Datong basin, northern China. Science of the Total Environment, 472, 809–817. https://doi.org/10.1016/j.scitotenv.2013.11.109

Wu, Y., Wang, Y., and Guo, W., 2019. Behavior and fate of geogenic uranium in a shallow groundwater system. Journal of Contaminant Hydrology, 222(June 2018), 41–55. https://doi.org/10.1016/j.jconhyd.2019.02.009

Yabusaki, S. B., Fang, Y., and Waichler, S. R., 2008. Building conceptual models of field-scale uranium reactive transport in a dynamic vadose zone-aquifer-river system. Water Resources Research, 44(12). https://doi.org/10.1029/2007WR006617

Zielinski, R. A., Asher-Bolinder, S., Meier, A. L., Johnson, C. A., and Szabo, B. J., 1997. Natural or fertilizer-derived uranium in irrigation drainage: A case study in southeastern Colorado, U.S.A. Applied Geochemistry, 12(1), 9–21. https://doi.org/10.1016/S0883-2927(96)00050-9

Zoriy, P., Ostapczuk, P., Dederichs, H., Höbig, J., Lennartz, R., and Zoriy, M., 2010. Biomonitoring of environmental pollution by thorium and uranium in selected regions of the Republic of Kazakhstan. Journal of Environmental Radioactivity, 101(5), 414–420. https://doi.org/10.1016/j.jenvrad.2010.02.014

CHAPTER 3: SIMULATING MULTI-YEAR NONPOINT-SOURCE URANIUM POLLUTION IN AN IRRIGATED STREAM-AQUIFER SYSTEM

Preface

This chapter, co-authored by Ibraheem A. Qurban, Timothy K. Gates, Eric D. Morway, John T. Cox, Jeremy T. White, Ryan T. Bailey, and Michael N. Fienen, was submitted to the Journal of Hydrology in April 2024. Ibraheem Qurban's contributions included modifying the MODFLOW-SFR2 input files developed by Morway and Cox, adapting the FORTRAN code for the RT3D-OTIS model developed by Bailey, calibrating the MODFLOW-RT3D-OTIS models using PESTPP-iES, discussing all research aspects, conceptualizing and creating numerous figures, writing the original manuscript, revising text and figures based on co-authors' feedback, and corresponding with the publisher. The chapter remains unchanged from the submitted paper, except for minor formatting adjustments to comply with CSU Graduate School guidelines for formatting and submission.

3.1.Summary

Uranium (U) in the rocks and soils of arid and semi-arid environments can be mobilized and transported by irrigation and fertilization of agricultural lands. Elevated levels of U, along with co-reactants like selenium (Se) and nitrate (NO_3), have environmental and health implications, necessitating careful monitoring and management practices to allay potential adverse effects on water resources. We have developed a physically-based distributed-parameter numerical model to assess U pollution over multiple years in a stream-aquifer system of a large irrigated region. To investigate the complex distribution of U and related contaminants, the model is applied to a 552 km² study region in the Lower Arkansas River Valley (LARV) of Colorado

over a period spanning 14 years. A version of the MODFLOW model for describing groundwater and stream flow is coupled with a form of the RT3D model simulating to portray reactive U, Se, and NO_3 transport in the shallow aquifer and in the Arkansas River stream network. Calibration of the resulting MODFLOW-RT3D model is carried out using the PESTPP-iES iterative ensemble smoother (iES) software. Simulated results indicate good agreement with observed U concentrations in groundwater and streams and with estimated mass loading to the Arkansas River. The overall average U concentrations in the non-riparian aquifer and river over the period are 126 μg/L and 61 μg/L, respectively, compared with 111.7 μg/L and 62 μg/L for measured values. The average 85^{th} percentile of simulated U concentrations over the period averaged across the non-riparian aquifer and river are 218.1 μg/L and 87 μg/L, respectively. These simulated U levels in groundwater exceed the chronic standard (85^{th} percentile = 30 μg/L) across 44% of the region. Additionally, over the simulation period, concentrations exceed the chronic standard along the entire reach of the Arkansas River by an average factor of 2.9. Average simulated U mass loading to the Arkansas River is 0.27 kg/day per km compared to estimated average unaccounted mass loading of 0.23 kg/day per km. Like U, Se concentrations substantially exceed the chronic standard, and there is slight to moderate NO_3 exceedance. Pollutant levels vary greatly over the region, highlighting hotspots which deserve special attention and may point to possible contributing factors. These results describe the severity and extent of the U problem in the LARV, providing a baseline for future comparison to simulated outcomes of alternative water and land best management practices (BMPs) in exploring prospects for pollution mitigation.

3.2.Introduction

Uranium (U) commonly occurs in the natural environment, being found in sedimentary, metamorphic, and igneous formations with an overall average concentration of about 2.7 mg/kg

(WHO 2012, Majumder and Wall 2017). Its release into aqueous settings results from natural hydrogeochemical processes and also can be triggered by a variety of human activities, such as mining, milling operations, energy production, coal combustion, and agriculture (Abdelouas 2006, Gavrilescu et al. 2009). This often leads to dissolved concentrations that exceed the maximum contaminant level of 30 μg/L set by the World Health Organization (WHO) and the United States Environmental Protection Agency (USEPA) and are potentially harmful to aquatic life, livestock, and humans, with infants being more vulnerable to U exposure (EFSA 2009). Hydrosystems near U mining sites face contamination from trace metals, affecting aquatic organisms (Fleeger et al. 2003). In lakes and streams U can induce acute renal failure and liver dysfunction in mammals and fish, while toxic levels affect kidney function and insulin levels in animals (Stopps and Todd 1982, Craft et al. 2004).

In the arid and semi-arid western United States, Cretaceous sedimentary rock, including Pierre and Niobrara shale, is a major source of U (Landis 1959, Ivahnenko et al. 2012). Most U in these formations and in their weathered residuum is in a chemically reduced form known as uraninite U(IV), existing as UO_2, which produces a dissolved and mobile form known as uranyl U(VI), which exists as UO_2^{2+} (Langmuir 1978) when exposed to oxic waters. The dissolution and mobilization of geogenic U is accelerated in regions of intensive irrigated agriculture. Canal seepage and water applied to fields in excess of crop consumptive use, laden with dissolved oxygen (O_2) and with nitrate (NO_3) derived from nitrogen (N)-based fertilizer, move through the surface and subsurface, causing reactions that lead to U pollution of aquifers and receiving streams. Such pollution has been documented in the San Joaquin River Valley, California (Nolan and Weber 2015, Thiros et al. 2015), the North Platte River Valley in western Nebraska (Böhlke et al., 2007), and the Arkansas River Valley in Colorado (Gates et al. 2009, Bern and Stogner 2017, Gates et al.

2018, Bern et al. 2020). Assessing and finding solutions to U contamination in these environments requires data and modeling that adequately account for major spatially and temporally varying hydrogeochemical processes over large scales.

Numerous laboratory-scale models have been developed and applied to simulate U interaction with sediment, leading to the description of reactive transport under limited conditions (Davis et al. 2004, Hay et al. 2011, Stoliker et al. 2013). Most studies of U in the field have been conducted over areas of relatively small scale (between 1 and 1000 ha) at sites affected by mining operations. Some field studies have utilized observed data, but datasets typically consist of a limited number of samples or do not span an extended period. Multiple groundwater aquifer models have been applied to simulate U solute transport at mill sites (Curtis et al. 2006, Yabusaki et al. 2008, Yabusaki et al. 2011, Fox et al. 2012, Ma et al. 2014, Jemison et al. 2020, Johnson et al. 2023, Kent et al. 2024). A summary description of these studies is provided in Table 2.

A study by Burow et al. (2017) marks the first nationwide assessment of U concentration changes in the US, with a focus on irrigated regions in the West. Utilizing a unique dataset collected over a decade, it examines U and bicarbonate (HCO_3) level fluctuations. Over a period of ten years, they found that 6% of 1105 groundwater monitoring wells throughout the United States exceeded the safety limits set by the EPA. Groundwater in the arid western regions exhibited elevated U levels, and changes in these levels, particularly in arid regions, are found to support the hypothesis of a connection between U and HCO_3 concentrations in irrigated areas. U occurrence was found to depend upon U-bearing rocks, oxidizing geochemical conditions, HCO_3 presence, and changes in chemistry, like HCO_3 fluctuations. The rise in irrigation activities and pumping at deeper levels of the groundwater system has resulted in the downward movement of water with high U and HCO_3 concentrations.

We are aware of no studies that have modeled U occurrence, mobilization, and reactive transport, including the coupling of groundwater and stream interactions over large expanses of irrigated agriculture. This highlights a critical gap in understanding U behavior in such environments where hydrogeochemical processes are influenced not only by natural sources but also by intensive human activity. The aim of the present study is to develop and apply such a computational model for simulating the mobilization and reactive transport of U in an irrigated stream-aquifer system. The distributed parameter model is calibrated at a regional scale of about 55,200 ha over an extended period of 14 years in application to a representative system in Colorado's Lower Arkansas River Valley (LARV). Irrigation practices along with coupled saturated and unsaturated flow and solute transport in groundwater and streams are simulated, accounting for major chemical reactions. In addition to U, attention is given to selenium (Se), a common co-constituent derived from Cretaceous rock known to be toxic, and to NO_3 which affects both U and Se and is itself a pollutant of concern. An ensemble method with data assimilation is employed for calibration of multiple model parameters by systematically reducing the discrepancy between observed field data and modelled equivalent outputs. The model is used for a spatiotemporal assessment of the severity and extent of U pollution over the LARV region in relation to the chronic standard and as affected by geology, irrigation, and other features, laying the groundwork for future exploration of best management practices (BMPs) for mitigation.

3.3.Conceptual Model of U Mobilization and Transport in an Irrigated Stream-Aquifer

In irrigated stream-aquifer systems, the mobility and retardation of U are governed in large part by oxidation-reduction (redox) biogeochemical reactions (Szecsody et al. 1998). U occurs in four oxidation states (+3, +4, +5, and +6), but in an aqueous environment, the most common are U(IV) and U(VI). U is mainly found in the earth's crust and all types of rocks (Prakash et al. 2020)

as three radioactive isotopes, U^{238} (99.27%), U^{235} (0.72%), and U^{234} (0.005%). U(VI) has the highest oxidation number, is the most common soluble form, and can migrate readily within groundwater and surface water (Ginder-Vogel and Fendorf 2007). U(IV) is found to be immobile, solid, adsorbed to organic matter, and of low solubility under reducing conditions (Ulrich et al. 2008).

Both U(IV) and U(VI) are abundant in aerobic (oxic) environments, with oxidation occurring at near-neutral pH values. U(VI) is highly active and mobile in aerobic zones, like the relatively shallow groundwater zone, where O_2 and other oxidants, like NO_3, may be present. NO_3 contamination is a common issue in shallow subsurface aquifers, stemming from agricultural application of N-based fertilizers and animal waste (Malakar et al. 2023). N fertilizers are commonly used in the form of ammonium (NH_4), which has the potential to leach into the groundwater where it may undergo conversion to NO_3 through the activity of nitrifying bacteria. This increase in NO_3 in groundwater can contribute to U contamination, as NO_3 can stimulate the oxidative dissolution of U(IV) minerals in rock or sediments through biotic and abiotic reactions (Malakar et al. 2023). Zielinski et al. (1997) found that the effect of phosphate (PO_4) as fertilizer on dissolved U in an area of the LARV is minimal, and that high dissolved U(VI) was derived primarily from geogenic sources.

Table 2. Summary of U transport modeling studies.

Reference	Model Dimension	Models Used	Study Area	Calibration Method	Simulated Variables	Calibration Target Data
Curtis et al. (2006)	3D	MODFLOW-RIVMT3DMS-SCM	Former U mill, near Naturita, CO (1.2 km^2)	UCODE	U(VI) groundwater concentration, alkalinity of recharge water in the source area, constant distribution coefficient	U(VI) groundwater concentration, alkalinity of recharge water in the source area, constant distribution coefficient
Yabusaki et al. (2008)	1D and 2D	SCM-STOMP	The Hanford Site, Columbia River, southeastern WA (0.4 km^2)	Manual	U(VI) and Ca groundwater concentrations, groundwater hydraulic head, and alkalinity	U(VI) and Ca groundwater concentration, groundwater hydraulic head, and alkalinity
Yabusaki et al. (2011)	3D	eSTOMP	U mill, in Rifle, CO (0.2 km^2)	N/A	U(VI) groundwater concentration	N/A
Fox et al. (2012)	1D	SCM-PHREEQC	The Old Rifle site mill, located in Rifle, CO	UCODE	U(VI) and U(IV), and Mn groundwater concentrations breakthrough curves., and Mn concentration	U(VI), U(IV), and Mn groundwater concentrations

Ma et al. (2014)	3D	MODFLOW-PHT3D-SCM-PHREEQC	IFRC mill, southeastern WA ($14km^2$)	Manual	U(VI), U(IV), and Br groundwater concentrations breakthrough curves, river stage, and intraborehole flow flux	U(VI), U(IV), and Br groundwater U(VI) concentrations, in groundwater, and river stage, and intraborehole flow flux
Jemison et al. (2020)	1D	CrunchTope-SCM	U mill, in Rifle, CO ($40\ cm^2$)	PEST	Br, acetate, Na, Ca, sulfate, Fe (II), and U concentrations in groundwater	Br, acetate, Na, Ca, sulfate, Fe (II), and U concentrations in groundwater
Johnson et al. (2023)	1D and 3D	MODFLOW-USG PHREEQC-PHT-USG	U mill, at Grand Junction CO ($0.2\ km^2$)	PESTPP-iES	Cl, sodium 2,6-difluorobenzoate, and U(VI) groundwater concentrations	Cl, sodium 2,6-difluorobenzoate, ,and U(VI) groundwater concentrations

Kent et al. (2024)	1D	MODFLOW-USG	U mill, in Southern Utah near the city of Monticello UT ($1.4\ km^2$)	PESTPP-iES	Groundwater level, streamflow, U(VI) groundwater concentration, U(VI) concentration in creek, and U(VI) cumulative mass removal	Groundwater level, streamflow, U(VI) groundwater concentration, U(VI) concentration in creek, and U(VI) cumulative mass removal

U(VI) can be reduced to U(IV) in the microbially active anaerobic zone (Wall and Krumholz 2006). Although at pH 6 U(VI) can be adsorbed strongly by iron (oxy)hydroxides to the sedimentary matrices, at a high pH the presence of carbonate (CO_3) and other cations inhibits the adsorption of U(VI) and its reduction to U(IV), which can lead to soluble U(VI)-CO_3 species (Langmuir 1978, Maher et al. 2013). U forms different soluble complexes with ions such as CO_3, NO_3, phosphite (PO_3), and calcium (Ca), which can retard U chemical reduction and sorption. Uranyl adsorption is limited when Ca ions are present due to the formation of two ternary uranyl-Ca-CO_3 complexes, $CaUO_2(CO_3)_3^{2-}$ and $Ca_2UO_2(CO_3)_3^0$ (Singer et al. 2009, Lopez et al. 2021). Uranyl complexes have a high resistance to chemical reduction; thus, the adsorption to organic matter or minerals is poor (Brooks et al. 2003, Stewart et al. 2010). Finally, these complexes are commonly the predominant U(VI) species in near-neutral to alkaline environments, which are frequently found in surface and groundwater systems of semi-arid and arid regions (Jurgens et al. 2010, Burow et al. 2017).

A conceptual sketch of an irrigated stream-aquifer system is provided in Fig. 6. Movement and storage of water in the system encompass various activities such as rainfall, irrigation from both canals and groundwater wells, runoff from fields, percolation through the unsaturated zone, canal seepage, groundwater storage and flow within the unconfined saturated zone, upflux from the shallow water table into the unsaturated zone, interactions between groundwater and streams, and flow within streams. Due to their major role in redox processes, O_2 and N species are also depicted along with U. Considered in the system are the cycling of U and N within the root zone; leaching of U and N in the vadose zone; the transport of U and N within the saturated zone through processes such as advection, dispersion, and chemical reactions; and the release of U(IV) from bedrock and near-surface layers and minerals. These include uraninite, vanadates, carnotite,

phosphates of autunite, and silicate uranophane (Langmuir 1978, Abdelouas et al. 1999). The presence of O_2 and NO_3, which are U(IV) oxidants, leads to the mobilization of U as U(VI). Also, the occurrence of these oxidants with CO_3 complexes in the groundwater is considered a primary control of U concentrations (Jurgens et al. 2010). Studies have shown a strong correlation between NO_3 and U(VI) and between Ca and U mobility; the NO_3 and Ca have the ability to dissolve, mobilize, and inhibit the chemical reduction of U(VI) in groundwater (Finneran et al. 2002, Senko et al. 2002, Wu et al. 2010, Nolan and Weber 2015, Lopez et al. 2021). Advection and dispersion are responsible for carrying U through the aquifer system; during this transport, U continues to react based on the presence of different species, including Se species [elemental Se, selenate (SeO_4), selenite (SeO_3), Selenomethionine (SeMet), and dimethyl diselenide (DMSe)] and other ions, depending on redox conditions (see Fig. 7) and pH.

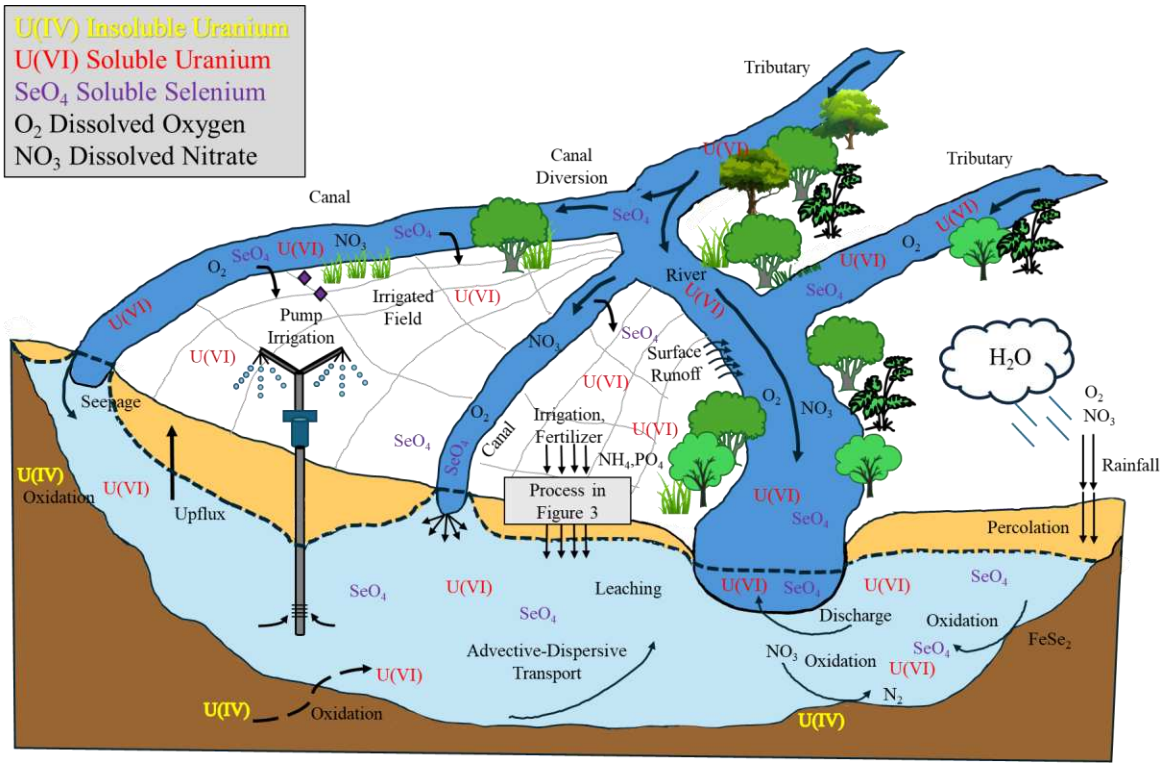

Figure 6. Conceptual model of an irrigated stream aquifer system showing the occurrence and movement of U and related constituents.

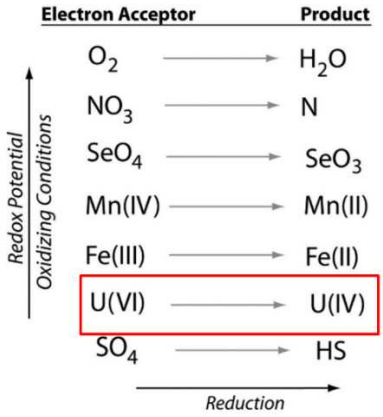

Figure 7. The chemical reduction ladder shows the succession of the terminal electron acceptor process (Gates et al. 2009). Top species are more readily reduced (left to right), whereas the bottom species are more favorable to oxidize (right to left).

Fig. 8 illustrates the cycling of O_2 N, Se, and U species in the vadose zone above the water table in an irrigated stream-aquifer system. These species can be introduced into the subsurface via fertilizer, irrigation water (either through surface or groundwater irrigation), and canal seepage water. In the root-soil zone, NH_4 can be converted to NO_3 through nitrification, and subsequently, NO_3 may undergo denitrification to form N_2, depending on the water content and the availability of organic carbon (OC). Additionally, both O_2 and NO_3 have the potential to undergo autotrophic chemical reduction in the presence of pyrite (FeS_2) and seleno-pyrite ($FeSe_2$) which are commonly found in bedrock shale formations and shale outcrops in numerous alluvial river valleys across the western United States (Seiler 1995, Bailey et al. 2012). Crop roots can take up N and Se species and then be plowed into the soil at the end of the harvest period. Three immobile species and seven mobile species represent organic soil matter. The immobile species are humus (H) (slow-decomposing), litter (L) (fast-decomposing), and manure (M), and the mobile species represent the dissolved phase, which includes O_2, U(VI), NH_4, NO_3, SeO_4, SeO_3, and SeMet. The N and organic Se are combined with the dead root mass of the crop that occurs in the harvest season, and these are connected to the litter pool. The organic matter may be mineralized to mobile U(VI), which then may undergo chemical redox reactions, a complex process that needs further

investigation and is not considered here. Both SeO_4 and SeO_3, can inhibit the reduction of U(VI) to U(IV). Also, U(IV) in rocks can be oxidized to U(VI) via O_2 and NO_3 autotrophic reduction.

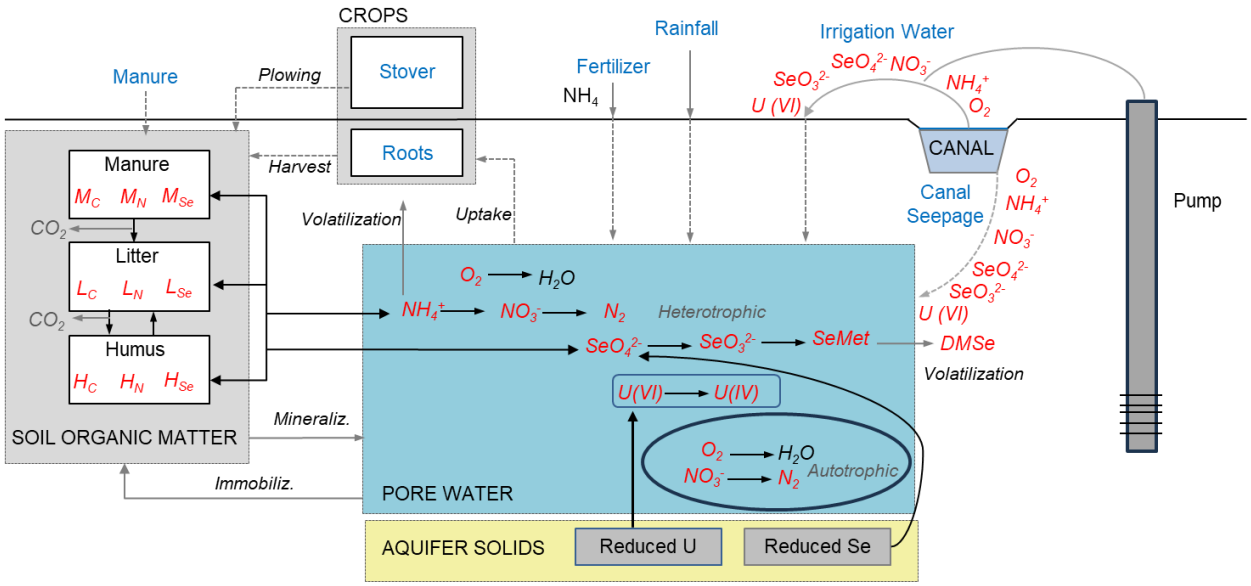

Figure 8. Conceptual model of U, N, and Se cycling processes in the vadose zone and shallow water table. Adapted from Bailey et al. (2014).

3.4.Redox Chemical Reactions in an Irrigated Stream-Aquifer System

There are several reactions by which U species are reduced in aqueous environments (Yabusaki et al. 2008) involving different mechanisms, pathways, and environmental conditions. The primary reaction of reduction U (VI) to U (IV) can be written as:

$$UO_2^{2+} + H_2O \leftrightarrow UO_2OH^+ + H^+ \quad (1)$$

$$UO_2^{2+} + 2H_2O \leftrightarrow UO_2(OH)_2 + 2H^+ \quad (2)$$

It is common for U to form soluble complexes with CO_3 which is often found at high concentrations in groundwater, at a neutral pH of 7, and with a 30 mM HCO_3 buffer. It also is possible for U to form soluble complexes with Se species under certain geochemical conditions, depending on factors such as U oxidation state, pH, ligand presence, and the specific chemical

environment. The formation of soluble complexes with SeO_4 and SeO_3 can enhance the mobility and transport of U in aquatic environments (Sladkov 2010):

$$UO_2^{2+} + SeO_4^{2-} \leftrightarrow UO_2SeO_4 \quad (3)$$

$$UO_2^{2+} + HSeO_3^{-} \leftrightarrow UO_2HSeO_3^{+} \quad (4)$$

In irrigated stream-aquifer systems nitrite (NO_2), solid manganese [Mn(IV)], and iron [Fe(III)] contribute to U(IV) oxidation. However, the key oxidizing agents are O_2 and NO_3, whose respective reactions are (Ulrich et al. 2008, Asta et al. 2020):

$$UO_2 + 2H^+ + 0.5O_2 \leftrightarrow UO_2^{2+} + H_2O \quad (5)$$

$$UO_2 + 0.4NO_3^- + 2.4H^+ \leftrightarrow UO_2^{2+} + 0.2N_2 + 1.2H_2O \quad (6)$$

This study considers the relationship between O_2, NO_3, and Se concentrations and their influence on U concentrations in a large irrigated agricultural setting. Field observations of U and NO_3 as co-contaminants have been reported by Riley and Zachara (1992), Senko et al. (2002), Senko et al. (2005), and Nolan and Weber (2015). Though a previous field study has suggested a positive but weak correlation between Ca and CO_3 concentrations with U, indicating their potential role in U mobilization and sorption (Singh et al., 2003), further investigation is needed and direct consideration is reserved for future research efforts. More detail about the interaction of CO_3 and Ca with U, including the formation of complexes, is presented in Supplemental Material in Appendix A.

3.5.Overview of the coupled flow and U transport model and calibration routine

The present study employs MODFLOW-RT3D (Fig. 9), a modeling assembly which couples the widely used groundwater flow model MODFLOW and the reactive solute transport model RT3D to holistically simulate the irrigated stream-aquifer system processes described in

Sections 3.3 and 3.4. The governing equations for flow in the groundwater system is described in Harbaugh (2005) and solved using MODFLOW-NWT (Niswonger et al., 2011). Streamflow in this connected stream-aquifer system is simulated with the streamflow routing package SFR (v.2) (Niswonger and Prudic 2010). The unsaturated-zone flow (UZF) package (Niswonger et al. 2006) is used to simulate flow through the vadose zone using a kinematic wave approximation, including consideration of evapotranspiration (ET) derived from groundwater upflux based on a linear function of water table depth (Harbaugh 2005, Morway et al. 2013).

RT3D (Clement 1997) simulates the reactive transport of multiple interacting solutes in the saturated zone of an aquifer, through the solution of the advection-dispersion-reaction equations. Bailey et al. (2013a) amended the RT3D code to simulate solute transport in coupled unsaturated-saturated subsurface environments, creating UZF-RT3D, followed by the inclusion of N and Se cycling packages (Bailey et al. 2014) to simulate the reactive transport of these species in an irrigated stream-aquifer system. To simulate the transport of N and Se species in coupled aquifer-stream systems, Shultz et al. (2018a) linked UZF-RT3D, with the N and Se cycling packages, to the stream solute transport model OTIS (Runkel 1998). Within this system, UZF-RT3D receives flow rates from MODFLOW and OTIS receives flow rates from the SFR package of MODFLOW, with volumetric exchange rates between the aquifer and the river network used to simulate the aquifer-stream mass transport of N and Se species. Forcing terms for flow including precipitation, applied irrigation, ET, runoff from fields, seepage from earthen canals, flow in the unsaturated and saturated zone, and exchange between the aquifer and river network. Each external forcing term contains specified solute mass. In this study, we amend the UZF-RT3D version of RT3D linked to OTIS as a tool to include the mobilization and reactive transport of U species (Sections 3.6 and 3.7).

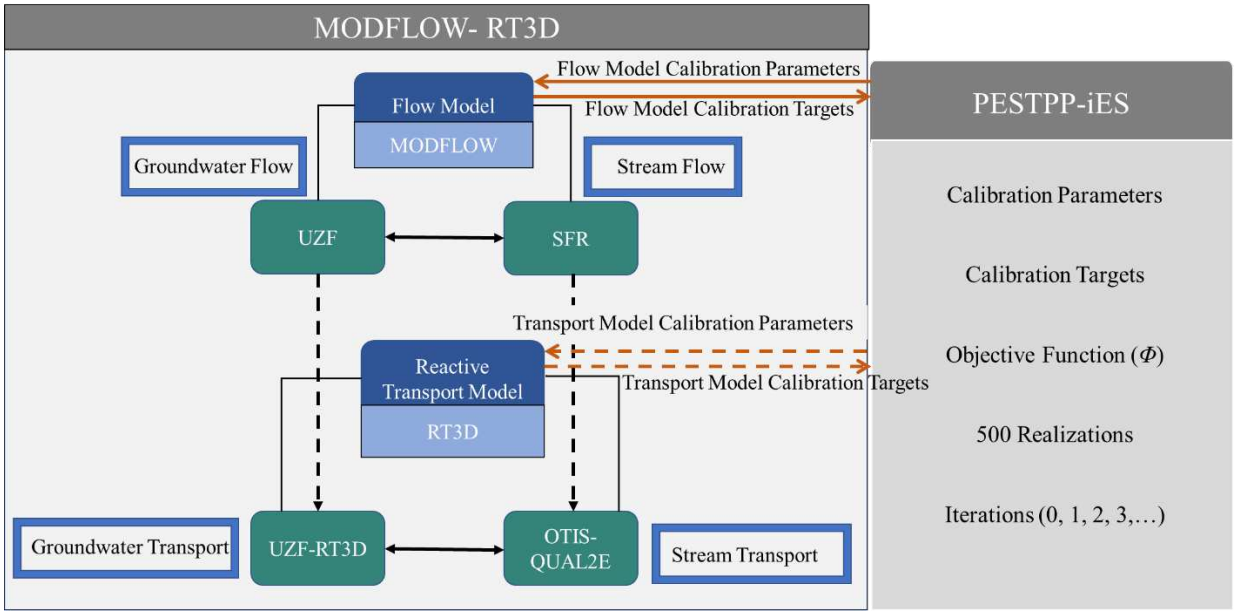

Figure 9. Schematic of coupled flow and reactive transport model (MODFLOW-RT3D) and calibration routine (PESTPP-iES). Calibration starts with the flow model followed by the reactive transport model.

For calibrating parameters in both the MODFLOW and RT3D packages of the coupled mode we use the iterative ensemble smoother iES (Chen and Oliver, 2013) algorithm as implemented in the PESTPP-iES parameter estimation software (White 2018). We first calibrate the groundwater flow parameters using observations of hydrologic state and, using the resulting parameter values, extend the calibration to the chemical reaction parameters for RT3D using solute concentration and mass loading data in a separate step. The PESTPP (White et al. 2020) suite is an object-oriented, model-independent code that builds on the model interface framework from the original PEST parameter estimation software (Doherty 2016) and includes new algorithms including the iES. The iES scales to efficiently estimate values of numerous model parameters by integrating model simulations and observed data while considering uncertainties (Zoccatelli et al. 2024).

The PESTPP-iES process involves starting with a prior estimate for the model parameter values based on knowledge or historical data, as represented by a prior parameter ensemble. The

goal, similar to other regression techniques, is to minimize a sum of squared errors objective function, which quantifies the differences between model outputs and observed data (calibration targets). The iES algorithm uses a Gauss Levenberg Marquardt algorithm, with an empirical Jacobian matrix calculated using ensembles, to systematically update an ensemble of parameter values parameters in a way that works toward a minimum value of the objective function. Due to nonlinearity of the relationship between model parameters and outputs, a linearization and iteration procedure is required to estimate parameters.

3.6. Equations and Numerical Models for Reactive U Transport in an Unconfined Aquifer System

UZF-RT3D (Bailey et al. 2013a) efficiently represents variably-saturated transport in 1D downward flow in the unsaturated zone and 3D flow in the saturated zone, using the finite-difference approach to approximate solutions to the following ADR mass balance equations for multiple reactive chemical species:

$$\frac{\partial(C_k\theta)}{\partial t}R_k = -\frac{\partial(\theta v_i C_k)}{\partial x_i} + \frac{\partial}{\partial x_i}\left[\theta D_{ij}\frac{\partial C_k}{\partial x_i}\right] + q_f C_{f_k} + F_k - \Upsilon_k + \theta r_{f_k}, \qquad k = 1,2,....,m \tag{7}$$

$$\frac{\partial(C_l\varepsilon)}{\partial t} = \alpha_l P_s + \varepsilon r_{s_k} \qquad l = 1,2,...,n \tag{8}$$

wherein:

m and n = total number of dissolved and solid-phase species, respectively

C_k = dissolved phase concentration of k^{th} species (M_f/L_f^3)

C_l = solid-phase concentration of l^{th} species (M_f/L_f^3) where f denotes the fluid phase, and s denotes the solid phase.

D_{ij} = hydrodynamic dispersion coefficient (L^2/T)

υ = pore velocity (L_b/T) with b denoting the bulk phase,

θ = volumetric water content (L_f^3/L_b^3).

ε = volumetric solid content (L_s^3/L_b^3) and is equal to 1 - φ, where φ is the porosity.

q_f = volumetric flux of water representing sources and sinks ($L_f^3/T/ L_b^3$) such as groundwater discharge, pumped groundwater, irrigation water, canal, and seepage

C_{f_k} = concentration of the source or sink (M_f/L_f^3) for k^{th} dissolved phase species

F_k = rate of input of the k^{th} species due to fertilizer application ($M_f L_b^3/T$)

Υ_k = the potential uptake rate of the k^{th} species ($M_f L_b^3/T$)

P_s = mass application rate for the l^{th} solid phase sources (M_s/ L_b^3)

α_l = fraction of P_s attributed to species l (-)

r_{f_k} = rate of all reactions that occur in the dissolved phase ($M_f L_f^3/T$) for the k^{th} species.

r_{s_k} = rate of all reactions that occur in the solid phase ($M_s L_s^3/T$) for the l^{th} species.

R_k = retardation factor for the k^{th} dissolved-phase species, equal to $1+\left(\rho_b + K_{d_k}\right)\Big/\theta$

ρ_b = bulk density of the porous media (M_b/L_b^3)

K_{d_k} = partitioning coefficient for the k^{th} species (L_f^3/M_b).

The finite-difference approximation of Eq. (7) is solved for C_k using UZF-RT3D within every finite-difference grid cell of the modeled domain during each transport time step (Clement 1997, Bailey et al. 2013a). The flow rates between cells and the water content for each cell required to solve the ADR equation are provided by the MODFLOW model. The sources and sinks (q_f) in an irrigated stream-aquifer system, such as infiltration from irrigation, canal seepage, and groundwater pumping, and various reactions (r_{f_k}), such as chemical reduction and oxidation,

mineralization, and immobilization, are described by Shultz et al. (2018a). The transport model of the dissolved phases of C_{Se} is also described by Shultz et al. (2018a).

Applications of Eq. (7) to represent the fate and transport model of the dissolved phases of O_2 and NO_3 , as shown in Fig. 8, are:

$$\frac{\partial(C_{O_2}\theta)}{\partial t} = -\frac{\partial(\theta v_i C_{O_2})}{\partial x_i} + \frac{\partial}{\partial x_i}\left[\theta D_{ij}\frac{\partial C_{O_2}}{\partial x_i}\right] + q_f C_{f_{O_2}} + \theta\left(-r_{f,O_2}^{het} - r_{f,O_2}^{auto}\right) \quad (9)$$

$$\frac{\partial(C_{NO_3}\theta)}{\partial t} = -\frac{\partial(\theta v_i C_{NO_3})}{\partial x_i} + \frac{\partial}{\partial x_i}\left[\theta D_{ij}\frac{\partial C_{NO_3}}{\partial x_i}\right] + q_f C_{f_{NO_3}} + F_{NO_3} - \Upsilon_{NO_3} + \theta\left(r_f^{nit} - r_{f,NO_3}^{het} - r_{f,NO_3}^{auto}\right) \quad (10)$$

wherein:

C_{O_2} = dissolved concentration O_2 (mg/L),

C_{NO_3} = dissolved concentration NO_3 expressed as equivalent NO_3-N (mg/L),

min and *imm* = mineralization and immobilization, respectively

auto and *het* = autotrophic and heterotrophic chemical reduction, respectively

nit = nitrification

In this study, we include the reactive transport of U:

$$\frac{\partial(C_U\theta)}{\partial t}R_U = -\frac{\partial(\theta v_i C_U)}{\partial x_i} + \frac{\partial}{\partial x_i}\left[\theta D_{ij}\frac{\partial C_U}{\partial x_i}\right] + q_f C_{f_U} + \varepsilon\left(r_{s,U}^{min} - r_{s,U}^{imm}\right) + \theta\left(r_{f,U}^{auto} - r_{f,U}^{het}\right) \quad (11)$$

wherein C_U = dissolved concentration of U(VI) (µg/L).

In our model, the reaction rates of all species are governed by first-order kinetics, with Monod terms accounting for the influence of additional reactants and influential species. The specific equations and comprehensive descriptions of the mass balance transport equations for O_2, NO_3, and Se can be found in the works of Bailey et al. (2013a), Bailey et al. (2013b) and Shultz et al. (2018a). The input rates associated with inorganic fertilizer application, F_{NO_3} and F_{Se} , are

incorporated into our model. However, F_U is assumed to be negligible based upon studies by Zielinski et al. 1997 and Rothbaum et al. (2006). Plant uptake rates, Υ_{NO_3} and Υ_{Se}, also are included in the ADR equation due to established effects on plant uptake. The uptake of trace elements by plants varies among species, but most plants tend to accumulate metals in the following order: Sr> Se > Cd > V > As > Cr > U. This suggests a correlation between the release of metals in soils and their absorption by plants, and U appears to be among the least absorbed trace elements (Bzour et al. 2017). Duhan et al. (2023) indicate that plant uptake of U primarily occurs from the dissolved fraction in the soil, indicating that U may be less available to plants. Also, plant uptake of U is typically assumed to be negligible, with transfer factors from soils to crop plants generally below 1% according to (Sheppard and Evenden 1988, Liesch et al. 2015, Schnug and Haneklaus 2015). Hence, the term Υ_U is neglected in the present study. Reactions involving C, N, and Se species in the litter, humus, and manure pools in soil organic matter (Fig. 8), as described in Bailey et al., (2013b), are included in the model. However, they are not included for U, as they do not significantly affect U cycling in the system. The terms, $r_{f_k}^{het}$ and $r_{f_k}^{auto}$ in Eqs. (9) – (11) that represent heterotrophic and autotrophic reduction rates are described in Bailey et al (2013b) for the Se species and in Supplemental Material in Appendix A for O_2, NO_3, and U.

3.7. Equations and Numerical Models for Reactive U Transport in an Alluvial Stream System

The basic mass balance differential equations modeled in the stream and storage zones are of the form (Runkel and Broshears 1991):

$$\frac{\partial C_j}{\partial t} = -\frac{Q}{A}\frac{\partial C_j}{\partial x} + \frac{1}{A}\frac{\partial}{\partial x}\left(AD\frac{\partial C_j}{\partial x}\right) + \frac{q_L}{A}\left(C_{L_j} - C_j\right) + S_j + r_j, \qquad j = 1, 2, ..., n \tag{12}$$

$$S_j = \bar{\rho}\lambda_{S_j}\left(C_j^* - K_{d_j}C_j\right) \tag{13}$$

Sorbate on the streambed is modeled as

$$\frac{\partial C_j^*}{\partial t} = -\frac{S_j}{\bar{\rho}} \tag{14}$$

Solid-phase species on the streambed are modeled by

$$\frac{\partial C_k^{sol}}{\partial t} = r_k^{sol}, \qquad k = 1,....,w \tag{15}$$

wherein

n = number of dissolved-phase species,

w = number of solid-phase species,

A = cross-sectional area of the stream channel (L^2),

C_j = main channel concentration (M/L^3) of the j^{th} dissolved-phase species,

C_{L_j} = lateral inflow solute concentration (M/L^3) of the j^{th} species

C_k^{sol} = main channel concentration (M/M) of the k^{th} solid-phase species,

r_k^{sol} = rate of all reactions occurs in the solid phase for the k^{th} species (ML^3/T),

D = dispersion coefficient (L^2/T),

Q = volumetric streamflow rate (L^3/T),

q_L = lateral inflow rate per unit length [(L^3/T)/ L],

x = distance along the thalweg axis of the stream channel (L),

$\bar{\rho}$ = mass of accessible sediment per volume of stream water (M/L^3),

λ_{S_j} = first-order sorption rate coefficient of the *j*th species (1/T),

C_j^* = solute concentration sorbed to streambed sediment (M/M),

K_{d_j} = streambed sorption partitioning (L^3/M), and

S_j = rate of change in solute mass concentration of the *j*th species on the streambed [(M/ L^3)/T].

In the present study, the OTIS code, modified to include U, functions as the engine for the approximation of the advection-dispersion solute transport. At the same time, QUAL2E simulates in-stream water quality mechanisms for O_2, N species, Se species, U, and algae dynamics. In a prior investigation conducted by Bailey and Ahmadi (2014), adjustments were made to the OTIS modeling code to facilitate the simulation of C_{O_2} and C_{NO_3} with N cycling within an interconnected stream network, incorporating the equations from QUAL2E. The UZF-RT3D model is coupled with the OTIS modeling code to allow for both groundwater and surface water chemical reactive transport, with chemical mass exchange between streams and the aquifer based on the exchange flow rates simulated by the SFR routine within the MODFLOW package. The solution to Eq. (12) is addressed through a Crank-Nicolson finite-difference method, as outlined by Runkel (1998). U is assumed to be conservative in highly oxic streams; thus, no in-stream reaction terms are included. Reactions for Se species are included, as fully described in (Shultz et al. 2018a). The concentration of U(VI) that attaches to the streambed is determined using Eq. (14), and the solid phase in the streambed is simulated using Eq. (15). The rate of change of U(VI) concentration between the streambed and the water column, denoted as S_U [ML^3/T], is modeled as follows:

$$S_U = \overline{\rho_U}\lambda_{Sorb_U}\left(C_U^* - K_{d_U}C_U\right) \tag{16}$$

$$\frac{\partial C_U^*}{\partial t} = -\frac{S_U}{\overline{\rho_U}} \tag{17}$$

Where, $\overline{\rho_U}$ = mass of streambed sediment per volume of stream water (g/m^3), λ_{Sorb_U} = first order sorption rate coefficient (1/sec), and K_{d_U} = streambed sorption partition coefficient (L/kg).

We model Se cycling in the system, including the first-order reaction rates equations for Se species following methods described by Shultz et al. (2018a). The system of ordinary differential equations for simulating the kinetics of interacting U species was solved using the 4th-order Runge-Kutta method. This facilitated the solution of mass-balance equations for both U and Se species.

3.8. Application of Coupled Flow and Reactive U Transport Model to A Representative Irrigated Stream-Aquifer System

3.8.1. Description of the Lower Arkansas River Valley Study Region

The LARV extends along the high plains in southeastern Colorado between the city of Pueblo eastward to the border with Kansas (Fig. 10). A vast earthen canal network, first constructed in the late nineteenth century, diverts flow from the Arkansas River to irrigate crops on alluvial and terrace soils covering a total area of about 109,000 ha (Morway et al. 2013, Shultz et al. 2018a). Thousands of irrigation pumping wells supplement the canal water with alluvial groundwater. Water allocation is governed by Colorado water law. The climate of the study area is semi-arid, with an average annual precipitation ranging between about 0.3 m in the west to 0.4 m near the Stateline, and the average monthly temperature in the LARV varies between about -1°C in winter and 25°C in summer. The region's geology consists of an alluvial aquifer underlain by a series of sedimentary formations of the late Cambrian to the Tertiary Period (Darton 1906, Barkmann et al. 2021). Soil types include clay loam, silty clay loam, loam, and sandy loam textural classes (Gates et al. 2012).

The irrigated stream-aquifer system of the LARV has been studied by Colorado State University (CSU) for over two decades with a focus on an Upstream Study Region (USR) and a Downstream Study Region (DSR) (Fig. 10). The USR is representative of valley conditions upstream of John Martin Reservoir, and the DSR of conditions downstream of John Martin Reservoir. Though it is one of Colorado's most productive agricultural zones, the LARV suffers in many areas from the effects of shallow water tables (Morway et al. 2013) and has substantial irrigation-induced water quality problems. Total dissolved solids (TDS), nutrients (especially NO_3 and phosphorus), and the trace elements Se and U, have been measured in high concentrations dissolved in groundwater and surface water at locations throughout the stream–aquifer system (Gates et al. 2009, Morway and Gates 2012, Bailey et al. 2012, Gates et al. 2016, Gates et al. 2018, Shultz et al. 2018a). Return flows from intensive and long-term irrigation have contributed to these high concentrations, which not only threaten crop productivity but often violate the Colorado Department of Public Health and Environment (CDPHE) chronic standards for aquatic, livestock, and human health. Field data indicate that U concentrations are markedly greater in the DSR than in the USR and broadly exceed CDPHE chronic standards (85^{th} percentile = 30 µg/L) in the aquifer and the streams (Gates et al. 2009, 2016). In the USR, insight into the nature and variability of Se, NO_3, phosphorus (P), and salinity (TDS) in relation to irrigation, geologic, and other factors has been enhanced by application of extensively calibrated coupled flow and solute transport models, forming a basis for remediation (Bailey et al. 2014, Shultz et al. 2018a, Tavakoli et al. 2019, Wei and Bailey 2021, Bailey and Hosseini 2023). The calibrated model presented herein constitutes a similar application to the characterization of irrigation-induced pollution in the DSR, with a primary focus on U.

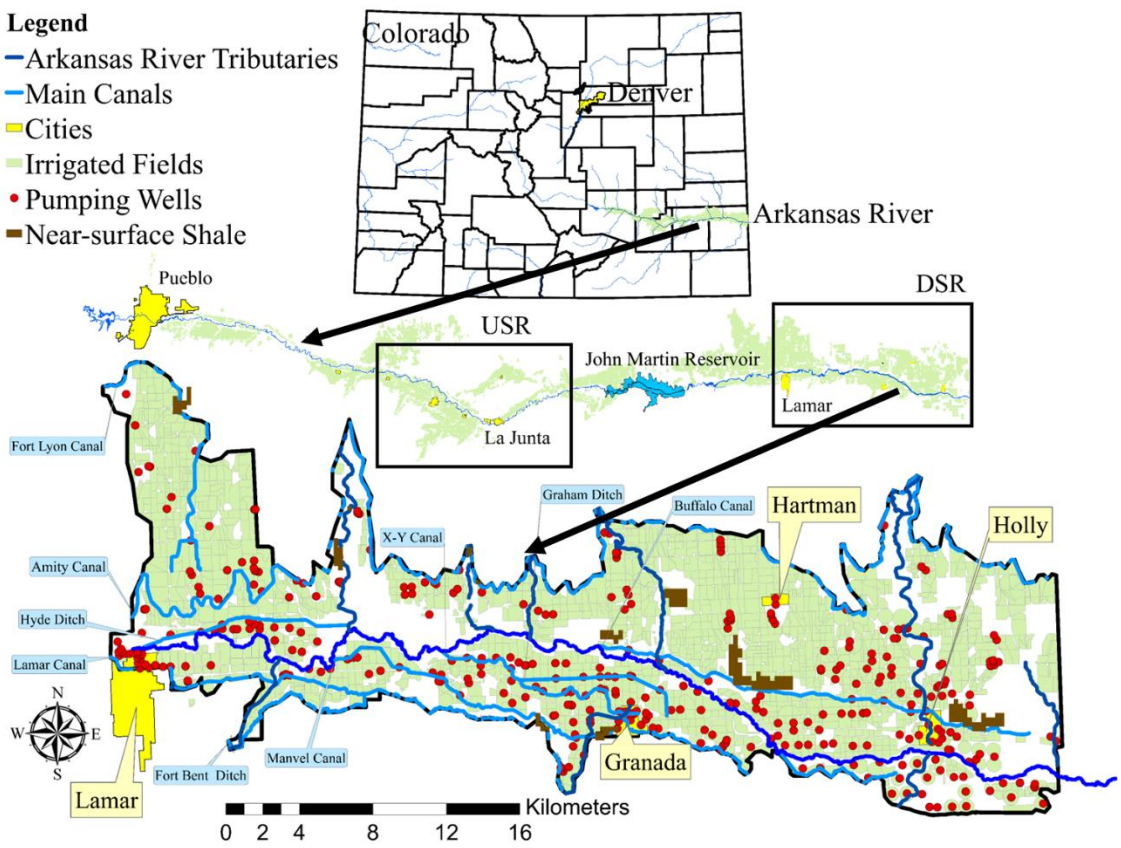

Figure 10. The LARV in Colorado, showing the USR and DSR, with details of the DSR.

The total area of the DSR is about 552 km^2 of which about 60% is irrigated with river water diverted into eight main canals in the region and from 392 groundwater pumping wells (Fig. 10). Major crops are alfalfa, corn, grass, wheat, and sorghum grown on soils consisting of various clay loam, loam, silty clay loam, silty loam, and sandy loam textural classes. The irrigation season begins in mid-to-late March and ends in mid-November. Surface irrigation is widely used in the DSR, while pressurized irrigation practices (mainly center-pivot sprinklers) have notably increased in the irrigated area since 2007.

The Arkansas River in the DSR stretches 71 km from the May Valley Drain near Lamar to the Colorado–Kansas state line, with four main tributaries: Clay Creek, Big Sandy Creek, Buffalo Creek, and Wild Horse Creek. These streams gain water from groundwater and surface return

flows, mainly from excess cropland irrigation. Four different streamflow gauges in the DSR are located at Lamar (ARKLAMCO), Granada (ARKGRACO), Big Sandy Creek (BIGLAMCO), and Wild Horse Creek (WILDHOCO). There is also a gauge at Coolidge, KS (ARKCOOKS) just downstream of the eastern boundary (Fig. 11). The bedrock geology beneath the DSR is predominantly Upper Cretaceous marine shale and limestone with minor sandstone. Beneath the Arkansas River the bedrock consists of the Fairport Chalky Shale, Blue Hill Shale, and Codell Sandstone members which are included in the Carlile Shale (Barkmann et al. 2021).

3.8.2. Field Data for Model Calibration and Support in the Study Region

Over the period 2003 - 2016, flow and water quality conditions in the irrigated stream-aquifer system of the DSR have been broadly monitored and studied. Data on flows and stages measured in tributary streams and the river, along with flows diverted into canals and quantities pumped by irrigation wells, have been compiled from the United States Geological Survey (USGS) and Colorado Division of Water Resources (CDWR) (Morway et al. 2013, Gates et al. 2016). Water balance studies have been conducted for numerous irrigation events on 18 surface irrigated fields and 20 sprinkler irrigated fields, allowing estimates of irrigation efficiency, deep percolation fraction, and surface runoff fraction (Gates et al. 2012). Weather variables, crop characteristics, and natural vegetation characteristics were assembled for computing ET. Weather data, including precipitation, were gathered at the Colorado Agricultural Meteorological (CoAgMet) stations in the region (Fig. 11) and from Next Generation Weather Rader (NEXRAD). Data on soil properties, geologic formations, unconfined alluvial aquifer properties, stream geometry, and canal seepage have been measured and/or compiled (Gates et al. 2012, Morway et al. 2013, Gates et al. 2016, Barkmann et. al 2021). Depth to the groundwater table along with water quality parameters have been measured multiple times annually from a network of 118 groundwater monitoring wells

shown in Fig. 11 (Gates et al. 2009, 2012, Morway et al. 2013, Gates et al. 2016).

Routine measurements of electrical conductivity (EC), temperature, pH, oxidation reduction potential, and C_{O_2} were made multiple times annually in groundwater monitoring wells and at surface water monitoring locations (Fig. 11). Periodic water quality samples also were gathered from monitoring wells and surface water sites and were analyzed in the laboratory for anions and cations. The major anions tested included chloride (Cl^-), sulfate (SO_4^{-2}), NO_3, CO_3^{-2}, HCO_3^-, and Mn^{+2}. Major cations examined included sodium (Na^+), potassium (K^+), Ca^{+2}, Magnesium (Mg^{+2}), and NH_4^+. Samples also were taken for the major trace elements Se, Fe, and U. Equipment, field methods, and laboratory procedures are described in Gates et al. (2009), Morway and Gates. (2012), Bailey et al. (2014), Gates et al. (2016), and Shultz et al. (2018a).

The total number of data samples collected and analyzed for NO_3, Se, U, and TDS (total of analyzed anion and cation concentrations) in the groundwater over the years of the study period 2003 – 2016, are 1066, 1870, 543, and 1126 samples, respectively. In the streams the corresponding total number of data samples collected and analyzed are 522, 759, 306, and 544, respectively. Samples for analysis of NO_3, Se, and TDS were collected regularly from the aquifer and streams from 2003 to 2011, then sporadically from 2015 to 2016. Samples for U were collected from groundwater regularly over 2005 to 2011, and from streams over 2006 to 2012. Only a few samples were collected in 2015 and 2016. Table S1 in Supplemental Material in Appendix A shows the number of samples gathered for each species for each year.

Summary statistics of C_U and co-reactant concentrations C_{NO_3} and C_{Se}, as well as TDS concentration (C_{TDS}), in groundwater are summarized in Table S2 and in streams are summarized

in Table S3 in Supplemental Material in Appendix A. In the present study, C_{Se} is the concentration of total dissolved Se species (SeO_3 + SeO_4). The average pH measured in the aquifer over the entire period 2003 – 2016 is 6.9, and in the Arkansas River is 7.9.

Values of C_U in groundwater ranged from 1.0 to 907 µg/L, with an overall average of 111.7 µg/L and an overall 85th percentile of 177 µg/L. Values of C_U along the Arkansas River were obtained from 249 samples, ranging from 6.7 to 252 µg/L, with an overall average of 61.4 µg/L and 85th percentile of 82 µg/L.

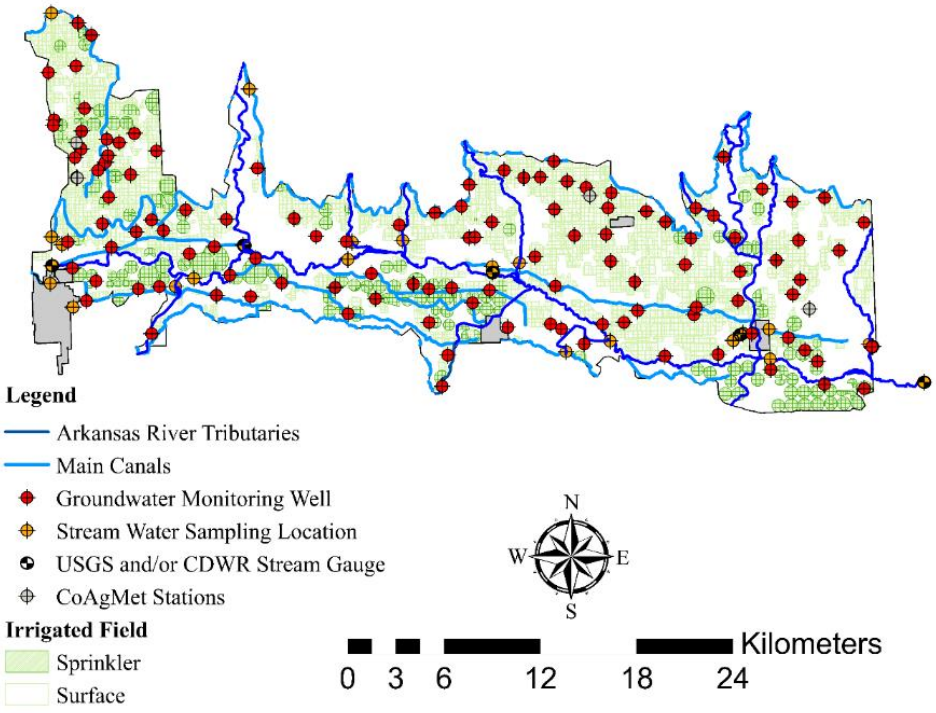

Figure 11. The DSR map showing all groundwater monitoring wells, stream water sampling locations, stream gauges, and CoAgMet stations.

3.8.3. Numerical Groundwater and Stream Flow Model Extension and Calibration

Morway et al. (2013) originally applied the UZF package to the DSR (Figure 11) for the period 2002 – 2007 employing the river (RIV) package to represent the stream network as a head-dependent flux boundary on the aquifer system (Harbaugh 2005). In the present study, the RIV

package was replaced with the SFR package for simulating time-varying flow in the stream network and the rate of groundwater flow exchange with the streams. In contrast to the RIV package, which simulates head-dependent flux boundaries to represent stream–aquifer interaction, SFR is applied to route flow along the Arkansas River and it is tributaries using an eight-point cross-sectional geometry for each stream segment. Darcy's Law is employed to quantify flow exchange rates between each SFR stream cell and adjacent groundwater aquifer cells. While the RIV package sets boundary conditions with specified head and conductance, SFR dynamically calculates water stage considering flow rates and channel characteristics, thus offering a comprehensive approach to simulating groundwater-surface water interactions.

The spatial domain of the unconfined aquifer in the DSR is discretized into 9311 active cells in MODFLOW (Fig.S1 in Supplemental Material in Appendix A). The uniform areal dimensions of each grid cell are 250 m x 250 m horizontally, with each cell having about the average area of irrigated fields in the study region. Two vertical layers are used for the alluvial aquifer (Morway et al. 2013). Layer one has an approximate thickness of 5 m, representing the maximum extent of deeply rooted crops (i.e., alfalfa). Layer two extends from the bottom of layer one to the impervious bedrock, typically shale or limestone.

Irrigation practices markedly changed in the DSR after 2007. In many fields, lower-efficiency surface irrigation systems were replaced with higher-efficiency sprinklers, resulting in the area under sprinkler irrigation rising from about 5% in 2007 to about 16% in 2016 (Fig S2 in Supplemental Material in Appendix A). This transition in irrigation methods required changes in field boundaries and in the simulation of irrigation water application over the study region over the extended period of 2002 – 2016. In the present study, this involved altering the mapping of field boundaries associated with transitions in irrigation methods to the underlying finite-

difference computational grid on a year-by-year basis. Data on weekly precipitation, climatic variables, well pumping, canal deliveries, and canal seepage were gathered or estimated. Crop ET and natural vegetation were calculated with the ASCE Penman-Monteith method (ASCE-EWRI 2005), and an irrigation scheduling and water balance algorithm was used to distribute effective precipitation and irrigation water supplies over the fields in the region and to calculate infiltration, tailwater runoff, and deep percolation. The methodology used, including the transfer of field properties to the computational grid, was essentially the same as that described by Morway et al. (2013) for the period 2002 – 2007. The extension of the model period to 2002 – 2016 was carefully checked to successfully simulate the distribution of weekly irrigation water deliveries (canals and wells) to about 3,000 irrigated parcels within the DSR, resulting in a total of about 2,000,000 individual field irrigation events.

Morway et al. (2013) applied the original PEST parameter estimation software to calibrate the MODFLOW model to the DSR for 2002 – 2007 (Doherty, 2002). The calibrated parameters hydraulic conductivity (K) [m/day] and specific yield (S_y) [m/m] were estimated using Kriging with pilot points situated at 163 model locations over the two layers in the DSR. The calibration targets were measured values of depth to water table (D_{wt}) converted to groundwater hydraulic head (h) [m] within monitoring wells spread over the region, and weekly unaccounted-for return flow per unit length along the Arkansas River [(m^3/week)/km] estimated from a river mass balance. In the current study, the DSR MODFLOW model was calibrated for the period extending from 2002 to 2016 using PESTPP-iES.

The objective function minimized in PESTPP-iES for parameter calibration of the MODFLOW model over the extended period in the DSR was:

$$\Phi_f = \sum_i^{N_f} \sum_j^{M_{f_i}} w_{f_{ij}} \left[S_{f_{ij}} - O_{f_{ij}} \right]^2 \quad (18)$$

where Φ_f is the objective function for the flow (*f*) model, N_f = the number of classes of flow calibration targets, M_{f_i} = the number of variables in the i^{th} class of flow calibration targets, $w_{f_{ij}}$ is the weight used to account for the uncertainty and/or expected importance of the j^{th} variable associated with the i^{th} class of flow calibration targets, $S_{f_{ij}}$ and $O_{f_{ij}}$ are the simulated and observed values, respectively, for the j^{th} flow variable in the i^{th} class of calibration targets. The difference $S_{f_{ij}} - O_{f_{ij}}$ is termed the residual associated with the j^{th} flow variable associated with the i^{th} class of flow calibration targets. Three (N_f = 3) classes of calibration targets were used to assess the MODFLOW simulations: (1) measured values of *h* [m] within each of 120 groundwater monitoring wells (Fig. 11), composing a total of M_{f_1}=11,027 values over the modeled period, (2) weekly average flow rate [m^3/s] measured over 761 weeks at three stream gauges within the Arkansas River and at two tributary stream gauges in tributaries (Fig. 11), composing a total of M_{f_2} = 3,805 values and (3) weekly unaccounted-for return flow per unit length along the Arkansas River [(m^3/week)/km] estimated from a river mass balance for 826 days within the period 5 October 2006 to 30 September 2010 (Gates et al. 2018), composing a total of M_{f_3} = 118 values. Together, this amounts to a total of 14,950 calibration targets, each associated with a weighted residual term in Eq. (18).

The weights for each calibration target residual in Eq. (18) were determined by taking the inverse of the variance of the observed values of variables associated with that class, as outlined by Hunt et al. (2006) and Tiedeman and Hill (2007). This strategy strives to result in a dimensionless residual for each variable, allowing for the evaluation of calibration targets with

different units, such as [L] for h, [L^3/T] for stream flow, and [(L^3/T)/L] for return flow within a unified objective function. Adjustment of weights to emphasize certain targets with more importance is a common procedure (Cooley and Naff, 1990, Doherty and Welter, 2012). Values of weights were assigned following the procedure detailed by Morway et al. (2013).

The calibrated parameters that yield a minimization of Φ_f in Eq. (18) included pilot points for K [m/day] and S_y [m/m] values over the region, using the same method described by Morway et al. (2013) and Doherty (2003). Values of streambed hydraulic conductivity c_{sb} [m^2/day] also were calibrated at a total of 522 computational cells representing the streams within the DSR.

The calibration process reaches convergence when the iteratively adjusted ensemble of calibrated parameter values fulfills the objective function criterion, typically occurring between iterations 3 and 5. The number of realizations selected for the MODFLOW calibration in the DSR was 500. PESTPP-iES generates several outputs, including the final calibrated parameter values that cause best alignment between model simulations and observed data, the distribution of values of variables associated with calibration targets and residuals, distribution of the objective function, and the posterior calibrated parameter distribution (White 2018, White et al. 2020). Upon completion of the optimization process, a file is produced that allows identification of $S_{f_{ij}}$ values in Eq. (18) for successful realizations. Once these realizations are pinpointed, a single model run can be executed using the calibrated parameters from the chosen realization to conduct a comprehensive comparison and assessment of the history-matching results. The calibrated parameter values associated with the minimum-error-variance parameter realization, commonly called the *base* realization (e.g. Moore and Doherty, 2005), after iteration 5 were selected for use in MODFLOW in coupling with the RT3D model package for the subsequent solute transport model calibration (Section 3.8.4) since it yielded the minimum Φ_f value.

3.8.4. Numerical Reactive Transport Model Calibration

The UZF-RT3D model with the amendment for U reactive transport was applied to approximate the ADR and related equations described in Sections 3.6 and 3.7 in simulating solute transport throughout the stream-aquifer system of the DSR employing the flows simulated by MODFLOW (see Fig. 9). The finite-difference grid applied to the region is composed of six vertical layers. The top four layers correspond to the first layer of the MODFLOW model, while the bottom two layers represent the second layer of MODFLOW, including the bedrock. The top two layers, each 0.5m thick, correspond to the root zone of cropped fields and naturally-vegetated areas. Along with layer three at 1-m thickness, these top three layers collectively represent the typical zone of unsaturated flow in the DSR. Layers 4 to 6 represent the saturated zone. Specifically, layer 4 denotes the approximate depth from which groundwater samples typically were extracted from monitoring wells in the region, serving as a basis for comparison of simulated solute concentrations with observed concentrations for use in model calibration, as detailed by Bailey et al. (2014). For application to the DSR, the UZF component was run on a daily time step, and OTIS-QUAL2E was run on an hourly time step to solve the stream reactive transport. Following a procedure like that described by Ajami et al. (2014), Bailey et al. (2014), and Shultz et al. (2018a), a 40-year spin-up simulation was used to generate the initial conditions for groundwater and surface water concentrations for the modeled period 2003 – 2016.

Additional components incorporated into the model involved calculation of C_{NO_3}, C_{Se}, and C_U in water diverted into canals having headgates located within the DSR and within canals entering the model domain across the eastern boundary and whose headgate diversions are situated upstream. These estimates are crucial for determining concentrations in irrigation water and canal seepage. Flows diverted into canals with headgates at locations along the Arkansas River within

the DSR were assigned the values of river concentrations computed by OTIS-QUAL2E for the corresponding river cell and time step. Concentrations in canals and in the Arkansas River crossing the western boundary into the DSR were estimated using regression relationships developed from stream samples in conjunction with EC and flow rate data available in the river near the western boundary or at locations further upstream corresponding to canal headgate diversions following procedures similar to those outlined in Gates et al. (2018).

To facilitate model calibration, the DSR domain is partitioned into 15 non-riparian groundwater aquifer subregions, riparian groundwater aquifer subregions, along with six Arkansas River segments and four tributary segments (Fig. 11). Aquifer subregions within the riparian corridor flanking the river and tributaries also were identified where it is expected that chemical reactions in the shallow aquifer will be affected by enhanced carbon cycling and heterotrophic microbial respiration associated with dense vegetation. The mapping of riparian areas was conducted by examining high-resolution satellite imagery obtained through the Google Earth tool to identify boundaries and spatial variations in the riparian landscape. The aquifer subregions and stream segments are composed of numerous MODFLOW-RT3D computational cells. The criteria for defining the subregions and segments include variations in geological formations, irrigation canal command area, sub-watersheds, crops and natural vegetation, definition of OTIS stream segments, and locations of monitoring wells and stream sampling.

Calibration of the RT3D package for the DSR used the same history matching approach with PESTPP-iES, as was used for the MODFLOW package, but in this case attention was given to capturing meaningful patterns and spatio-temporal statistics of measured solute data over a historic period rather than on the exact replication of data time series at specific measurement points in the region (Konikow 2011). The following objective function for the RT3D package

was minimized:

$$\Phi_{st} = \sum_{i}^{N_{st}} \sum_{j}^{M_{st_i}} w_{st_{ij}} \left[\frac{\left(S_{st_{ij}} - O_{st_{ij}} \right)}{O_{st_{ij}}} \right]^2 \tag{19}$$

where Φ_{st} is the objective function for the solute transport (*st*) model, N_{st} = number of classes of solute transport calibration targets, M_{st_i} = the number of variables in the i^{th} class of solute transport calibration targets, $w_{st_{ij}}$ = the weight attributed to the j^{th} variable associated with the i^{th} class of solute transport calibration targets, $S_{st_{ij}}$ and $O_{st_{ij}}$ are the simulated and observed values, respectively, of the j^{th} solute transport variable in the i^{th} class of calibration targets.

Three classes (N_{st} = 3) of calibration targets were used to assess the RT3D simulations: (1) average measured values of C_{NO_3}, C_{Se}, and C_U over the simulation period within each non-riparian groundwater subregion (Fig. 12), composing a total of M_{st_1} = 45 values over the modeled period; (2) weekly average values of mass loading of NO_3, Se, and U to the Arkansas River [(kg/week)/km] estimated by Gates et al (2018) using a stochastic river mass balance model to account for groundwater and unaccounted surface loading for a total of 48 weeks within the period October 1, 2006, to September 30, 2010, composing a total of M_{st_2} = 144 values; and (3) the 85th percentile measured values C_{NO_3}, C_{Se}, and C_U over the simulation period within each of the six Arkansas River segments and the four tributary segments, composing a total of M_{st_3} = 30 values over the modeled period. In total, there are 219 calibration targets across the three classes, each linked to a weighted residual term in Eq. (19).

Values of the weights, $w_{st_{ij}}$, for the three classes of calibration targets were assigned to incorporate the following considerations: (i) relative importance of the class of calibration target

(Cooley and Naff, 1990), with classes of higher importance assigned proportionally higher weights, $w_{st_{imp_{i,j}}}$, and (ii) an assumed level of uncertainty associated with the available observed data for the variables within each class of calibration target, $w_{st_{unc_{i,j}}}$. The level of uncertainty was assessed using three main criteria: (a) number of available observations, with fewer available samples implying greater relative uncertainty, (b) coefficient of variation (CV) in the observed values, with higher CV indicating higher relative uncertainty, and (c) measurement error, with higher measurement error indicating higher relative uncertainty. Details are provided in Supplemental Material in Appendix A.

Model parameters that were selected for calibration to achieve the minimization of Φ_{st} in Eq. (19) included 13 parameters associated with reactive transport in the non-riparian groundwater aquifer, with values set for all cells within each of the 15 non-riparian groundwater subregions; six parameters associated with reactive transport in the riparian groundwater aquifer, with values set for all cells within 20 riparian subregions north and south of the Arkansas River and 8 riparian subregions east and west of the tributaries; and 16 parameters associated with reactive transport in the streams, with values of six of them set for all cells within each of the Arkansas River and tributary segments, values of nine of them set across all stream segments, and one value at the downstream boundary cell of the Arkansas River. These parameters were selected after exploring the sensitivity of model calibration target variables by making manual adjustments to the parameter values based upon multiple model runs and guided by the findings of Bailey et al (2013b) and Shultz et al (2018a). They are listed in Table 3. Accounting for the spatial distribution of the 34 parameters across the DSR, there were a total of 543 areas where distinct parameter values were adjusted in the calibration process. Upper and lower bounds on parameter values are specified to define range limits (Table 3) in PESTPP-iES for automated calibration, and initially were guided

by ranges reported in the literature. However, since parameter values reported in the literature typically are derived from small scales, such as laboratory settings, which may not apply to the regional scale, range limits were adjusted.

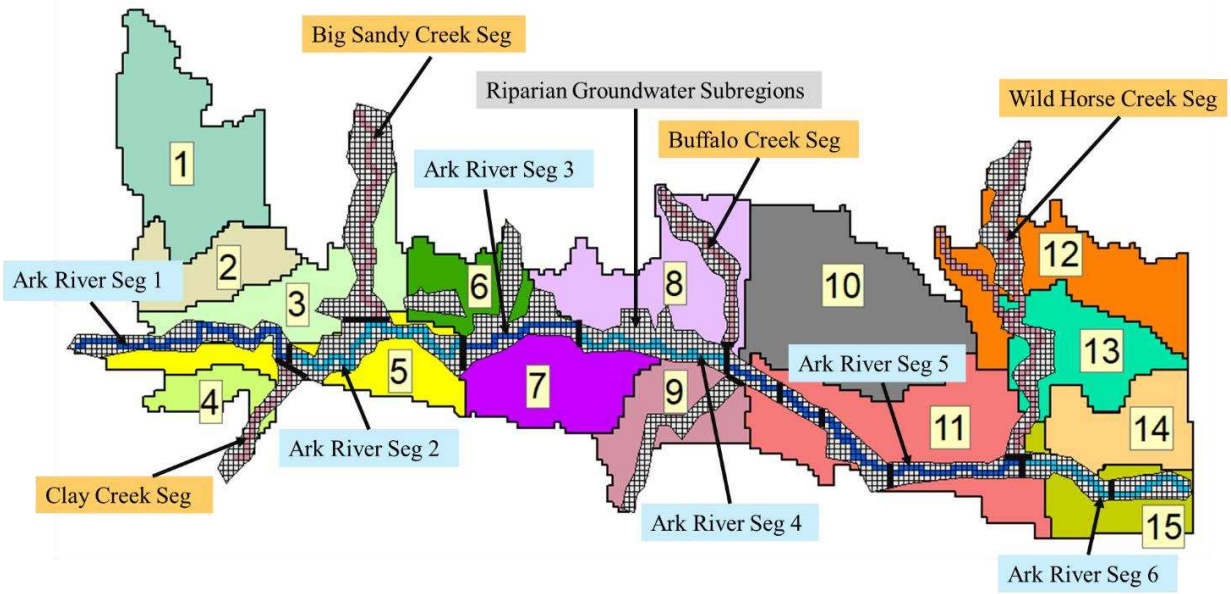

Figure 12. Model domain showing 15 non-riparian aquifer subregions, riparian groundwater aquifer, six Arkansas River segments, and four tributary segments

Table 3. RT3D parameters calibrated using PESTPP-iES.

		Values Calibrated by PESTPP-iES		
	Range limit in PESTPP-iES	Min	Average	Max
Non-riparian groundwater aquifer parameters				
Rate constant for the reaction in which O_2 is reduced, and U is oxidized, $\lambda_{UO_2}^{auto}$ (1/day)	3.00E-07 - 6.50E+00	3.06E-07	1.41E-04	1.40E-03
Rate constant for the reaction in which NO_3 is reduced and U is oxidized, $\lambda_{NO_3-U}^{auto}$ (1/day)	3.00E-07 - 6.50E+00	4.91E-07	6.23E-05	2.36E-04
Rate of heterotrophic reduction of U, $\lambda_{U_{(VI)}}^{het}$ (1/day)	3.00E-07 - 6.50E+00	4.97E-06	1.12E-01	9.95E-01
Rate of autotrophic reduction of O_2 in the presence of shale, $\lambda_{O_2}^{auto}$ (1/day)	3.00E-07 - 6.50E+00	3.00E-07	1.45E+00	6.50E+00
Rate of autotrophic reduction of NO_3 in the presence of shale, $\lambda_{NO_3}^{het}$ (1/day)	3.00E-07 - 6.50E+00	3.19E-07	1.17E+00	6.50E+00

Rate of heterotrophic chemical reduction of NO_3, $\lambda_{NO_3}^{auto}$ (1/day)	3.00E-07 - 6.50E+00	6.35E-07	1.06E+00	5.65E+00
Rate of heterotrophic chemical reduction of SeO_4, $\lambda_{SeO_4}^{het}$ (1/day)	3.00E-07 - 6.50E+00	4.74E-07	2.79E-01	2.85E+00
Rate of heterotrophic chemical reduction of SeO_3, $\lambda_{SeO_3}^{het}$ (1/day)	3.00E-07 - 6.50E+00	1.51E-06	9.05E-01	6.50E+00
U_6 groundwater sorption partitioning, $Kd_{U_{(VI)}}$ (L/kg)	5.00E+01 - 5.00E+03		1.88E+02	
Rate of nitrification, λ_{nit} (1/day)	1.00E-01 - 2.00E+00	1.20E-01	8.50E-01	1.90E+00
Monod half-saturation constant for NO_3, K_{NO_3} (g/m^3)	5.00E+00 - 1.50E+01	5.00E+00	7.64E+00	1.45E+01
Rate of heterotrophic chemical reduction of SeO_3 to mobile SeMet, $\lambda_{SeO_3}^{het(SeMet)}$ (1/day)	2.00E-03 - 2.00E+00	2.93E-03	2.13E-01	1.79E+00
The Monod half-saturation constant for Se, K_{Se} (g/m^3)	5.00E+02 - 2.00E+03	5.03E+02	1.01E+03	1.89E+03
Riparian groundwater aquifer parameters				
Rate of heterotrophic chemical reduction of U, $\lambda_{U_{(VI)}}^{het}$ (1/day)	3.00E-09 - 6.50E+00	1.02E-08	2.22E+00	6.50E+00
Rate of heterotrophic chemical reduction of NO_3, $\lambda_{NO_3}^{het}$ (1/day)	3.00E-09 - 6.50E+00	3.00E-09	4.57E-01	6.00E+00
Rate of heterotrophic chemical reduction of SeO_3, $\lambda_{SeO_3}^{het}$ (1/day)	3.00E-09 - 6.50E+00	3.00E-09	9.25E-02	2.28E+00

Rate of heterotrophic chemical reduction of SeO_4, $\lambda_{SeO_4}^{het}$ (1/day)	3.00E-09 - 6.50E+00	3.00E-09	2.64E-01	3.55E+00
Rate of nitrification, λ_{nit} (1/day)	1.00E-01 - 2.00E+00	1.00E-01	9.04E-01	2.00E+00
The Monod half-saturation constant for NO_3, K_{NO_3} (g/m^3)	5.00E+00 - 1. 50E+01	5.00E+00	1.03E+01	1.50E+01
Stream parameters				
Mass of accessible sediment per unit volume of water for U sorption for streams and tributaries for each segment, $\overline{\rho_{U_{(VI)}}}$ (g/m^3)	4.00E+03 - 2.00E+04	4.00E+03	4.39E+03	5.79E+03
Mass of accessible sediment per unit volume of water for SeO_4 sorption for streams and tributaries for each segment, $\overline{\rho_{SeO_4}}$ (g/m^3)	4.00E+03 - 2.00E+04	4.00E+03	5.86E+03	9.49E+03
Mass of accessible sediment per unit volume of water for SeO_3 sorption for streams and tributaries for each segment, $\overline{\rho_{SeO_3}}$ (g/m^3)	4.00E+03 - 2.00E+04	4.37E+03	1.16E+04	1.16E+04
$U_{(VI)}$ partitioning coefficient in sediments in the streams and tributaries for each segment, $Kd_{U_{(VI)}}$ (L/kg)	2.00E-03 - 3.00E-02	2.02E-03	4.66E-03	9.57E-03
SeO_4 partitioning coefficient in sediments in the streams and tributaries for each segment, Kd_{SeO_4} (L/kg)	2.00E-07 - 3.00E-02	4.91E-07	3.98E-03	2.38E-03

SeO_3 partitioning coefficient in sediments in the streams and tributaries for each segment, Kd_{SeO_3} (L/kg)	2.00E-07 - 3.00E-02	5.32E-07	6.29E-03	2.06E-02
Rate constant for SeO_4 sorption to sediment, $\lambda_{Sorb_{SeO_4}}$ (1/sec)	5.00E-07 - 5.00E-04		6.01E-07	
Rate constant for SeO3 sorption to sediment, $\lambda_{Sorb_{SeO_3}}$ (1/sec)	5.00E-07 - 5.00E-04		5.8E-07	
Rate constant for U_6 sorption to sediment, $\lambda_{Sorb_{U(VI)}}$ (1/sec)	5.00E-06 - 5.00E-04		1.7E-04	
Rate constant for the chemical reduction of SeO_4 to SeO_3, λ_{SeO_4} (1/day)	1.00E-02 - 3.00E+00		1.6E-01	
Rate coefficient for the assimilation of selenate to SeMet, $\lambda_{SeO_4}^{assim}$ (1/day)	1.00E-02 - 3.00E+00		8.0E-04	
Rate constant for the volatilization of SeO_4, $\lambda_{SeO_4}^{vol}$ (1/day)	1.00E-02 - 3.00E+00		8.3E-04	
Michaelis-Menton half-saturation constant for nitrogen, K_N (mg N / L)	4.00E-03 - 1.00E-01		9.12E-02	
Dispersive flux at the downstream boundary for the last segment of the river and the last within that segment, DSBOUND	1.17E-03 - 5.00E+00		1.17E-03	

A total of 500 realizations were set for the prior parameter ensemble to be explored in each iteration of PESTPP-iES. It is uncommon, however, to complete a full set of PESTPP-iES runs with all 500 realizations without encountering failures. Various factors can lead to realization failures, including an inability to meet the convergence criteria or prolonged convergence issues during the solution process in the iES model, leading to their abandonment, as reported in Prieto-Estrada et al. (2023), Delottier et al. (2023), and Kent et al. (2024). In the PESTPP-iES calibration of the RT3D package in the DSR the number of successful realizations per iteration ranged from 270 to 500. The values of the calibrated parameters obtained by PESTPP-iES for the minimum Φ_{st} realization were amended slightly by manual adjustment to a few parameters to enhance compliance with calibration targets. This refinement process is essential to address discrepancies between algorithmically derived parameter values and empirically determined values, ensuring a more accurate and reliable representation of the model dynamics. This final set of values was then used in MODFLOW-RT3D to simulate the solute transport variables across the DSR.

3.8.5. Calibration Uncertainty and Results

Here we summarize representative results for the PESTPP-iES calibration of the solute transport parameters in the coupled MODFLOW-RT3D model (Section 3.8.4) to minimize the function Φ_{st}. A brief discussion of results of the calibration of the MODFLOW flow model to minimize Φ_f for the extended period is provided in Supplemental Material in Appendix A, along with values of the calibrated parameters summarized in Table S4 in the Supplemental Material in Appendix A**.**

Employing the iterative iES method described in Sections 3.8.3 and 3.8.4, PESTPP-iES provides insight into uncertainty in the coupled MODFLOW-RT3D model simulation of flow and solute

transport variables in the DSR in relation to the uncertainty in estimation of the values of the calibrated parameters. In each PESTPP-iES iteration, model runs using multiple realizations (ensemble) of calibrated parameter values provide corresponding realizations of the simulated values of flow and solute transport variables, including the calibration targets and the objective function. In the current study, an iteration was considered successful if 270 out of the 500 realizations resulted in a feasible MODFLOW-RT3D simulation. A realization within iteration 6 of the PESTPP-iES calibration run resulted in a minimum value Φ_{st} = 13.9 which was slightly smaller than that for the base realization. Calibrated parameter values for this minimum Φ_{st} realization are quite close to the values obtained for the base realization, as illustrated in plots of several randomly-selected calibrated parameters in Supplemental Material in Appendix A (see Fig. S4), but resulted in a closer history match to calibration targets across the region and over the simulated period. Values of about 20 parameters were further adjusted manually to enhance matches to calibration targets resulting in a reduction of the Φ_{st} value by less than 5%. Figs. 13 – 15 illustrate the uncertainty in the parameter estimation procedure through display of the prior and posterior (iteration 6) frequency histograms of the ensemble of feasible values of a few selected representative variables that served as calibration targets. Findings for model calibration using PESTPP-iES were reported in a similar way by Abbas et al. (2024) who presented prior and posterior frequency distributions for the SWAT groundwater flow model, by Zoccatelli et al. (2024) for precipitation and rainfall-runoff models, by Askar et al. (2023) for modeling of steady flow and transient solute transport conditions using FEFLOW, and by Martin and White (2023) for modeling discharge in several Texas rivers.

Fig. 13 displays prior and posterior distributions of simulated values of the calibration target variables of average C_{NO_3}, C_{Se}, and C_U in groundwater over the modeled period in subregions

1, 9, and 15 over the ensemble of realizations of the calibrated parameter values. Shown in each plot is the value of the calibration target variable for the realization associated with the minimum Φ_{st} value. Also shown is the observed value from field data. Similar plots are presented in Fig. 14 for the calibration targets of total groundwater mass loading of NO_3, Se, and U to the Arkansas River for the representative months May 2008, December 2008, and April 2009. The frequency histograms over the simulated ensemble of realizations of the calibration targets of average C_{NO_3}, C_{Se}, and C_U over the modeled period in segments 2, 4, and 6 of the Arkansas River are shown in Fig. 15. The spread in the distribution of simulated values indicates the degree of uncertainty. The plots reveal how the spread narrows from the prior to the posterior, indicating how PESTPP-iES closes in with increasing confidence on an ensemble of estimated parameter values that yield acceptable matches to observed data across multiple targets. A few additional plots, illustrating the progression of uncertainty reduction across the six iterations within the PESTPP-iES framework, are presented in Fig. S5 in Supplemental Material in Appendix A for four representative calibration targets.

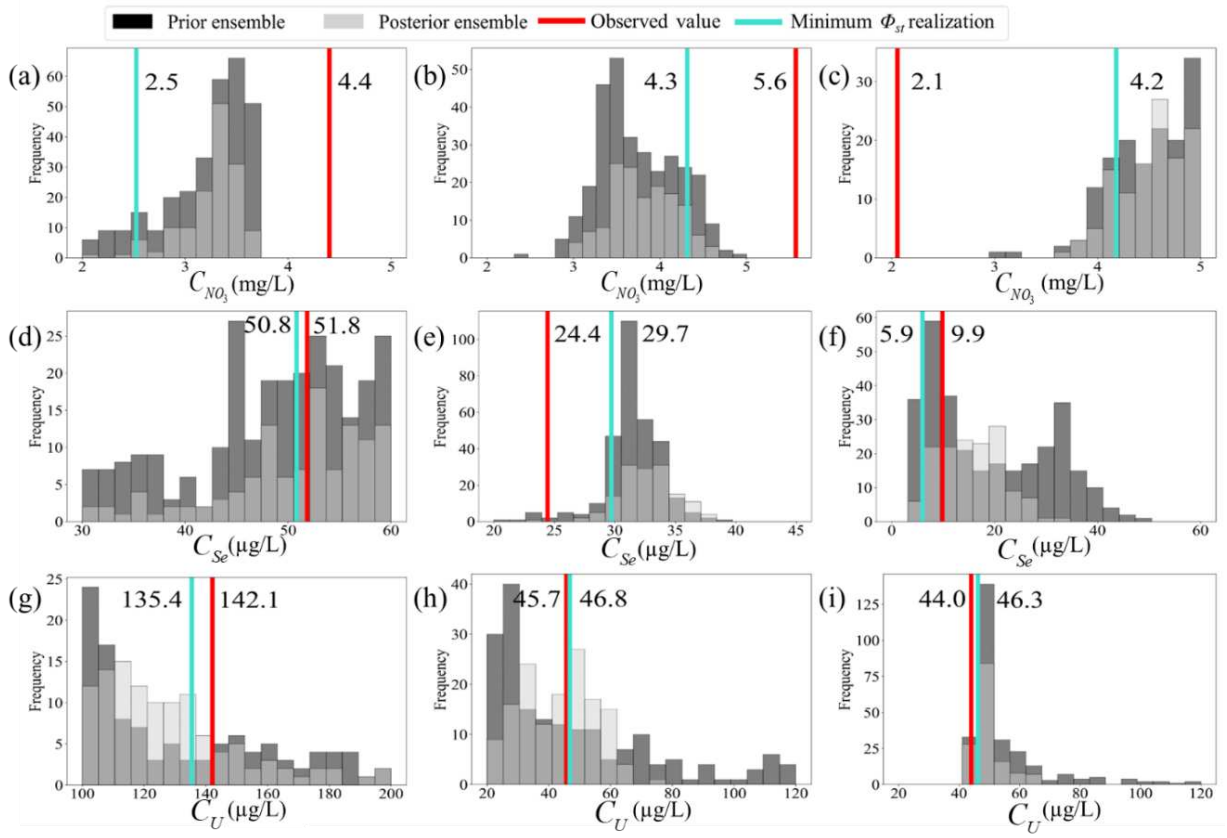

Figure 13. Prior and posterior frequency histograms of the ensemble of realizations of values of the calibration target variables in selected groundwater subregions: (a) average C_{NO_3} in subregion 1, (b) average C_{NO_3} in subregion 9, (c) average C_{NO_3} in subregion 15, (d) average C_{Se} in subregion 1, (e) average C_{Se} in subregion 9, (f) average C_{Se} in subregion 15, (g) average C_U in subregion 1, (h) average C_U in subregion 9, and (i) average C_U in subregion 15. Refer to Fig. 12 for the location of each groundwater subregion.

Sections 3.8.6 and 3.8.7 describe the results of implementing this final set of values in MODFLOW-RT3D to simulate solute transport variables across the DSR to represent conditions over the period 2003 – 2016. Out of the 543 calibrated model parameters, 356 have values that fall within 20% of the lower bound specified in PESTPP-iES. Table 3 summarize the statistics of the calibrated parameters to which Φ_{st} was found to be most sensitive by an earlier manual adjustment of parameter values. Table 3 provides the range and average of the calibrated parameters for the groundwater aquifer in non-riparian areas, groundwater aquifer in riparian areas, and stream parameters over all segments in the Arkansas River and the tributary segments

across the DSR. These calibrated parameters are within the range of values reported in the literature. Summaries of the values of calibrated parameters for each non-riparian groundwater subregion, each riparian area, and each stream segment can be found in Table S5 – S7 in Supplementary Material in Appendix A.

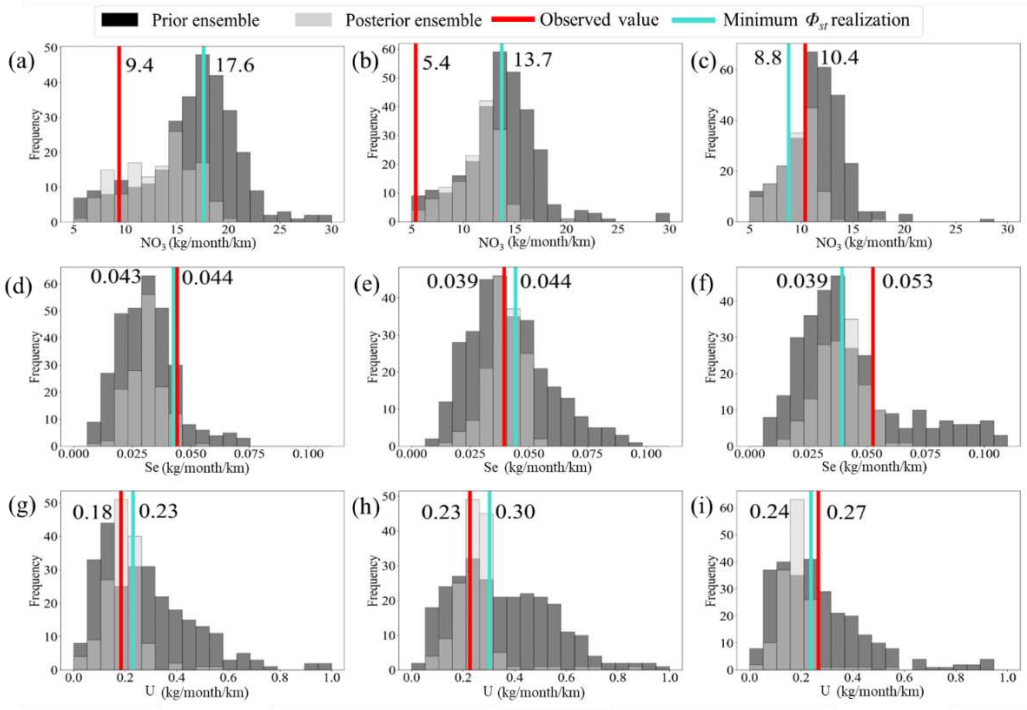

Figure 14. Prior and posterior frequency histograms of the ensemble of realizations of the values of the calibration target variables (a) NO_3 mass loading to Arkansas River May 2008, (b) NO_3 mass loading to Arkansas River December 2008, (c) NO_3 mass loading to Arkansas River April 2009, (d) Se mass loading to Arkansas River May 2008, (e) Se mass loading to Arkansas River December 2008, (f) Se mass loading to Arkansas River April 2009, (g) U mass loading to Arkansas River May 2008, (e) U mass loading to Arkansas River December 2008, and (f) U mass loading to Arkansas River April 2009.

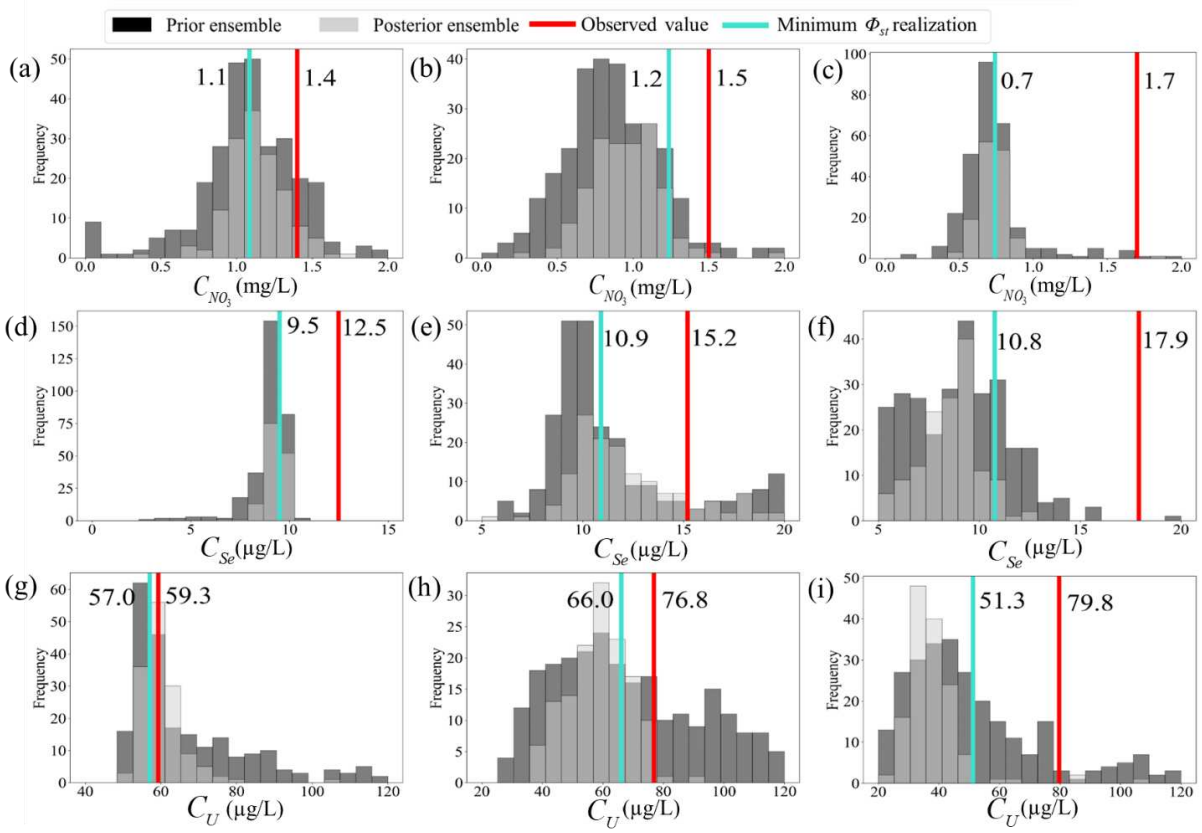

Figure 15. Prior and posterior frequency histograms of the ensemble of realizations of the values of the calibration target variables in selected Arkansas River segments: (a) average C_{NO_3} in segment 2, (b) average C_{NO_3} in segment 4, (c) average C_{NO_3} in segment 6, (d) average C_{Se} in segment 2, (e) average C_{Se} in segment 4, (f) average C_{Se} in segment 6, (g) average C_U in segment 2, (h) average C_U in segment 4, and (i) average C_U in segment 6. Refer to Fig. 12 for the location of each Arkansas Rive segment.

3.8.6. Simulated Groundwater and Stream Flows in the LARV DSR

Groundwater and stream flow variables in the DSR simulated with the MODFLOW package over the extended period 2002 – 2016 using the calibrated flow parameter values for the minimum Φ_f realization in PESTPP-iES were found to match well with available data. Frequency histograms of residuals for *h* are plotted in Fig. 16 using observed data from the 118 groundwater monitoring wells in the DSR for the simulation over the extended period, as well as for the simulation by Morway et al. (2013) for the period 2002 - 2007. The average residual for *h* is 0.57

m for the simulation over the extended period. Fig. 17 shows the average groundwater table elevation and average depth to water table (D_{wt}) from the ground surface simulated by the calibrated MODFLOW model over the irrigation seasons within the extended period 2002 – 2016. In addition to illustrating the variability in the groundwater level and gradient throughout the DSR, that drives advective transport of solutes, this figure indicates the large fraction of the region subjected to shallow groundwater tables which affects solute movement between the unsaturated and saturated zones and contributes to waterlogging and salinity under cropped lands (Morway and Gates 2012, Tavakoli-Kivi et al. 2019).

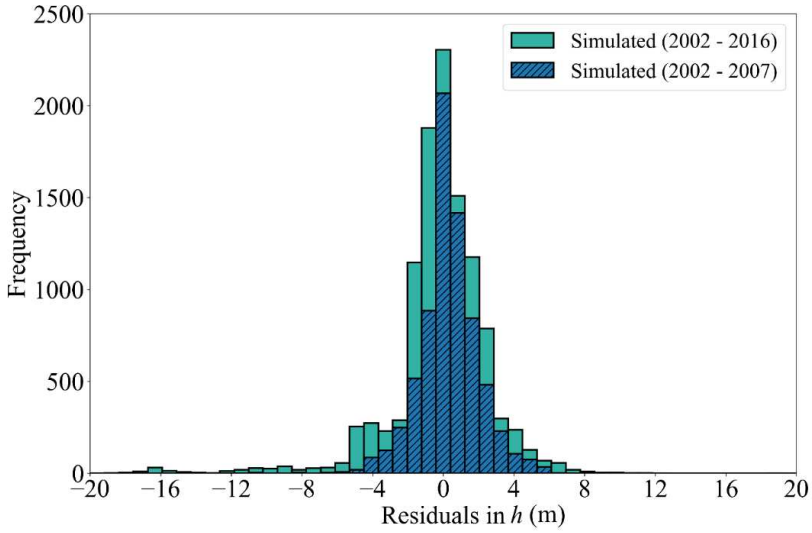

Figure 16. Frequency histograms of residuals in h in the DSR in the calibrated MODFLOW simulation over the extended period 2002 – 2016 and in the simulation by Morway et al (2013) over the period 2002 – 2007.

Fig. 18 plots the weekly total groundwater return flow to the Arkansas River in the DSR simulated by the MODFLOW model calibrated for the extended period. The plot shows results in comparison to the mean and 95% inter-percentile range of weekly total groundwater return flow and unaccounted surface return flow estimated by Gates et al. (2018) using a stochastic river mass balance for the period October 2006 to September 2010. Unaccounted water sources emerge from the ungauged tributaries, such as Clay Creek and Buffalo Creek, and from direct

overland runoff to the river. Positive return flow values indicate gains to the river. The stochastic model reveals spikes over short periods, that may be due in part to significant precipitation and runoff from the desert area outside the model domain. The MODFLOW model, however, only routes precipitation within the model domain and does not predict these spikes. The time-averaged groundwater return flow simulated by the calibrated MODFLOW model is 0.032 m^3/day per km. As expected, this value falls below the stochastic mass balance model prediction of 0.043 m^3/day per km for the average which includes unaccounted surface water return flow (Gates et al., 2018).

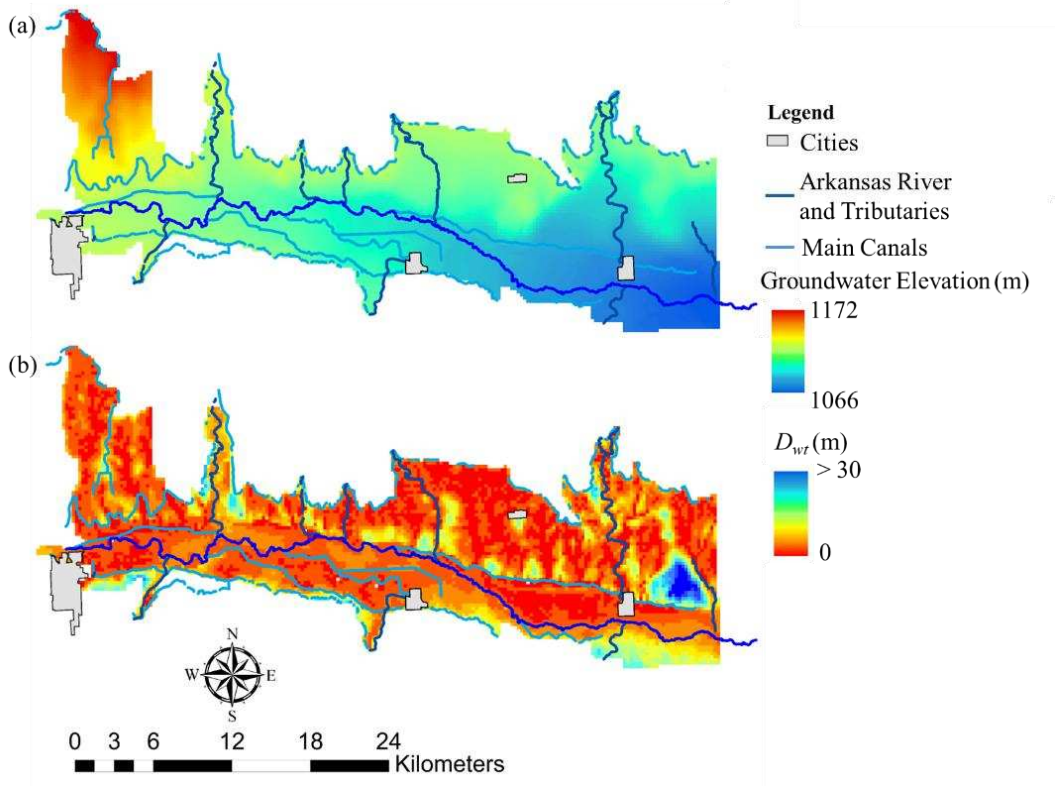

Figure 17. Simulated (a) groundwater table elevation and (b) Dwt in the DSR averaged over the irrigation seasons within 2002 – 2016.

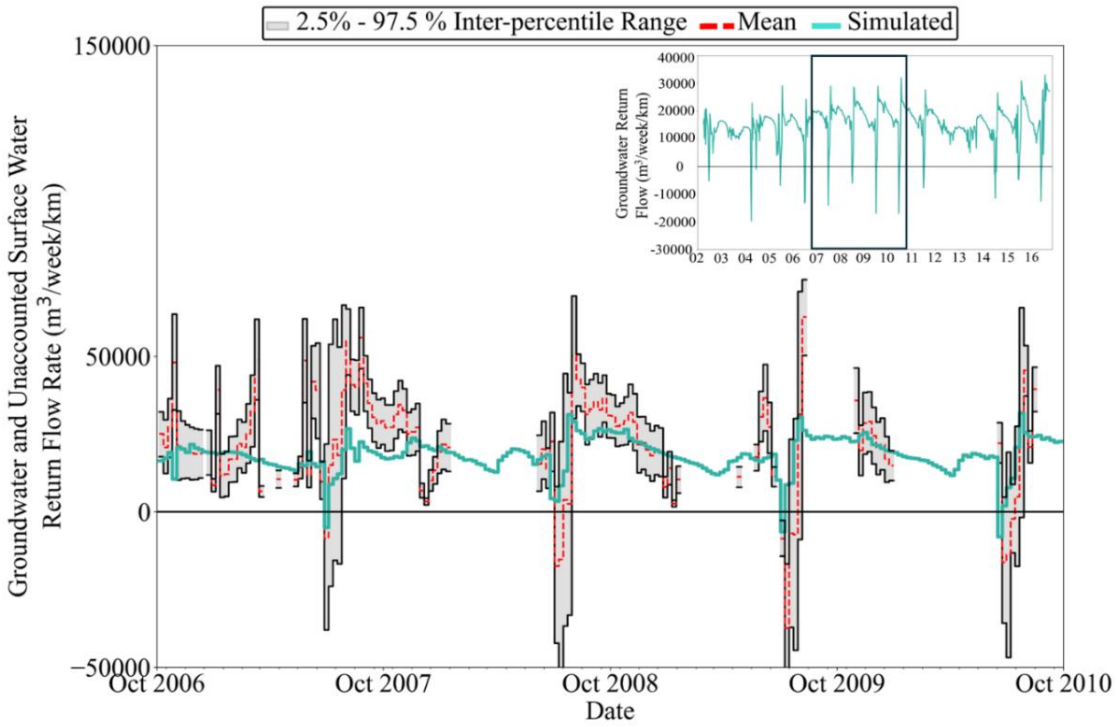

Figure 18. Groundwater return flow simulated by the MODFLOW model calibrated for the extended period compared to groundwater return flow and unaccounted surface water return flow estimated by the stochastic river mass balance model of Gates et al (2018). The inset plot shows the MODFLOW simulated groundwater return flow for the full extended period 2002 - 2016. The box within the inset plot represents the same period as the analysis by Gates et al. (2018).

Weekly average flow rates simulated using the SFR package in MODFLOW in the computational cells containing stream gauge locations are compared with weekly average data gathered at 15-minute intervals at the gauge locations. Fig. 19 plots the simulated values compared to the data at the Lamar, Granada, and Coolidge gauge locations, indicating a good match. The model-simulated values in the cell adjacent to the Colorado-Kansas state line are compared with data at the nearby Coolidge station, which lies 3.6 km downstream. Similar comparisons of simulated and measured flow rates are provided in Fig. 20 for the Big Sandy Creek and Wild Horse Creek tributaries. Table 4 summarizes several computed performance measures of simulated compared to measured flows: the Nash-Sutcliffe Coefficient of Efficiency (NSCE) (Nash and Sutcliffe, 1970), coefficient of determination (R^2), the Kling-Gupta Efficiency (KGE) (Gupta et

al., 2008), and the Normalized Root Mean Square Error (NRMSE) which is the root mean square error (RMSE) divided by the mean of the observed values. NSCE varies from -∞ to 1, Performance levels are considered acceptable when they fall between 0.0 and 1.0, while values below 0.0 suggest that the observed mean value is a more reliable predictor than the simulated value, indicating unsatisfactory performance (Moriasi et al., 2007). R^2 values range from 0 to 1, where 1 indicates a perfect match of simulated values to observed data and 0 indicates no match. The KGE values range from -∞ to 1.0, with the optimal KGE value being 1, 0 indicating a weak match of simulated to observed values, and a negative value indicating poor model performance (Knoben et al., 2019). The poorer match of simulated flows with data in the tributaries, compared to the match at the Arkansas River gauges, could be due in part to measured tributary flows emerging from outside the model domain and to the difficulty of aligning simulated flows to the observed timing and magnitude of flashy overland flows in the tributaries.

3.8.7. Simulated Solute Concentrations and Mass Loads in the LARV DSR

Application of the coupled MODFLOW-RT3D model using the calibrated flow and solute transport parameter values obtained in PESTPP-iES for the minimum Φ_f and minimum Φ_{st} realizations provides a depiction of the spatiotemporal distribution of U and related pollutants across the DSR. Simulated values of C_{NO_3}, C_{Se}, and C_U averaged over the over the period 2003 - 2016 are shown in the color contour maps in Fig. 21, revealing similarity to plotted average observed values and revealing substantial variability over the region. Markedly high concentrations, frequently exceeding CDPHE chronic standards, occur in some areas, especially in the central part of the region north of Granada and within the irrigated areas commanded by the Lamar, Buffalo, and Amity canals. Areas of high C_{NO_3} often correspond to high C_{Se}, and C_U, reflecting NO_3 contribution to the inhibition of chemical reduction, as well as to the oxidative

mobilization of Se and U. Significant related factors that contribute to the elevated simulated levels of C_{NO_3}, C_{Se}, and C_U are bedrock and near-surface shale formations that occur within the region (Fig. 10). These formations are sources for the release of Se and U through oxidation.

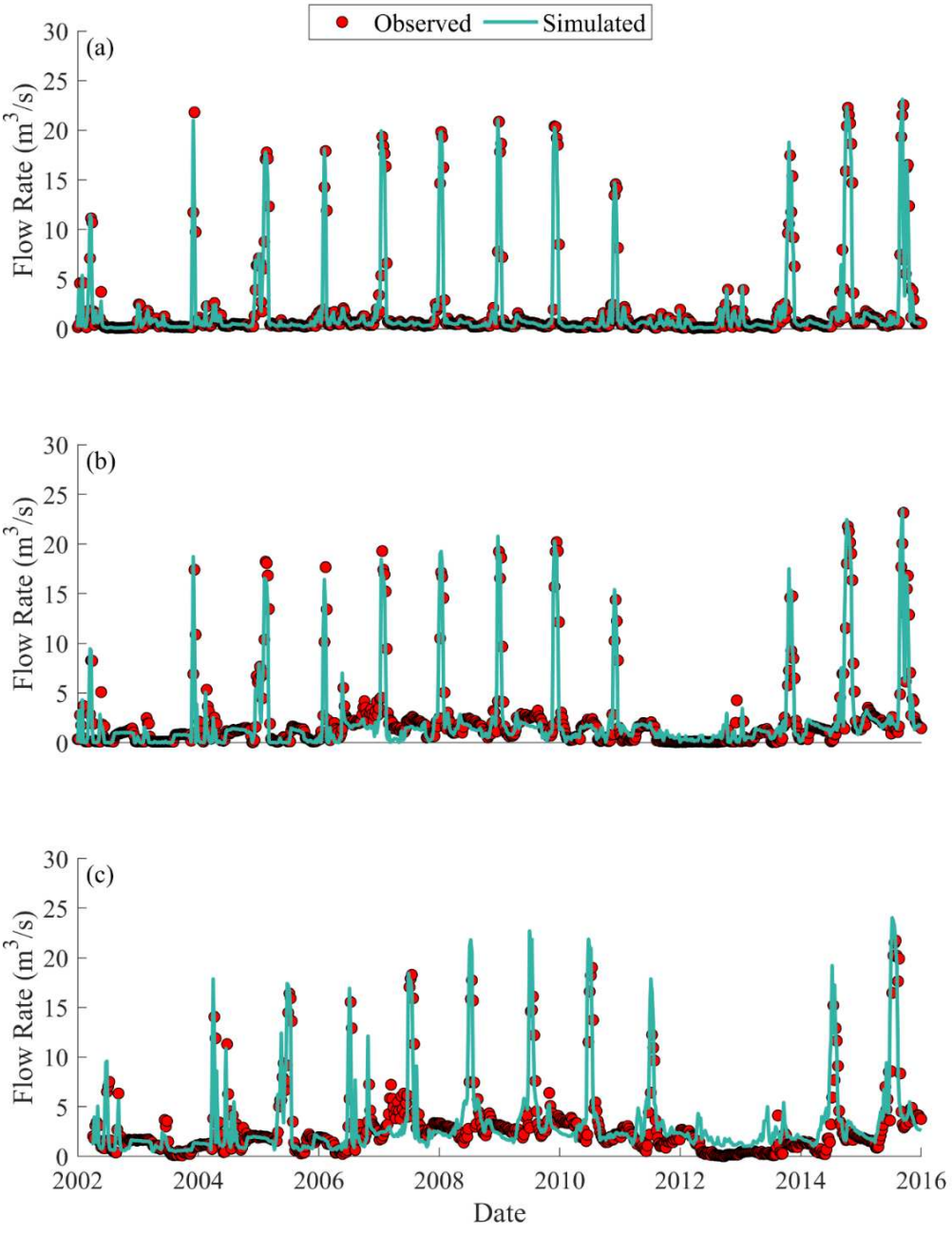

Figure 19. Weekly average flow rate simulated by the calibrated MODFLOW model compared to data at the river gauge locations at (a) Lamar, (b) Granada, and (c) Coolidge.

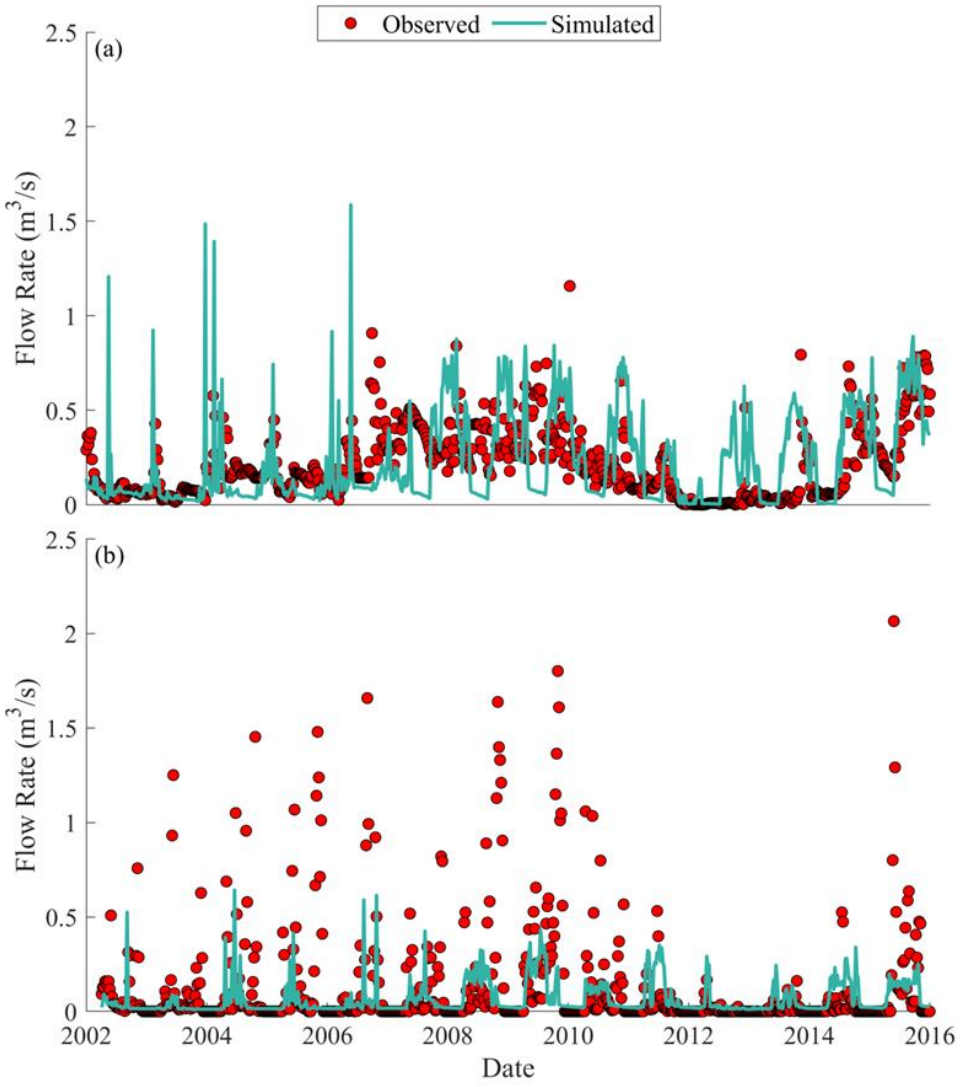

Figure 20. Weekly average flow simulated by the calibrated MODFLOW model compared to data at the tributary gauge locations in (a) Big Sandy Creek and (b) Wild Horse Creek.

Table 4. Performance measures for comparing simulated and observed flow rates in the vicinity of the five USGS stream gauges within the DSR.

	NSCE	R^2	KGE	NRMSE
Lamar (m^3/sec)	0.7	0.7	0.9	1.2
Granada (m^3/sec)	0.6	0.7	0.8	1.1
Coolidge (m^3/sec)	0.4	0.5	0.7	0.96
Big Sandy Creek (m^3/sec)	-0.8	0.1	0.3	1.1
Wild Horse Creek (m^3/sec)	-0.03	0.04	-0.2	2.1

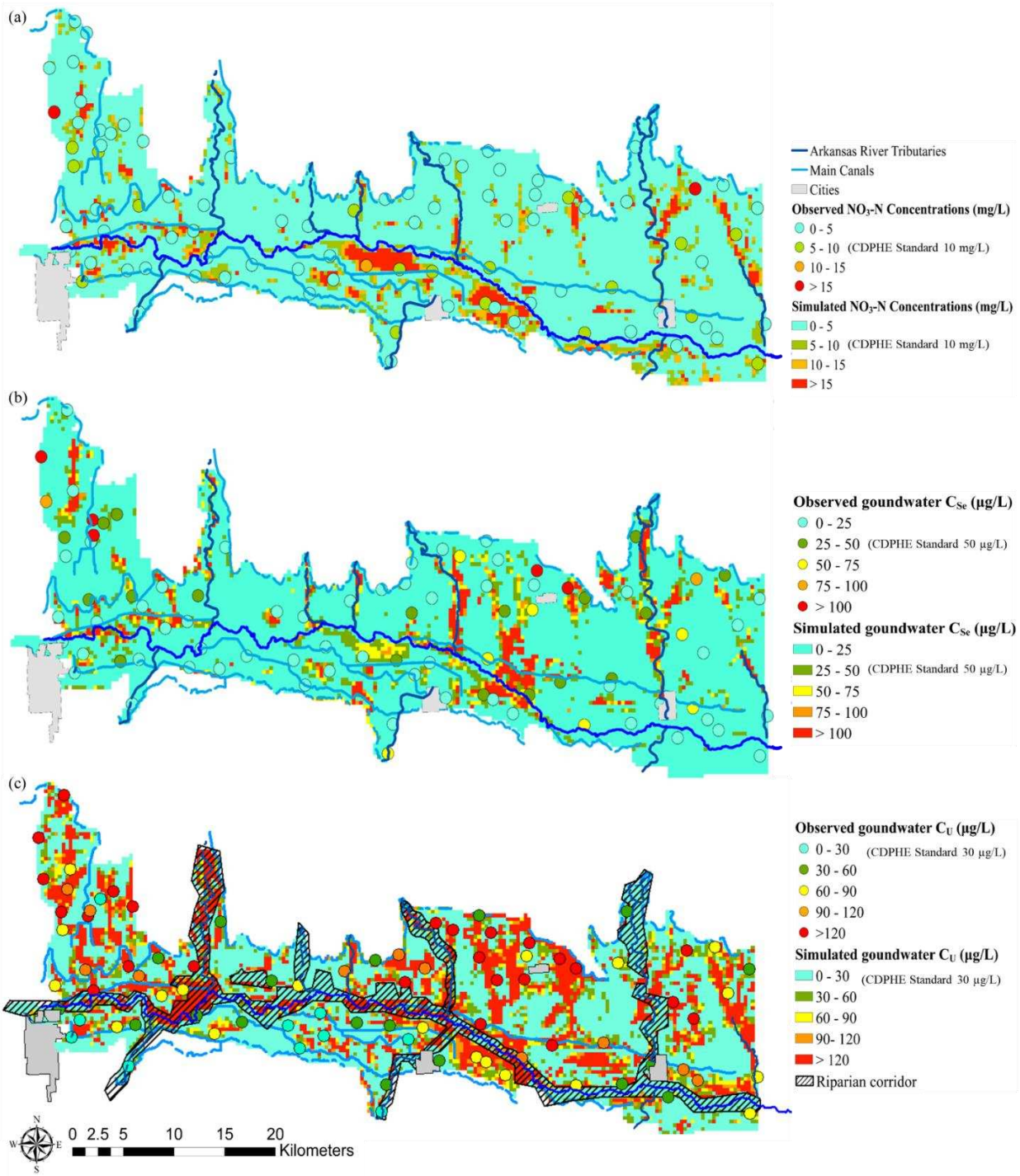

Figure 21. Simulated and observed groundwater concentrations in the DSR averaged over the period 2003-2016 for (a) C_{NO_3}, (b) C_{Se}, and (c) C_U.

High organic matter and enhanced microbial activity in stream riparian corridors often contributes to increased heterotrophic reduction in shallow groundwater aquifers (Sahu and Gu

2009, Dosskey et al. 2010, Bailey et al. 2015a, Shultz et al. 2018b) . Hence, statistics for simulated groundwater concentrations were computed separately for non-riparian and riparian areas, highlighted in Fig. 21C. Spatiotemporal average simulated C_{NO_3}, C_{Se}, and C_U for non-riparian areas in the DSR stand at 3.6 mg/L, 41 µg/L 126 µg/L, respectively. This aligns closely with respective average C_{NO_3}, C_{Se}, and C_U in monitoring wells of 3.9 mg/L, 53.3 µg/L, and 111.7 µg/L. The average 85th percentile of simulated C_{NO_3}, C_{Se}, and C_U for non-riparian areas stands at 5.8 mg/L, 50.2 µg/L, and 218.1 µg/L, respectively. By contrast, the spatiotemporal average simulated C_{NO_3}, C_{Se}, and C_U for riparian areas are 2.9 mg/L, 25.6 µg/L, and 72.2 µg/L, respectively, with average 85th percentile values being 4.8 mg/L, 41.3 µg/L 152.2 µg/L. The lower simulated concentrations in riparian areas are attributed in part to higher reaction rate parameters calibrated by PESTPP-iES, in keeping with expected higher levels of chemical reduction in these areas.

Plotted in Fig. 22 are the spatiotemporal average simulated C_{NO_3}, C_{Se}, and C_U within each of the 15 groundwater subregions (Fig. 12) over 2003 – 2016, along with the corresponding average values in groundwater monitoring wells. Also shown are whiskers on each plotted bar of the average observed value representing $\pm$ one standard deviation from the average. The CDPHE standard 85th percentile limit for C_{Se} is 50 µg/L in groundwater, and for C_{NO_3} is 10 mg/L.

Overall, results indicate good agreement between average simulated values and average values measured in monitoring wells spanning the DSR. Discrepancies are due in part to (a) errors in model formulation and parameter calibration, (2) errors in collection and analysis of water samples, and (3) differences between model scale and observation scale. The model simulates concentration values over a 6.25-ha grid cell and a one-day period whereas observed values are derived from instantaneous samples taken from 6.3-cm diameter monitoring wells at a point

below ground surface typically located within the model grid layer 4. Overall, results in Figs. 21 and 22 indicate the ability of the calibrated MODFLOW-RT3D model to reasonably depict the larger patterns of solute contamination and transport throughout the aquifer system in the DSR in relation to observed data, considering that the available data themselves do not comprehensively represent conditions across the entire irrigated command area. Predictions of C_U are especially comparable. Fig. S6 in Supplemental Material in Appendix A depicts the spatial simulated C_{O_2} in groundwater compared with observed data. Also, Fig. S7 shows a comparison of C_{O_2} in groundwater for each subregion.

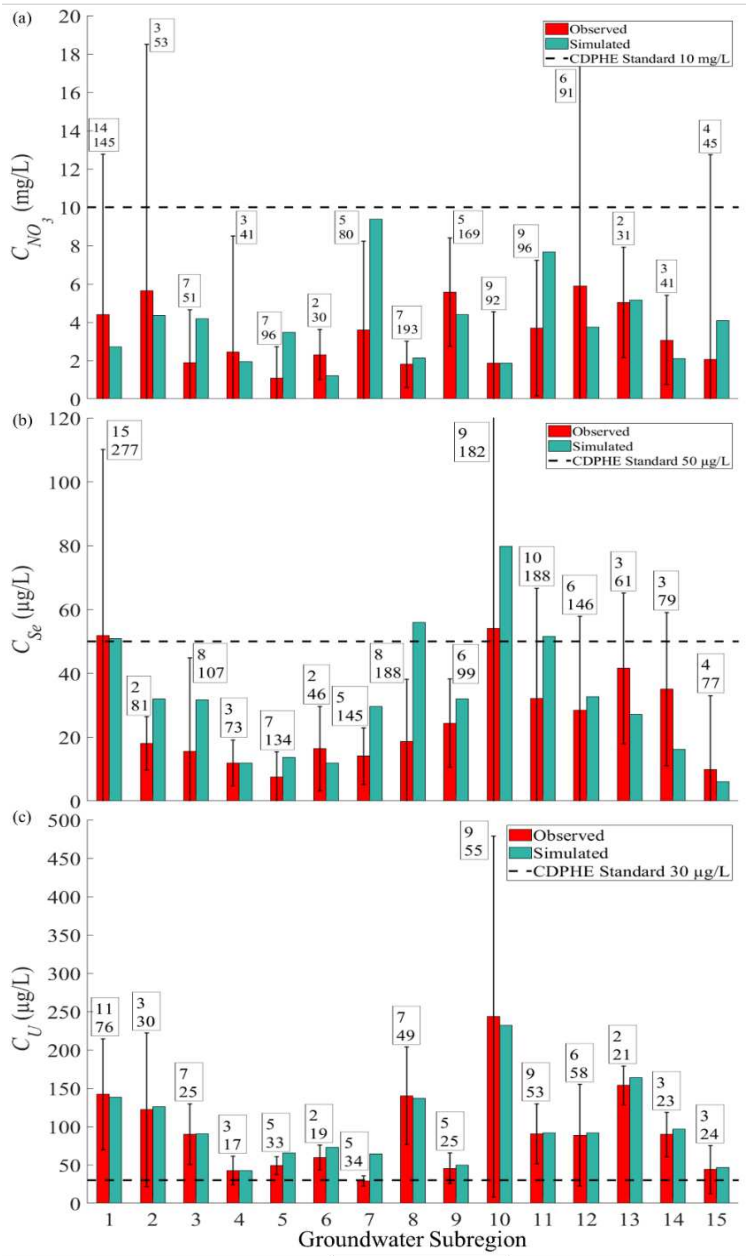

Figure 22. Spatiotemporal average simulated and observed groundwater concentrations within the 15 subregions for (a) C_{NO_3}, (b) C_{Se}, and (c) C_U. Upper and lower whiskers depict plus or minus one standard deviation associated with uncertainty from the discrepancy in the observed values' spatial and temporal scales and measurement error. The top numeral in each box above the bars represent the number of monitoring wells within and the bottom numeral is the number of observations with each sub-region over the simulation period.

Another sense of the model's ability to capture the spatiotemporal distribution of constituent concentrations over the DSR may be gained from Fig. 23a that shows the relative

frequency histogram of simulated values of C_U in all non-riparian groundwater cells compared to the relative frequency histogram of all observed values. The Brier Score (BS) (Brier 1950, Tavakoli et al. 2019) is employed to assess the performance of the relative frequency distributions of the simulated values in relation to the observed values:

$$BS = \left(\frac{1}{n_b}\right)\sum_{1}^{n_b}\left(f_i - o_i\right)^2 \tag{20}$$

wherein n_b is the number of bins, f_i is the simulated relative frequency in the i^{th} bin, and o_i is the observed relative frequency in the i^{th} bin. The value of $\sqrt{BS}$ ranges between 0 and 1 with a value closer to 0 signifying a better alignment between the simulated and observed distributions. The $\sqrt{BS}$ of C_U simulated across all non-riparian groundwater cells over the entire period is 0.1, indicating a reasonably close match between simulated and observed distributions.

Fig. 24 shows the simulated groundwater mass loading of NO_3, Se, and U (kg/day per km) to the Arkansas River. It is compared with results from the stochastic mass balance model of groundwater and unaccounted mass loading to the river reported by Gates et al. (2018) for the period October 2006, to September 2010. Simulated values follow the general pattern of the estimated values and typically fall within the 95th inter-percentile range for all three constituents. The simulated average mass loading rates for NO_3, Se, and U are 8.8 kg/day/km, 0.051 kg/day/km, and 0.27 kg/day/km, compared to the respective stochastic mass balance estimates of 9.2 kg/day/km, 0.055 kg/day/km, and 0.23 kg/day/km.

Simulated values of C_U along the Arkansas River are presented in Fig. 25 for the computational cell within each of the six river segments (Fig. 12) that contains a sampling location, along with the measured concentrations at each sampling location. Similar plots for

C_{NO_3}, C_{Se}, and C_U are presented in Fig. 26 for the cells corresponding to sampling locations within representative segment 2, upstream; stream segment 4, mid-stream; and stream segment 6, downstream. The CDPHE standard shown for C_{NO_3} in the plots in Figure 26 is an interim standard for total dissolved N species $\left(C_{NO_3-N} + C_{NO_2-N} + C_{NH_4-N}\right)$. Table 5 summarizes the average and 85th percentile values of the simulated and observed concentrations for each sampled cell within each stream segment in the Arkansas River and for all sampled cells along the entire river. In comparing simulated and observed concentrations, the spatial and temporal discrepancies in the model and observation scales must be kept in mind. Water samples for laboratory analysis are about 100 mL in size and are taken at points within the river. However, simulated concentrations are over a model cell containing the sampling location and ranging in size from 40 m to 200 m. Samples typically are collected over about five-minute intervals, predominantly in the morning or early afternoon in contrast to simulated concentrations over a model time step of one day. Given this disparity, the match between simulated and observed values is quite acceptable. Even in downstream segments where differences appear greater, simulated concentrations still follow the overall periodic trends in observed concentrations. Figs. S8 – S14 in Supplemental Materials in Appendix A represent the simulated C_{O_2}, C_{NO_3}, C_{Se}, and C_U in the river and in its tributaries compare with the observation data.

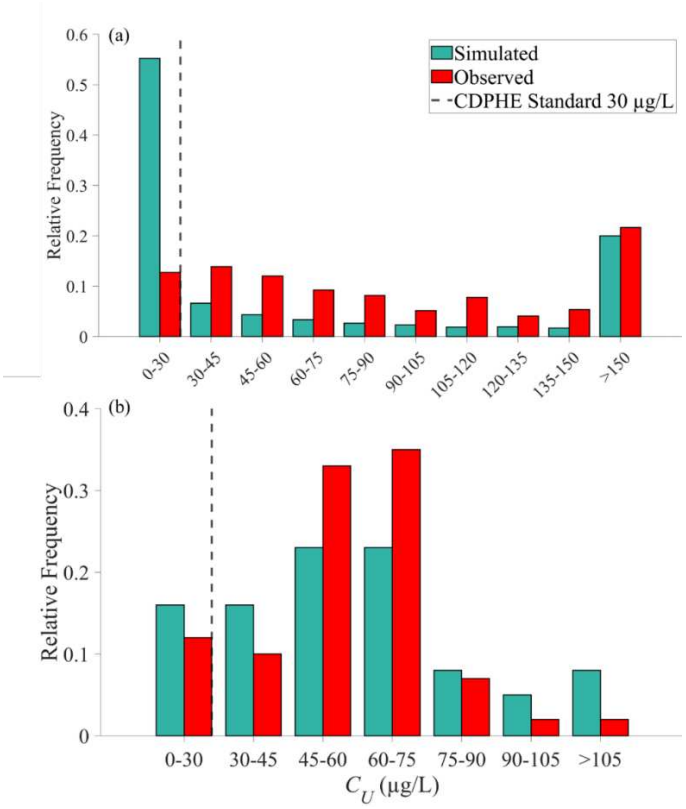

Figure 23. Relative frequency histograms of (a) simulated values of C_U in all non-riparian groundwater cells over the DSR and the simulation period compared to all observed values, and (b) simulated values of C_U in stream segment cells of the Arkansas River in the DSR and over the simulation period compared to all observed values.

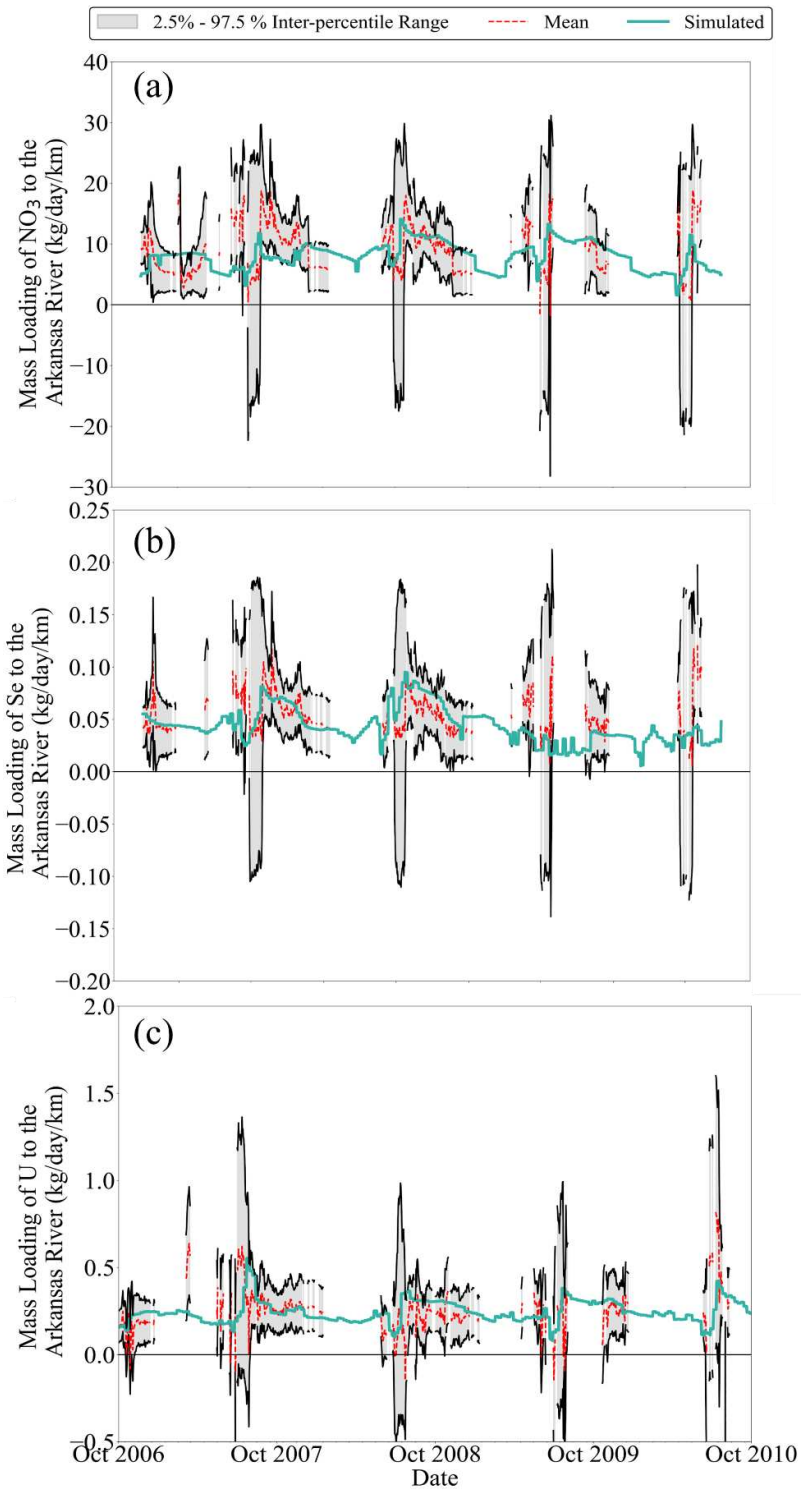

Figure 24. Simulated groundwater mass loading of (a) NO_3, (b) Se, and (c) U to the Arkansas River compared with the statistics of groundwater and unaccounted mass loading estimated by Gates et al (2018).

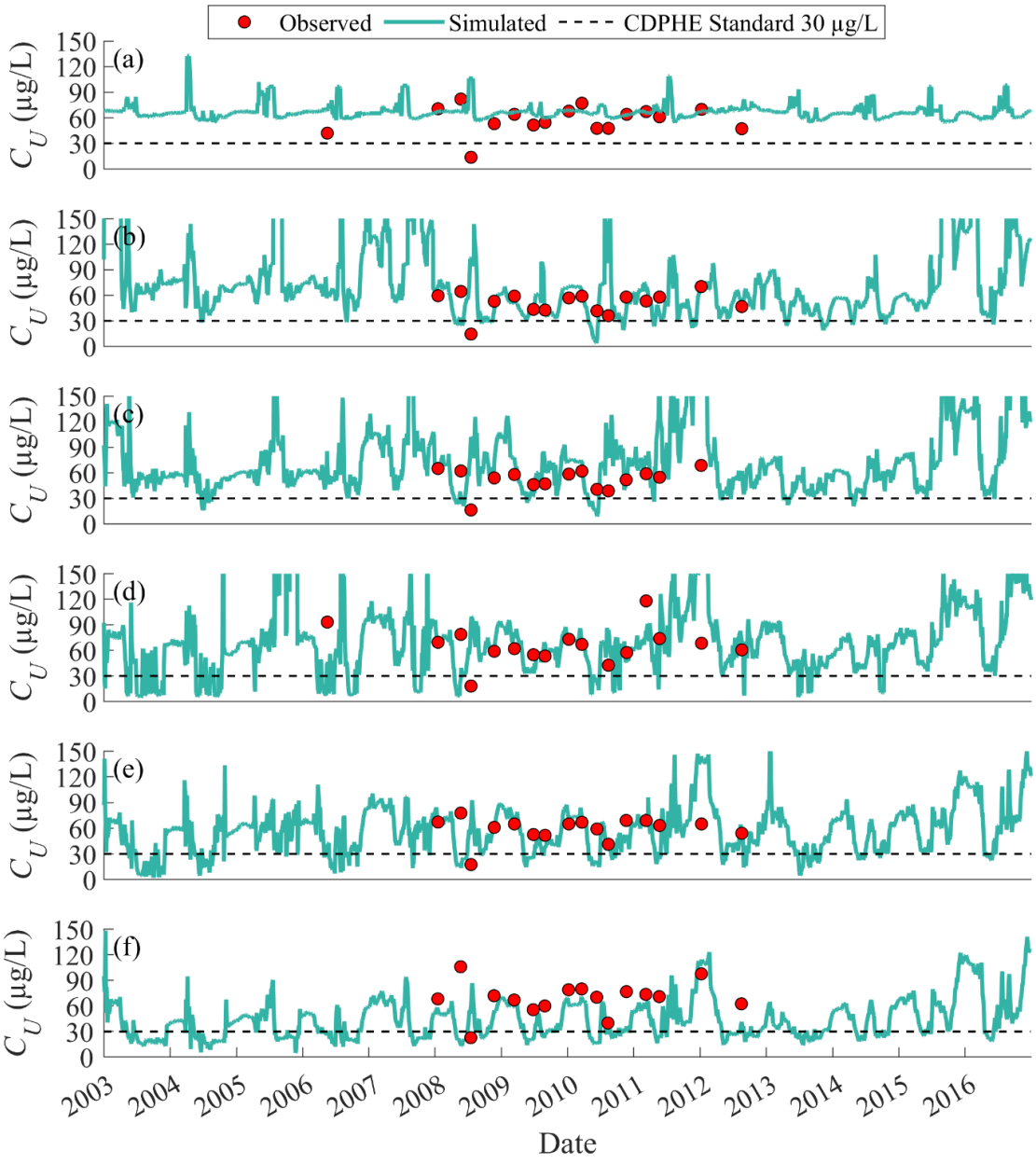

Figure 25. Simulated C_U values in the Arkansas River for the computational cell corresponding to the sample location in (a) stream segment 1, (b) stream segment 2, (c) stream segment 3, (d) stream segment 4, (e) stream segment 5, and (f) stream segment 6 (ordered upstream to downstream). Also shown is the CDPHE chronic standard.

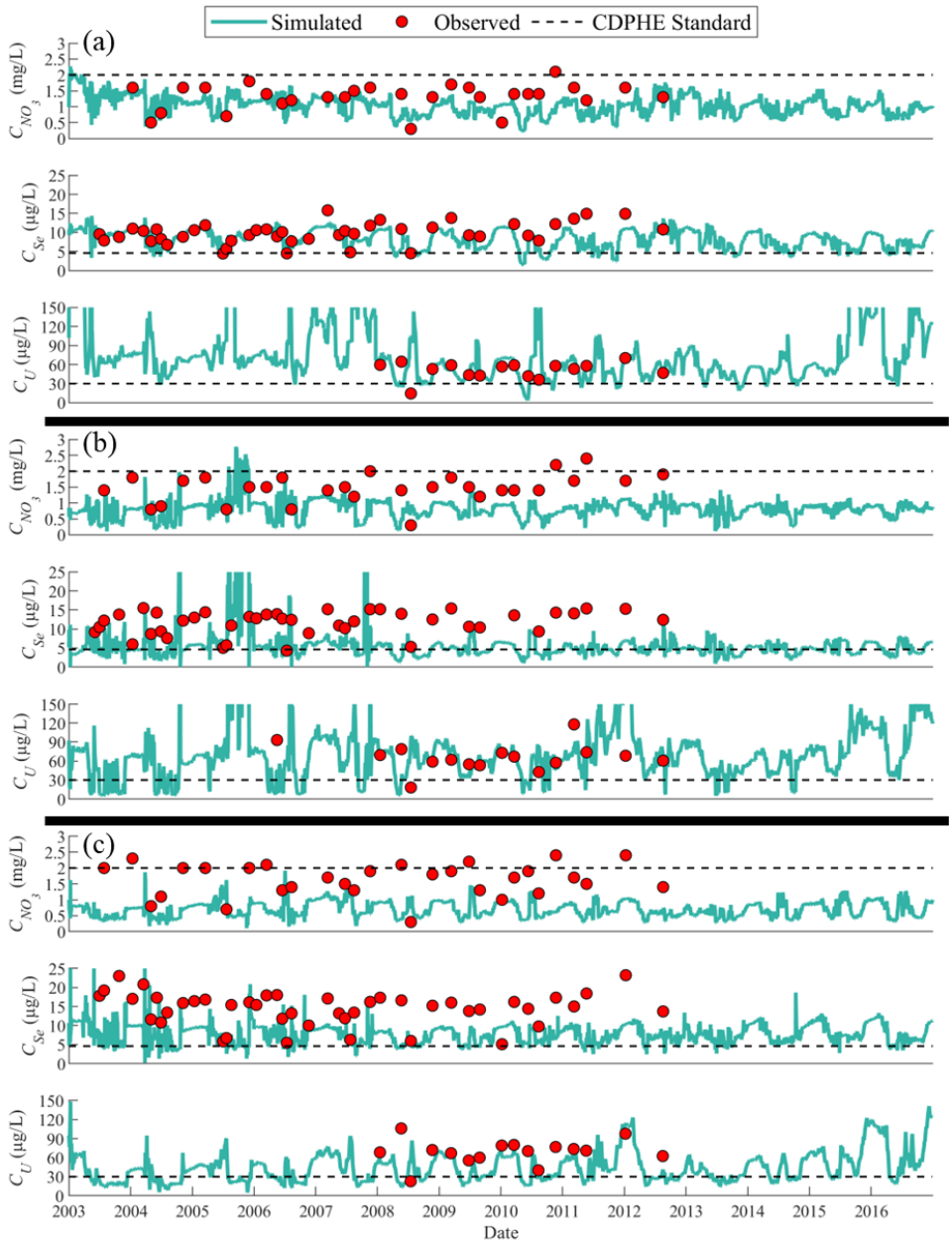

Figure 26. Simulated C_{NO_3}, C_{Se}, and C_U values in the Arkansas River for the computational cell corresponding to the sample location in representative (a) stream segment 2 (upstream), (b) stream segment 4 (mid-stream), and (c) stream segment 6 (downstream). Refer to Fig. 12 for the location of each stream segment. Also shown are the CDPHE chronic and interim standards.

The relative frequency histogram of simulated values of C_U in all stream segments of the Arkansas River in the DSR over the simulation period compared to the relative frequency

histogram of all observed values is depicted in Fig. 23b. The $\sqrt{BS}$ value is 0.07, again indicating a strong correspondence between the spatiotemporal distribution of simulated concentrations compared to observed concentrations. The 85th-percentile value of C_U simulated over the period is mapped for every computational cell along the Arkansas River in Fig. 27. Also shown are frequency histograms and related statistics of simulated C_U over the simulated period at three representative arbitrary locations along the river along with frequency histograms at three sampling locations along the river. Variation in C_U along the river is attributed to the influence of tributary inflows and canal diversions along the river, distinctions in adjacent irrigation and fertilization practices, differences in aquifer storage and transmission properties, the presence of bedrock and near-surface geologic formations, and patterns of riparian vegetation type and density, among other factors. These results underscore the substantial exceedance of the chronic standard, with simulated concentrations ranging from 1.9 to 5.0 times the standard along the entire river reach, underscoring the growing concern about U pollution in the LARV. It is noteworthy that the average 85th percentile of simulated C_U at the most downstream computational cell is 63.2 µg/L, comparing favorably with the average 85th percentile measured value of 73.4 µg/L for 31 water samples collected over 2009 – 2016 at the Coolidge stream gauge about 3.6 km downstream by the Kansas Department of Health and Environment (KDHE, 2024) and not used in the model calibration.

Table 5. Statistics of observed and simulated concentrations for all constituents for each sampled cell within each stream segment in the Arkansas River within the DSR.

	River Segment	Average		85th percentile	
		Simulated	Observed	Simulated	Observed
C_{NO_3} (mg/L)	1	1	1.1	1.3	1.5
	2	1.1	1.4	1.3	1.6
	3	1	1.2	1.1	1.6
	4	1. 2	1.5	1	1.8
	5	1	1.7	1.2	2
	6	0.7	1.7	1	2.1
	Total	0.9	1.4	1.2	2
C_{Se} (µg/L)	1	10.8	10.4	12.3	14.9
	2	9.9	9.8	10.9	12.5
	3	6.4	10.1	8.2	13.7
	4	10.1	11.7	6.8	15.2
	5	11.1	11.9	14.1	15
	6	9.1	14.4	10.5	17.9
	Total	8	14.1	11.3	22.4
C_U (µg/L)	1	66.2	57.6	70	70.1
	2	53	51	70.4	59.3
	3	67.2	52.2	109	62.2
	4	66.2	65.6	94.3	76.8
	5	59.1	59.1	81.5	68.3
	6	48.5	70	70	79.8
	Total	61	61.8	87.3	82

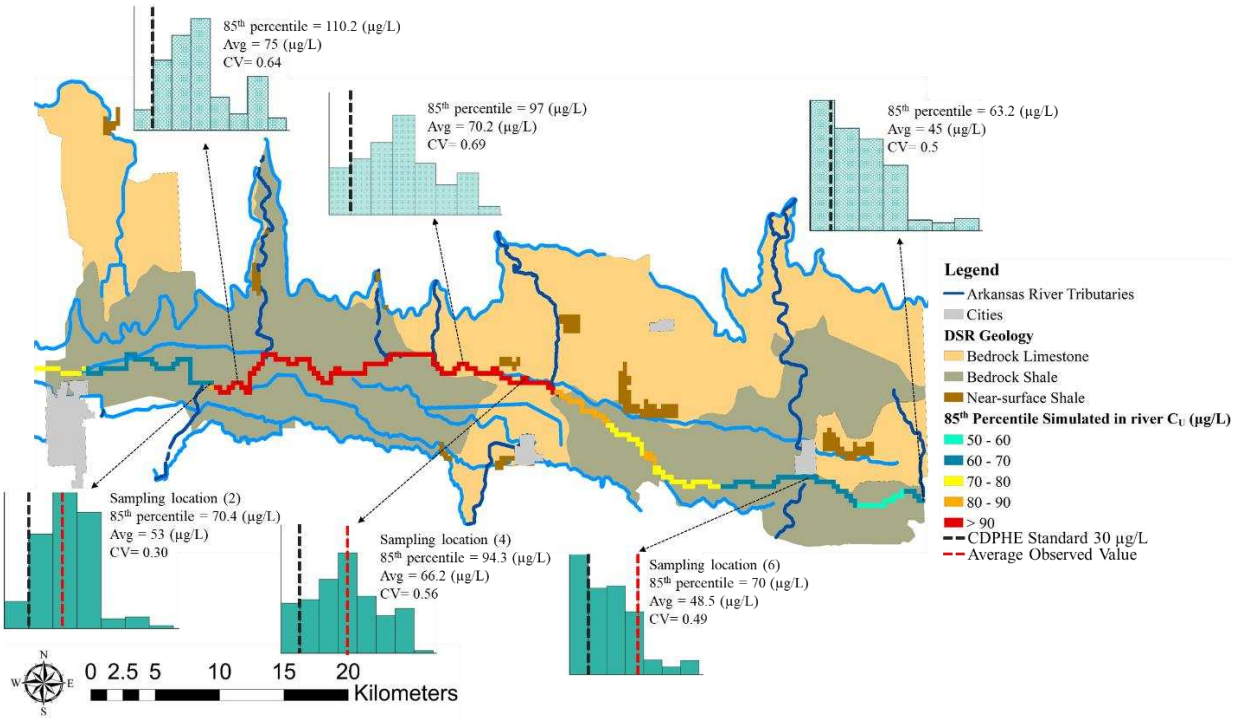

Figure 27. The 85th percentile of simulated C_U over the entire period 2003 – 2016 in each computational cell along the Arkansas River is depicted. Also shown are frequency histograms of simulated values in computational cells at three representative arbitrary locations along the river, along with frequency histograms at three representative sampling locations along the river. The black dash line on each histogram depicts the CDPHE chronic standard, and the red dash line on each sampling location histogram is the average observed value.

3.9. Summary and Conclusions

To sustain irrigated agriculture in its contribution to feeding the world, the intertwining concerns of land management, water management, and environmental protection will need heightened understanding and attention. Water quality in the aquifers and streams of vast irrigated regions is often diminished by patterns of irrigation return flows that interact with fertilizers, soils, and geology to create elevated concentrations of harmful solutes. For characterizing these problems and exploring feasible solutions, calibrated distributed parameter flow and solute transport models will play an increasingly important role.

We consider here a representative region in the irrigated stream-aquifer system of Colorado's Lower Arkansas River Valley (LARV), where extensive irrigation practices over the last 130 years have led to notable challenges, including elevated concentrations of U, along with co-reactants Se and NO_3, that pose threats to human health and cause adverse impacts on fish and waterfowl. This location has been extensively monitored for many years, offering a rich and varied collection of targets for calibrating and verifying computational models. This study applies MODFLOW-RT3D, a coupled spatially-distributed and physically-based finite-difference model designed to simulate the movement and behavior of mainly U, Se, and NO_3 species within interconnected groundwater and surface water systems. Notably, the model accounts for the influence of O_2 and NO_3 on U and Se chemistry and transport, as well as the cycling and transport of these species due to their interconnected dynamics. The MODFLOW-RT3D application focuses on key processes and factors governing U mobilization and transport in agriculturally affected aquifers and streams, including sorption, redox reactions, marine shale release, soil interactions, crop uptake, groundwater extraction, canal seepage, irrigation inputs, and relations between groundwater and surface water. Saturated and unsaturated zone flow rates and sources/sinks are accounted for in the base MODFLOW algorithm and activated packages. The UZF-RT3D and OTIS-QUAL2E components address the reactive transport of solutes within the RT3D package.

The PESTPP-iES parameter estimation software was used to calibrate the coupled MODFLOW-RT3D model against a wide array of available historical data on groundwater head, streamflow, return flow and mass loading to the river, and U, Se, and NO_3 concentrations in the aquifer and stream network over a 14-year period. This calibration was performed in two stages – first adjusting only the flow components using hydrologic data and MODFLOW package, and

subsequently adjusting the reactive transport components with concentration data and the RT3D package. PESTPP-iES uses an optimization algorithm to adjust parameter values through multiple realizations and iterations to suitably correspond with calibration targets based on observed data and using weights. Results are presented that describe uncertainty in the MODFLOW-RT3D model simulation of flow and solute transport variables in the LARV in relation to uncertainty in the estimated values of the calibrated parameters. The calibration process used 500 realizations for both the flow and solute transport models and was considered "calibrated" after 5 and 6 PESTPP-iES iterations, respectively. Only about 4% of calibrated parameters required further manual adjustment to enhance the match of model simulations to calibration targets.

Application of MODFLOW-RT3D to the study region in the LARV using the calibrated parameter values determined with PESTPP-iES demonstrates a strong agreement between simulated and observed values, with consistent trends for the model's flow and solute transport components. Results provide a more comprehensive picture of the magnitude, extent, and severity of irrigation-induced pollution in the LARV, revealing how U, Se, and NO_3 concentrations are dispersed across the region over the 14-year simulation period, including the appearance of hotspots, variations in concentration peaks, and critical time intervals when contamination levels exceed the chronic standards. The RT3D model identifies areas with elevated C_U in groundwater and predicts stream concentrations that align well with observed values and trends. In non-riparian aquifer areas, the average simulated value for C_U deviates by about 13% from the average observed concentrations in monitoring wells. The simulated mass loading rates for U differ by approximately 17% from values estimated from a river mass balance. The difference between the average simulated and observed values of C_U in streams is approximately 2%. Chronic standards are severely violated, with the 85th percentile simulated C_U in exceedance by about 627% in

groundwater and 190% in the Arkansas River. Almost half of the entire groundwater aquifer extents are in violation. Modeled Se concentrations also substantially exceed WHO and CDPHE standards and there is moderate violation by modeled NO_3 concentrations of the CDPHE interim standard for total N.

Modeled groundwater concentrations do not change much over time, having an average coefficient of variation of 0.25 and no significant trends. In contrast, river concentrations display an expected seasonal variability. We find that simulated C_U values in the streams for the non-irrigation season (mid-November – mid-March), when precipitation runoff and reservoir releases to streams are small and groundwater discharge contributes a large fraction, are markedly greater than values in the irrigation season (mid-March – mid-November). Over the 14 modeled non-irrigation seasons, the simulated 85th percentile of C_U averaged across all computational cells in the river is 102 µg/L, while over the irrigation seasons, the average is 69.2 µg/L. This finding is consistent with fluctuations at stream sampling locations, where simulated values align with high observed concentrations during winter and low flow periods.

The model provides valuable insights into potential sources of U contamination. Examining the simulated concentrations in both groundwater and the streams in relation to regional properties and processes suggests the possible origins of elevated concentrations. We find high simulated U levels in groundwater, especially in areas with near-surface shale layers, and close to irrigation canals. We notice a particularly high simulated level of C_U in the northwestern portion of the modeled region near the Fort Lyon canal (Figure 10), where geological materials and irrigation with surface water play significant roles. Similarly, areas north of the Buffalo canal and near the Amity canal (Figure 10) in the mid-east reveal elevated U levels due to geological sources and relatively plentiful irrigation water from senior water rights.

Like any numerical model, this model cannot perfectly replicate field processes. Reactive transport models, which involve complex interactions between multiple transport and chemical reaction parameters, result in predicted concentrations that vary across several orders of magnitude. Several challenges have emerged in this research, including the limitations associated with calibrating flow and reactive transport model packages sequentially using PESTPP-iES. This calibration approach involves adjusting each package independently. Enhancing this method to calibrate flow and transport parameters altogether in the coupled model might significantly improve the accuracy of the model outputs, given the complex interactions between flow and reactive transport dynamics. Another limitation is related to the application of the ADR equations on a large scale. Typically, the processes represented in these equations, along with their associated parameters, are defined and validated at small scales. Scaling up these equations to a region the size of the DSR in the LARV undoubtedly leads to error, but the extent to which parameters originally defined at small scales can be properly interpreted as averages over cells within larger domains remains unclear. Moreover, a large-scale model resolution is rarely compatible with the scales at which field data can be feasibly measured for use in model calibration. Nevertheless, the modeling tool we present here satisfactorily conforms to flow and solute mass balance, complies with current understanding of major hydrogeochemical processes, and matches the overall magnitude and trends observed in the field over a multi-year period. Hence, we conclude that it provides a comparative baseline for use in evaluating the potential impacts of various water and land BMPs designed for pollution mitigation.

Model results underscore the need to develop targeted remediation strategies to move conditions in the LARV closer to regulatory compliance. Future work is intended to apply the calibrated model to simulate pollution conditions in the region that could be expected if BMPs

were to have been implemented within the same historic period, allowing changes in pollutant concentrations and loads to be evaluated relative to the baseline. Such an analysis aims to facilitate well-informed decision-making about the prospective implementation of these BMPs in the future. Guided by results from similar studies by Bailey et al. (2015) and Shultz et al. (2018b) for managing Se and NO_3 pollution in the USR in the LARV, attention will be given in the DSR to water BMPs that include reducing irrigation on fields, selectively removing irrigation from rotationally fallowed land, and sealing canals to reduce seepage. Land BMPs will include enhancing riparian buffers and reducing N fertilizer applications. Noteworthy among the BMPs identified as showing the most promise for lowering Se and NO_3 concentrations in the USR are canal sealing as well as a combination of water and land management strategies, such as connecting canal sealing with both reduced fertilizer use and enhanced riparian buffers (Shultz et al., 2018b). A similar approach will be employed in a future assessment of these BMPs to reduce U, along with NO_3 and Se, concentrations in the LARV. Findings suggest that this methodology can be applied for assessing pollution in comparable irrigated stream-aquifer systems worldwide.

3.10. References

Abbas, S. A., Bailey, R. T., White, J. T., Arnold, J. G., White, M. J., ˇCerkasova, N., and Gao, J., 2024. A framework for parameter estimation, sensitivity analysis, and uncertainty analysis for holistic hydrologic modeling using SWAT+. Hydrology and Earth System Sciences, 28(1), 21–48. https://doi.org/10.5194/hess-28-21-2024

Abdelouas, A., Lutze, W., and Nuttall, H. E., 1999. Oxidative dissolution of uraninite precipitated on Navajo sandstone. Journal of Contaminant Hydrology, 36(3–4), 353–375. https://doi.org/10.1016/S0169-7722(98)00151-X

Abdelouas, A., 2006. Uranium mill tailings: Geochemistry, mineralogy, and environmental impact. Elements, 2(6), 335–341. https://doi.org/10.2113/gselements.2.6.335

Ajami, H., McCabe, M., Evans, J., and Stisen, S., 2014. Assessing the impact of model spin-up on surface water-groundwater interactions using an integrated hydrologic model. Water Resources Research, 50. https://doi.org/10.1002/2013WR014258

ASCE-EWRI., 2005. The ASCE standardized reference evapotranspiration equation. American Society of Civil Engineers. https://doi.org/10.1061/9780784408056

Asic, A., Kurtovic-Kozaric, A., Besic, L., Mehinovic, L., Hasic, A., Kozaric, M., Hukic, M., and Marjanovic, D., 2017. Chemical toxicity and radioactivity of depleted uranium: The evidence from in vivo and in vitro studies. Environmental Research, 156(December 2016), 665–673. https://doi.org/10.1016/j.envres.2017.04.032

Askar, A. H., White, J. T., and Illangasekare, T. H., 2023. Identifying the source settings of deep brine leakage from CO2 geological repositories using observations from shallow overlying formations. Advances in Water Resources, 179(July), 104505. https://doi.org/10.1016/j.advwatres.2023.104505

Asta, M. P., Beller, H. R., and O'Day, P. A., 2020. Anaerobic dissolution rates of u(iv)-oxide by abiotic and nitrate-dependent bacterial pathways. Environmental Science and Technology, 54(13), 8010–8021. https://doi.org/10.1021/acs.est.0c01019

Bailey, R. T., Hunter, W. J., and Gates, T. K., 2012. The influence of nitrate on selenium in irrigated agricultural groundwater systems. Journal of Environment Quality, 41(3), 783. https://doi.org/10.2134/jeq2011.0311

Bailey, R. T., Morway, E. D., Niswonger, R. G., and Gates, T. K., 2013a. Modeling variably saturated multispecies reactive groundwater solute transport with MODFLOW-UZF and RT3D. Groundwater, 51(5), 752–761. https://doi.org/10.1111/j.1745-6584.2012.01009.x

Bailey, R. T., Gates, T. K., and Halvorson, A. D., 2013b. Simulating variably-saturated reactive transport of selenium and nitrogen in agricultural groundwater systems. Journal of Contaminant Hydrology, 149, 27–45. https://doi.org/10.1016/j.jconhyd.2013.03.001

Bailey, R. T., and Ahmadi, M., 2014. Spatial and temporal variability of in-stream water quality parameter influence on dissolved oxygen and nitrate within a regional stream network. Ecological Modelling, 277, 87–96. https://doi.org/10.1016/j.ecolmodel.2014.01.015

Bailey, R. T., Gates, T. K., and Ahmadi, M., 2014. Simulating reactive transport of selenium coupled with nitrogen in a regional-scale irrigated groundwater system. Journal of Hydrology, 515, 29–46. https://doi.org/10.1016/j.jhydrol.2014.04.039

Bailey, R. T., Gates, T. K., and Romero, E. C., 2015a. Assessing the effectiveness of land and water management practices on nonpoint source nitrate levels in an alluvial stream-aquifer system. Journal of Contaminant Hydrology, 179(3), 102–115. https://doi.org/10.1016/j.jconhyd.2015.05.009

Bailey, R. T., Romero, E. C., and Gates, T. K., 2015b. Assessing best management practices for remediation of selenium loading in groundwater to streams in an irrigated region. Journal of Hydrology, 521, 341–359. https://doi.org/10.1016/j.jhydrol.2014.11.079

Bailey, R. T., and Hosseini, P., 2023. Comprehensive simulation of salinity transport in irrigated watersheds using an updated version of SWAT-MODFLOW. Environmental Modelling and Software, 159(March 2022), 105566. https://doi.org/10.1016/j.envsoft.2022.105566

Barkmann, P. E., Palkovic, M. J., Sebol, L. A., Broes, L. D., Bird, K. S., Gates, T. K., Bailey, R. T., Cox, J. T., Underwood, E. N., and Diker, K., 2021. Natural sources of mobile uranium in the downstream reach of Colorado ' s Arkansas River Valley and Evaluation of Best Management Practices for Mitigation.

Bern, C. R., and Stogner, R. W., 2017. The Niobrara Formation as a challenge to water quality in the Arkansas River, Colorado, USA. Journal of Hydrology: Regional Studies, 12(April), 181–195. https://doi.org/10.1016/j.ejrh.2017.05.001

Bern, C. R., Holmberg, M. J., and Kisfalusi, Z. D., 2020. Salt flushing, salt storage, and controls on selenium and uranium: a 31-year mass-balance analysis of an irrigated, semiarid valley. JAWRA Journal of the American Water Resources Association, 56(4), 647–668. https://doi.org/10.1111/1752-1688.12841

Böhlke, J. K., Verstraeten, I. M., and Kraemer, T. F., 2007. Effects of surface-water irrigation on sources, fluxes, and residence times of water, nitrate, and uranium in an alluvial aquifer. Applied Geochemistry, 22(1), 152–174. https://doi.org/10.1016/j.apgeochem.2006.08.019

Brier, G. W., 1950. Verification of forecasts expressed in terms of probability. Monthly Weather Review, 78(1), 1–3. https://doi.org/10.1175/1520-0493(1950)078<0001:vofeit>2.0.co;2

Brooks, S. C., Fredrickson, J. K., Carroll, S. L., Kennedy, D. W., Zachara, J. M., Plymale, A. E., Kelly, S. D., Kemner, K. M., and Fendorf, S., 2003. Inhibition of bacterial U(VI) reduction by calcium. Environmental Science and Technology, 37(9), 1850–1858. https://doi.org/10.1021/es0210042

Brown, L.C., Barnwell, T.O., 1987. The Enhanced stream water quality models QUAL2E and QUAL2E-UNCAS: Documentation and User Manual EPA/600/3-87/

007. U.S. Environmental Protection Agency, Environmental Research Laboratory, Athens, GA.

Burow, K. R., Belitz, K., Dubrovsky, N. M., and Jurgens, B. C., 2017. Large decadal-scale changes in uranium and bicarbonate in groundwater of the irrigated western U.S. Science of the Total Environment, 586, 87–95. https://doi.org/10.1016/j.scitotenv.2017.01.220

Bzour, A. F., Khoury, H. N., and Oran, S. A., 2017. Uptake of arsenic (As), cadmium (Cd), chromium (Cr), selenium (Se), strontium (Sr), vanadium (V) and uranium (U) by wild plants in Khan Al-Zabib area/Central Jordan. Jordan J Earth Environ Sci, 8(1), 45–53.

Chen, Y., and Oliver, D. S., 2013. Levenberg-Marquardt forms of the iterative ensemble smoother for efficient history matching and uncertainty quantification. Computational Geosciences, 17(4), 689–703. https://doi.org/10.1007/s10596-013-9351-5

Clement, T.P., 1997. RT3D-A modular computer code for simulating reactive multi-species transport in 3-dimensional groundwater aquifer. Draft report. PNNL-SA-28967. Pacific Northwest National Laboratory, Richland, Washington: Pacific Northwest National Laboratory

Cooley, R.L., Naff, R.L., 1990. Regression modeling of ground-water flow: U.S. Geological Survey Techniques in Water-Resources Investigations, Book 3, Chap B4, 232p. . http://pubs.usgs.gov/twri/twri3-b4/

Craft, E. S., Abu-Qare, A. W., Flaherty, M. M., Garofolo, M. C., Rincavage, H. L., and Abou-Donia, M. B., 2004. Depleted and natural uranium: Chemistry and toxicological effects. In Journal of Toxicology and Environmental Health - Part B: Critical Reviews (Vol. 7, Issue 4, pp. 297–317). https://doi.org/10.1080/10937400490452714

Curtis, G. P., Davis, J. A., and Naftz, D. L., 2006. Simulation of reactive transport of uranium(VI) in groundwater with variable chemical conditions. Water Resources Research, 42(4), 1–15. https://doi.org/10.1029/2005WR003979

Darton, N. H., 1906. Geology and underground waters of the Arkansas Valley in eastern Colorado: USGS Professional Paper 52, 90 p

Delottier, H., Doherty, J., and Brunner, P., 2023. Data space inversion for efficient uncertainty quantification using an integrated surface and sub-surface hydrologic model. Geoscientific Model Development, 16(14), 4213–4231. https://doi.org/10.5194/gmd-16-4213-2023

Doherty, J., 2002. Manual for PEST, fifth ed. Watermark numerical computing, Brisbane, Australia.

Doherty, J., 2003. Ground water model calibration using pilot points and regularization. Ground Water 41 (2), 170–177.

Doherty, J., Welter, D., 2010. A short exploration of structural noise. Water Resour. Res. 46 (5), http://dx.doi.org/10.1029/2009WR008377

Doherty, J., 2016. PEST user manual. Watermark numerical computing, Brisbane, Queensland, Australia.

Dosskey, M. G., Vidon, P., Gurwick, N. P., Allan, C. J., Duval, T. P., and Lowrance, R., 2010. The role of riparian vegetation in protecting and improving chemical water quality in streams. Journal of the American Water Resources Association, 46(2), 261–277. https://doi.org/10.1111/j.1752-1688.2010.00419.x

Duhan, S. S., Khyalia, P., Solanki, P., and Laura, J. S., 2023. Uranium sources, uptake, translocation in the soil-plant system and its toxicity in plants and humans: A Critical Review. Oriental Journal Of Chemistry, 39(2), 303–319. https://doi.org/10.13005/ojc/390210

EFSA., 2009. Uranium in foodstuffs, in particular mineral water. EFSA Journal, 7(4). https://doi.org/10.2903/j.efsa.2009.1018

Finneran, K. T., Housewright, M. E., and Lovley, D. R., 2002. Multiple influences of nitrate on uranium solubility during bioremediation of uranium-contaminated subsurface sediments. Environmental Microbiology, 4(9), 510–516. https://doi.org/10.1046/j.1462-2920.2002.00317.x

Fleeger, J. W., Carman, K. R., and Nisbet, R. M., 2003. Indirect effects of contaminants in aquatic ecosystems. In Science of the Total Environment (Vol. 317, Issues 1–3, pp. 207–233). Elsevier. https://doi.org/10.1016/S0048-9697(03)00141-4

Fox, P. M., Davis, J. A., Hay, M. B., Conrad, M. E., Campbell, K. M., Williams, K. H., and Long, P. E., 2012. Rate-limited U(VI) desorption during a small-scale tracer test in a heterogeneous uranium-contaminated aquifer. Water Resources Research, 48(5), 1–18. https://doi.org/10.1029/2011WR011472

Fredrickson, J. K., Zachara, J. M., Kennedy, D. W., Duff, M. C., Gorby, Y. A., Li, S. M. W., and Krupka, K. M., 2000. Reduction of U(VI) in goethite (α-FeOOH) suspensions by a dissimilatory metal-reducing bacterium. Geochimica et Cosmochimica Acta, 64(18), 3085–3098. https://doi.org/10.1016/S0016-7037(00)00397-5

Gates, T. K., Cody, B. M., Donnelly, J. P., Herting, A. W., Bailey, R. T., and Mueller Price, J., 2009. Assessing selenium contamination in the irrigated stream–aquifer system of the Arkansas River, Colorado. Journal of Environmental Quality, 38(6), 2344–2356. https://doi.org/10.2134/jeq2008.0499

Gates, T. K., Garcia, L. A., Hemphill, R. A., Morway, E. D., and Elhaddad, A., 2012. Irrigation practices, water consumption, and return flows in Colorado's Lower Arkansas River Valley. 221, 116.

Gates, T. K., Steed, G. H., Niemann, J. D., and Labadie, J. W., 2016. Data for improved water management in Colorado's Arkansas River Basin: hydrological and water quality studies. Colorado Water Institute Special Report No. 24, 24, 122.

Gates, T. K., Cox, J. T., and Morse, K. H., 2018. Uncertainty in mass-balance estimates of regional irrigation-induced return flows and pollutant loads to a river. Journal of Hydrology: Regional Studies, 19(June), 193–210. https://doi.org/10.1016/j.ejrh.2018.09.004

Gavrilescu, M., Pavel, L. V., and Cretescu, I., 2009. Characterization and remediation of soils contaminated with uranium. Journal of Hazardous Materials, 163(2–3), 475–510. https://doi.org/10.1016/j.jhazmat.2008.07.103

Ginder-Vogel, M., and Fendorf, S., 2007. Chapter 11 Biogeochemical uranium redox transformations: potential oxidants of uraninite. Developments in Earth and Environmental Sciences, 7(07), 293–319. https://doi.org/10.1016/S1571-9197(07)07011-5

Gupta, H. V, Wagener, T., and Liu, Y., 2008. Reconciling theory with observations: elements of a diagnostic approach to model evaluation. Hydrological Processes, 22(18), 3802–3813. https://doi.org/https://doi.org/10.1002/hyp.6989

Harbaugh, A. W., 2005. MODFLOW-2005, The U.S. Geological Survey modular ground-water model — the ground-water flow process: U.S. Geological Survey Techniques and Methods 6-A16. In Modeling techniques. http://water.usgs.gov/software/ground_water.html/.

Hay, M. B., Stoliker, D. L., Davis, J. A., and Zachara, J. M., 2011. Characterization of the intragranular water regime within subsurface sediments: Pore volume, surface area, and mass transfer limitations. Water Resources Research, 47(10). https://doi.org/10.1029/2010WR010303

Hunt, R. J., Feinstein, D. T., Pint, C. D., and Anderson, M. P., 2006. The importance of diverse data types to calibrate a watershed model of the Trout Lake Basin, Northern Wisconsin, USA. Journal of Hydrology, 321(1), 286–296. https://doi.org/https://doi.org/10.1016/j.jhydrol.2005.08.005

Ivahnenko, T., Ortiz, R. F., and Robert W. Stogner, S., 2012. Characterization of streamflow, water quality, and instantaneous dissolved solids, selenium, and uranium loads in selected reaches of the Arkansas River, southeastern Colorado, 2009-2010. In Scientific Investigations Report.

Jemison, N. E., Bizjack, M. T., Johnson, T. M., and Druhan, J. L., 2020. Influence of physical and chemical hydrology on bioremediation of a U-contaminated aquifer informed by reactive transport modeling incorporating 238U/235U ratios. Geochimica et Cosmochimica Acta, 269, 303–328. https://doi.org/10.1016/j.gca.2019.10.031

Johnson, R. H., Kent, R. D., Tigar, A. D., Richardson, C. D., Paradis, C. J., and Reimus, P. W., 2023. Cross-hole and vadose-zone infiltration tracer test analyses to determine aquifer reactive transport parameters at a former uranium mill site (Grand Junction, Colorado). Minerals, 13(7). https://doi.org/10.3390/min13070947

Jurgens, B. C., Fram, M. S., Belitz, K., Burow, K. R., and Landon, M. K., 2010. Effects of groundwater development on uranium: Central Valley, California, USA. Ground Water, 48(6), 913–928. https://doi.org/10.1111/j.1745-6584.2009.00635.x

Kansas department of health and environment, KDHE., 2024. Data requested by the author on January 11, 2024 from the website https://khap2.kdhe.state.ks.us/KORARequestForm/KORARequestForm.aspx

Kent, R. D., Johnson, R. H., Laase, A. D., and Nyman, J. L., 2024. Modeling evaluation of the impact of residual source material on remedial time frame at a former uranium mill site. Journal of Contaminant Hydrology, 261(January), 104298. https://doi.org/10.1016/j.jconhyd.2024.104298

Knoben, W. J. M., Freer, J. E., and Woods, R. A., 2019. Technical note: Inherent benchmark or not? Comparing Nash-Sutcliffe and Kling-Gupta efficiency scores. Hydrology and Earth System Sciences, 23(10), 4323–4331. https://doi.org/10.5194/hess-23-4323-2019

Konikow, L. F., 2011. The secret to successful solute-transport modeling. Groundwater, 49(2), 144-159. https://doi.org/10.1111/j.1745-6584.2010.00764.x

Landis, E. R., 1959. Radioacti'Vity and uranium content of the Sharon Springs member of the Pierre shale and associated rocks in western Kansas and eastern Colorado Trace Elements Investigations Report 573.

Langmuir, D., 1978. Uranium solution-mineral equilibria at low temperatures with applications to sedimentary ore deposits. Geochimica et Cosmochimica Acta, 42(6 PART A), 547–569. https://doi.org/10.1016/0016-7037(78)90001-7

Liesch, T., Hinrichsen, S., and Goldscheider, N., 2015. Uranium in groundwater - fertilizers versus geogenic sources. Science of the Total Environment, 536, 981–995. https://doi.org/10.1016/j.scitotenv.2015.05.133

Lopez, A. M., Wells, A., and Fendorf, S., 2021. Soil and aquifer properties combine as predictors of groundwater uranium concentrations within the Central Valley, California. Environmental Science and Technology, 55(1), 352–361. https://doi.org/10.1021/acs.est.0c05591

Lovley, D. R., Phillips, E. J. P., Gorby, Y. A., and Landa, E. R., 1991. Microbial reduction of uranium. Nature, 350(6317), 413–416. https://doi.org/10.1038/350413a0

Ma, R., Zheng, C., Liu, C., Greskowiak, J., Prommer, H., and Zachara, J. M., 2014. Assessment 118 of controlling processes for field-scale uranium reactive transport under highly transient flow conditions. Water Resources Research, 50(2), 1006–1024. https://doi.org/10.1002/2013WR013835

Maher, K., Bargar, J. R., and Brown, G. E., 2013. Environmental speciation of actinides. Inorganic Chemistry, 52(7), 3510–3532. https://doi.org/10.1021/ic301686d

Majumder, E. L.-W., and Wall, J. D., 2017. Uranium bio-transformations: chemical or biological processes? open journal of inorganic chemistry, 07(02), 28–60. https://doi.org/10.4236/ojic.2017.72003

Malakar, A., Ray, C., D'Alessio, M., Shields, J., Adams, C., Stange, M., Weber, K. A., and Snow, D. D., 2023. Interplay of legacy irrigation and nitrogen fertilizer inputs to spatial variability of arsenic and uranium within the deep vadose zone. Science of the Total Environment, 897(July), 165299. https://doi.org/10.1016/j.scitotenv.2023.165299

Martin, N., and White, J., 2023. Flow regime-dependent, discharge uncertainty envelope for uncertainty analysis with ensemble methods. Water (Switzerland), 15(6), 1–23. https://doi.org/10.3390/w15061133

Moriasi, D. N., Arnold, J. G., Liew, M. W. Van, Bingner, R. L., Harmel, R. D., and Veith, T. L., 2007. Model evaluation guidelines for systematic quantification of accuracy in watershed simulations. 50(3), 885–900.

Morway, E. D., and Gates, T. K., 2012. Regional assessment of soil water salinity across an intensively irrigated river valley. Journal of Irrigation and Drainage Engineering, 138(5), 393–405. https://doi.org/10.1061/(asce)ir.1943-4774.0000411

Morway, E. D., Gates, T. K., and Niswonger, R. G., 2013. Appraising options to reduce shallow groundwater tables and enhance flow conditions over regional scales in an irrigated alluvial aquifer system. Journal of Hydrology, 495, 216–237. https://doi.org/1. Journal of Hydrology, 495, 216–237. https://doi.org/10.1016/j.jhydrol.2013.04.047

Moore, C., Doherty, J., 2006. The cost of uniqueness in groundwater model calibration. Adv. in Water Resour. 29, 605–623.

Nash, J. E., and Sutcliffe, J. V., 1970. River flow forecasting through conceptual models part I — A discussion of principles. Journal of Hydrology, 10(3), 282–290. https://doi.org/10.1016/0022-1694(70)90255-6

Niswonger, R. G., Prudic, D. E., and Regan, S. R., 2006. Documentation of the unsaturated-zone flow (UZF1) package for modeling unsaturated flow between the land surface and the water table with MODFLOW-2005. U.S. Geological Survey Techniques and Methods, 71.

Niswonger, R. G., and Prudic, D. E., 2010. Documentation of the streamflow-routing (sfr2) package to include unsaturated flow beneath streams—a modification to SFR1: U.S. Geological Survey Techniques and Methods 6-A13. US Geological Survey Techniques and Methods 6, April 2010, 59. http://pubs.er.usgs.gov/publication/tm6A13

Niswonger, R. G., Panday, S., and Motomu, I., 2011. MODFLOW-NWT , A Newton formulation for MODFLOW-2005. USGS Reports, 44.

Nolan, J., and Weber, K. A., 2015. Natural uranium contamination in major u.s. aquifers linked to nitrate. Environmental Science and Technology Letters, 2(8), 215–220. https://doi.org/10.1021/acs.estlett.5b00174

Prakash, R., Bhartariya, K. G., Singh, S., Singh, K., Rajak, M., and Kaushik, Y. B., 2020. Uranium and its correlation with other geogenic contaminants in ground water of Ganga Yamuna Doab, Fatehpur District, Uttar Pradesh, India. Journal of the Geological Society of India, 95(4), 359–365. https://doi.org/10.1007/s12594-020-1444-x

Prieto-Estrada, A. E., Widdowson, M. A., and Stewart, L. D., 2023. Numerical modeling and data-worth analysis for characterizing the architecture and dissolution rates of a multicomponent dnapl source. Water Resources Research, 59(5), 1–20. https://doi.org/10.1029/2022WR034351

Riley, R. G., and Zachara, J. M., 1992. Chemical contaminants on DOE lands and selection of contaminant mixtures for subsurface science research. https://doi.org/10.2172/10147081

Rothbaum, H., McGaveston, D., Wall, T., Johnston, A., and Mattingly, G., 2006. Uranium accumulation in soils from long-continued applications of superphosphate. Journal of Soil Science, 30, 147–153. https://doi.org/10.1111/j.1365-2389.1979.tb00972.x

Runkel, R. L., and Broshears, R. E., 1991. One-dimensional transport with inflow and storage (OTIS): a solute transport model for small streams. Final Report, Univ. Colo. Center for Advanced Decision Support for Water and Environmental Systems, Boulder, Colorado.

Runkel, R. L., 1998. One-dimensional transport with inflow and storage (OTIS): a solute transport model for streams and rivers. U.S. Geological Survey WaterResources Investigation Report 98-4018, Denver, Colorado.

Sahu, M., and Gu, R. R., 2009. Modeling the effects of riparian buffer zone and contour strips on stream water quality. Ecological Engineering, 35(8), 1167–1177. https://doi.org/10.1016/j.ecoleng.2009.03.015

Sani, R., Peyton, B., Smith, W., Apel, W., and Petersen, J., 2002. Dissimilatory reduction of Cr(VI), Fe(III), and U(VI) by Cellulomonas isolates. Applied Microbiology and Biotechnology, 60(1–2), 192–199. https://doi.org/10.1007/s00253-002-1069-6

Schnug, E., and Haneklaus, N., 2015. Uranium in phosphate fertilizers – review and outlook BT - Uranium - Past and Future Challenges (B. J. Merkel and A. Arab (eds.); pp. 123–130). Springer International Publishing.

Seiler, R. L., 1995. Prediction of areas where irrigation drainage may induce selenium contamination of water. Journal of Environmental Quality, 24(5), 973–979.

Senko, J. M., Istok, J. D., Suflita, J. M., and Krumholz, L. R., 2002. In-situ evidence for uranium immobilization and remobilization. Environmental Science and Technology, 36(7), 1491–1496. https://doi.org/10.1021/es011240x

Senko, J. M., Suflita, J. M., and Krumholz, L. R., 2005. Geochemical controls on microbial nitrate-dependent U(IV) oxidation. Geomicrobiology Journal, 22(7–8), 371–378. https://doi.org/10.1080/01490450500248911

Sheppard, S. C., and Evenden, W. G., 1988. Critical compilation and review of plant/soil concentration ratios for uranium, thorium and lead. Journal of Environmental Radioactivity, 8(3), 255–285. https://doi.org/https://doi.org/10.1016/0265-931X(88)90051-3

Shultz, C. D., Bailey, R. T., Gates, T. K., Heesemann, B. E., and Morway, E. D., 2018a. Simulating selenium and nitrogen fate and transport in coupled stream-aquifer systems of irrigated regions. Journal of Hydrology. https://doi.org/10.1016/j.jhydrol.2018.02.027

Shultz, C. D., Gates, T. K., and Bailey, R. T., 2018b. Evaluating best management practices to lower selenium and nitrate in groundwater and streams in an irrigated river valley using a calibrated fate and reactive transport model. Journal of Hydrology, 566, 299–312. https://doi.org/10.1016/J.JHYDROL.2018.09.005

Singer, D., Maher, K., and Brown, G., 2009. Uranyl–chlorite sorption/desorption: evaluation of different U(VI) sequestration processes. Geochimica et Cosmochimica Acta, 73, 5989–6007. https://doi.org/10.1016/j.gca.2009.07.002

Sladkov, V., 2010. Interaction of uranyl with Se(IV) and Se(VI) in aqueous acid solutions by means of capillary electrophoresis. Electrophoresis, 31(20), 3482–3491. https://doi.org/10.1002/elps.201000247

Stewart, B. D., Mayes, M. A., and Fendorf, S., 2010. Impact of uranyl−calcium−carbonato complexes on uranium(vi) adsorption to synthetic and natural sediments. Environmental Science and Technology, 44(3), 928–934. https://doi.org/10.1021/es902194x

Stoliker, D. L., Liu, C., Kent, D. B., and Zachara, J. M., 2013. Characterizing particle-scale equilibrium adsorption and kinetics of uranium(VI) desorption from U-contaminated sediments. Water Resources Research, 49(2), 1163–1177. https://doi.org/10.1002/wrcr.20104

Stopps, G. J., and M. Todd.,1982 The chemical toxicity of uranium with special reference to effects on the kidney and the use of urine for biological monitoring. No. INFO--0074. Atomic Energy Control Board.

Singh, S., Asha Rani, Kumar Mahajan, R., and Singh Walia, T. P., 2003. Analysis of uranium and its correlation with some physico-chemical properties of drinking water samples from Amritsar, Punjab. Journal of Environmental Monitoring, 5(6), 917–921. https://doi.org/10.1039/B309493F

Szecsody, J. E., Cantrell, K. J., Krupka, K. M., Resch, C. T., Williams, M. D., and Fruchter, J. S., 1998. Uranium mobility during in situ redox manipulation of the 100 areas of the handford site. PNNL-12048, Pacific Northwest National Laboratory, Richland WA, November 1998. http://www.pnl.gov/main/publications/external/technical_reports/PNNL-12048.pdf

Tanwer, N., Arora, V., Kant, K., Singh, B., Singh Laura, J., and Khosla, B., 2023. Prevalence of uranium in groundwater of rural and urban regions of india. in water resources management for rural development: challenges and mitigation (First Edit). Elsevier Ltd. https://doi.org/10.1016/B978-0-443-18778-0.00002-7

Tavakoli, S., Bailey, R., and Gates, T., 2019. A Salinity reactive transport and equilibrium chemistry model for regional-scale agricultural groundwater systems. Journal of Hydrology, 572. https://doi.org/10.1016/j.jhydrol.2019.02.040

Thiros, S. A., Paul, A. P., Bexfield, L. M., and Anning, D. W., 2015. The quality of our nation's waters: water quality in basin-fill aquifers of the southwestern United States: Arizona, California, Colorado, Nevada, New Mexico, and Utah, 1993-2009. In Circular. https://doi.org/10.3133/cir1358

Tiedeman, C. R., and Hill, M. C., 2007. Model calibration and issues related to validation, sensitivity analysis, post-audit, uncertainty evaluation and assessment of prediction data needs. In Groundwater: Resource Evaluation, Augmentation, Contamination, Restoration, Modeling and Management (pp. 237–282). Springer Netherlands. https://doi.org/10.1007/978-1-4020-5729-8_9

U.S. Environmental Protection Agency (USEPA)., 2011. EPA radiogenic cancer risk models and projections for the US population, EPA 402-R11-001. Washington, DC: US EPA.

Ulrich, K.-U., Singh, A., Schofield, E. J., Bargar, J. R., Veeramani, H., Sharp, J. O., Bernier-Latmani, R., and Giammar, D. E., 2008. Dissolution of biogenic and synthetic UO2 under varied reducing conditions. Environmental Science andamp; Technology, 42(15), 5600—5606. https://doi.org/10.1021/es800647u

Wall, J. D., and Krumholz, L. R., 2006. Uranium reduction. annual review of microbiology, 60(1), 149–166. https://doi.org/10.1146/annurev.micro.59.030804.121357

Wei, X., and Bailey, R. T., 2021. Evaluating nitrate and phosphorus remediation in intensively irrigated stream-aquifer systems using a coupled flow and reactive transport model. Journal of Hydrology, 598(April), 126304. https://doi.org/10.1016/j.jhydrol.2021.126304

White, J. T., 2018. A model-independent iterative ensemble smoother for efficient history-matching and uncertainty quantification in very high dimensions. Environmental Modelling and Software, 109(June), 191–201. https://doi.org/10.1016/j.envsoft.2018.06.009

White, J.T., Hunt, R.J., Fienen, M.N., and Doherty, J.E., 2020, Approaches to highly parameterized inversion: PEST++ version 5, a software suite for parameter estimation, uncertainty analysis, management optimization and sensitivity analysis: U.S. Geological Survey Techniques and Methods 7C26, 52 p., https://doi.org/10.3133/tm7C26.

World Health Organization, 2001. Depleted uranium: Sources, exposure and health effects, No. WHO/SDE/PHE/01.1. World Health Organization.

Wu, W. M., Carley, J., Green, S. J., Luo, J., Kelly, S. D., Van Nostrand, J., Lowe, K., Mehlhorn, T., Carroll, S., Boonchayanant, B., Löfller, F. E., Watson, D., Kemner, K. M., Zhou, J., Kitanidis, P. K., Kostka, J. E., Jardine, P. M., and Criddle, C. S., 2010. Effects of nitrate on the stability of uranium in a bioreduced region of the subsurface. Environmental Science and Technology, 44(13), 5104–5111. https://doi.org/10.1021/es1000837

Yabusaki, S. B., Fang, Y., and Waichler, S. R., 2008. Building conceptual models of field-scale uranium reactive transport in a dynamic vadose zone-aquifer-river system. Water Resources Research, 44(12). https://doi.org/10.1029/2007WR006617

Yabusaki, S. B., Fang, Y., Williams, K. H., Murray, C. J., Ward, A. L., Dayvault, R. D., Waichler, S. R., Newcomer, D. R., Spane, F. A., and Long, P. E., 2011. Variably saturated flow and multicomponent biogeochemical reactive transport modeling of a uranium bioremediation field experiment. Journal of Contaminant Hydrology, 126(3–4), 271–290. https://doi.org/10.1016/j.jconhyd.2011.09.002

Zielinski, R. A., Asher-Bolinder, S., Meier, A. L., Johnson, C. A., and Szabo, B. J., 1997. Natural or fertilizer-derived uranium in irrigation drainage: A case study in southeastern Colorado, U.S.A. Applied Geochemistry, 12(1), 9–21. https://doi.org/10.1016/S0883-2927(96)00050-9

Zoccatelli, D., Wright, D. B., White, J. T., Fienen, M. N., and Yu, G., 2024. Precipitation uncertainty estimation and rainfall-runoff model calibration using iterative ensemble mmoothers. Advances in Water Resources, 186(August 2023), 104658. https://doi.org/10.1016/j.advwatres.2024.104658

CHAPTER 4: DISCUSSION AND CONCLUSION

4.1. Discussion

In the following, further elaboration is provided for several issues described in the Journal Article presented in Chapter 3:

- NH_4 is not prone to leaching through the unsaturated zone because of its positive charge, which causes attachment to negatively charge soil particles and inhibits its downward movement to the water table. As it moves downward through the profile, NH_4 can undergo nitrification, a process driven by nitrifying bacteria that converts it into NO_3. The movement of NH_4 can be retarded by various physical-chemical and biological processes, like sorption (including cation exchange) and microbially induced transformations (Böhlke et al. 2006) . This depends on the geochemistry of the aquifer and how groundwater flows. Studies have shown that NH_4 transport can be retarded in contaminated groundwater, leading to longer times for the aquifer to flush out NH_4 compared to other more mobile substances (Ceazan et al. 1989, DeSimone and Howes 1998, Van Breukelen et al. 2004). Ammonium oxidation, which is often associated with nitrification and possibly Mn-oxide reduction, results in the production of nitrite (NO_2) and then NO_3. The resulting NO_3 is more mobile and can leach into groundwater. This transformation of NH_4 into NO_3 can contribute to groundwater contamination issues, including interactions with substances like U.

- U is found in small amounts in phosphate-containing fertilizers. A notable increase in U content in fertilizers compared to natural soils could indicate that fertilizers introduce detectable levels of dissolved U into irrigation drainage (Zielinski et al. 1997). In the process of producing fertilizer from phosphate rock, the majority of U remains in superphosphate and phosphoric acid. This occurs through acidulation or the dissolution of phosphate rock using concentrated acids (Guimond and Windham 1975, Roessler et al. 1979). Phosphate fertilizers have been studied as a potential factor in enriching U levels in soils and groundwater. However, Zielinski et al. (1997) investigated the impact of using U-rich fertilizer over several decades on the U concentration in irrigation drainage in the LARV in Colorado and found that the contribution of fertilizer-derived U was minimal compared to naturally occurring U derived from nearby soils, some of which likely derived from shale. This suggests that while phosphate fertilizers can contain U, their long-term use does not significantly increase U levels in irrigation drainage in the LARV when compared to U naturally present in the environment and mobilized by irrigated agriculture.
- Utilizing river mass balance methods with field data on flows and concentrations can offer valuable insights into understanding the scale and scope of nonpoint source (NPS) return flows and pollutant loads along a river. By calculating river NPS inputs and outputs from or to the adjacent landscape and groundwater aquifer, a river system mass balance enables comparisons with NPS inputs to or outputs from the river that are computed using distributed parameter (DP) models for flow and mass transport processes within the landscape-aquifer system (Gates et al. 2018). Anderson et al. (2015) and Hill and Tiedeman (2007) recommend calibrating DP groundwater models against estimates of groundwater

flow, although such estimates can be uncertain, rather than solely relying on estimates of groundwater head.

Here, groundwater flows and mass loads (along with a relatively small quantity of unaccounted-for surface flows and mass loads) to the Arkansas River computed using from stochastic river mass balance models (Gates et al 2018) were used as calibration targets for groundwater return flows and mass loads computed by MODFLOW-RT3D.

- The solute mass balance in calculations performed by the RT3D package was checked for numerous randomly selected groundwater and river computational cells in the LARV DSR model, at various locations and times. Cell mass balances revealed on average less than a 1% error, in support of computational accuracy.
- A manual sensitivity analysis was conducted to discover which model parameters most affect model output. Parameter values were systematically varied from low to medium to high over expected ranges to determine the resulting relative magnitude of model-simulated variables, including calibration targets. This involved many runs testing 34 calibrated parameters, revealing that model simulations were very sensitive to 28 of them.
- The terms “calibration”, “validation”, and “verification” have sparked philosophical discussions due to the conflicting perspectives on the degree to which computational models can represent reality (Oreskes et al. 1994). The definition of model validation has prompted considerable debate within groundwater literature, as discussed by Konikow and Bredehoeft (1992), Bredehoeft and Konikow (1993, 2012), Anderson and Bates (2001), Hassan (2004a, 2004b), and Moriasi et al. (2012). Some argue that simulation models cannot be validated and can only be enhanced through invalidation (Konikow and Bredehoeft 1992). In model calibration, particularly within hydrology and environmental

modeling, a common practice is to divide available data into a calibration period and a validation (or testing) period. This approach is supported by many researchers because it helps to assess the model's predictive capability under conditions that were not used during the model development phase. However, some studies suggest using all available data for calibration, arguing that this method can optimize the model parameters better as more data points are available for comparison. Considering the large number of parameters required for calibrating field-based groundwater models, Doherty and Hunt (2010) recommend using all accessible data during the calibration process rather than reserving data for validation purposes. In this study, we utilized all data available, opting not to split the data into separate periods for calibration and testing, to ensure the best match to calibration targets over the full model simulation period. However, the calibrated model underwent an independent test using observed data from a location just outside the model's domain, specifically at the Arkansas River monitoring location at Coolidge, Kansas, situated approximately 3.6 km away from the last computational cell in the model. The average 85th percentile of simulated C_U at the last computational cell downstream is 63.2 µg/L, compared with the average 85th percentile measured value of 73.4 µg/L at the Coolidge stream gauge.

Finally, while models serve as tools for critical analysis and organizing thinking, their predictive capability is limited, and terms like validation and verification can create a false sense of confidence in model predictions. The focus should shift toward gaining a deeper understanding of hydrogeological systems with the model rather than relying solely on model validation (Konikow and Bredehoeft 1992).

4.2. Major Findings

In vast irrigated areas, water quality in aquifers and streams often suffers due to irrigation return flows interacting with fertilizers, soils, and geological factors, increasing harmful solute levels. Remediating this environmental impact is vitally important to sustaining irrigated agriculture in its crucial role of feeding the world's population.

In this dissertation, a numerical model is built to simulate flow and U, Se, and N species in a representative irrigated stream-aquifer system in the Lower Arkansas River Valley (LARV) in Colorado. Extensive irrigation practices spanning over a century have created significant challenges, relatively high NO_3 concentrations arise from fertilizer application on farmland to achieve high crop yields, potentially causing groundwater contamination that can then seep into surface water. Conversely, U and Se primarily originate from geological formations, resulting from oxidative dissolution of bedrock and shale outcrops. These contaminants pose risks to human health and negatively impact aquatic life. The LARV has been extensively monitored, providing valuable data for calibrating, and supporting a computational model for use in assessment and later mitigation.

Versions of the MODFLOW and RT3D models, incorporating a variety of subroutines, were utilized to model flow and solute transport within the study region. Incorporating the SFR and UZF routines into MODFLOW enabled the simulation of groundwater-surface water interactions. RT3D, coupled with OTIS and QUAL2E, was employed to simulate U, Se, and NO_3 chemical transport throughout the alluvial aquifer and the Arkansas River network. Calibration of both MODFLOW and RT3D involved automated and adjustments. PESTPP-iES software was utilized to fine-tune the groundwater head, streamflow, return flow and mass loading to the river, and U, Se, and NO_3 concentrations and loads within the aquifer and stream network, aligning the

model outputs with observation data over a 14-year period. PESTPP-iES output provides a representation of the uncertainty in model predictions associated with the model parameter calibration. Adoption of the minimum-error-variance set of parameter values results in a calibrated model used to provide a more complete picture of the current spatiotemporal distribution of pollutants in the LARV.

Utilizing the calibrated parameter values derived from PESTPP-iES, the application of MODFLOW-RT3D in the LARV study region demonstrates a robust agreement between modeled and observed data, showing consistent trends in flow and solute transport components. Analysis of the outcomes reveals the distribution of U, Se, and NO_3 concentrations across the region over a 14-year simulation period, highlighting hotspots, variations in peak concentrations, and critical periods when contamination levels surpass chronic standards. The RT3D-OTIS model effectively identifies areas with elevated U in groundwater and predicts stream concentrations that closely match observed values. In non-riparian aquifer zones, the average values of C_{NO_3}, C_{Se}, and C_U deviate by 8%, 23%, and 13%, respectively, from the average observed field data in monitoring wells, while the NO_3, Se, and U mass loading rates differ by around 4%, 7% and 17%, respectively, compared to estimates from river mass balance. Also, the average values of C_{NO_3}, C_{Se}, and C_U in the Arkansas River deviate by 36%, 43%, and 1%, respectively, from the average observed data in the stream sample location. Finally, simulated 85th percentile C_{NO_3}, C_{Se}, and C_U values in the Arkansas River are 1.2 mg/L, 11.3 µg/L, and 87.3 µg/L, respectively.

The model offers valuable insights into potential U contamination sources, particularly noting high concentrations near surface shale layers and in irrigation with surface water. It identifies specific areas, like near the Fort Lyon canal and other irrigation channels, where geological factors and irrigation practices combine to contribute to high U levels. Groundwater

concentrations remain relatively stable over time, while river concentrations exhibit seasonal variability, markedly higher during non-irrigation seasons.

The findings indicate substantial violations of chronic standards, necessitating targeted remediation strategies to achieve compliance. Groundwater's 85th percentile simulated C_U exceeds the standard by 627% and in the Arkansas River the standard is surpassed by 190%. Almost half of the groundwater aquifer area fails to meet standards. Se concentrations also exceed WHO and CDPHE standards, with moderate NO_3 violations.

The calibrated model used in the LARV study region for a multi-year historic period acts as a baseline to compare against in a future application of the model to evaluate land and water best management practices (BMPs) for pollution mitigation in the LARV. By simulating pollution conditions with and without these BMPs, changes in pollutant concentrations and loads can be assessed relative to baseline conditions, aiding informed decision-making for future BMP implementation.

The model presented here, like any numerical model, cannot perfectly replicate complex field conditions. Therefore, it is essential to acknowledge that the physical and chemical processes integrated into the model are broad approximations of the real processes. This is particularly notable in reactive transport models, which involve multiple parameters of movement and chemical reaction that yield concentrations spanning several orders of magnitude. As a result, these models are better suited as investigative rather than precise prediction tools. As such, the model presented here provides great value for enhanced understanding of factors that contribute to the magnitude and variability of pollutants induced by intensive irrigation and point toward possible solutions, described in Chapter 5. This approach can potentially be applied to assess pollution in similar irrigated systems globally.

Some notable limitations of the MODFLOW-RT3D model are:

i. MODFLOW legacy code

The MODFLOW model was integrated with a legacy code for irrigation water allocation to individual fields. This code generated the UZF input file. The Information Technology office at Colorado State University mandated using computers that have legacy code for security reasons since they are in Windows 7. Consequently, certain input files produced by the legacy code were manually adjusted based on experts using their domain knowledge.

ii. ADR equation limitation

The ADR equations for solutes are typically validated under controlled conditions where the environmental properties can be more easily measured and constrained. These conditions are usually representative of small scales. However, when these equations are applied to resolutions over large scales, like that in the current study, the assumptions suitable to small scales often no longer hold true. Variations in soil, topography, geology, microbiology, vegetation cover, microbiology, water sinks and sources, and other factors across larger landscapes introduce heterogeneities that can significantly affect the transport and fate of substances modeled by the ADR equation. As a result, scaling up from a smaller to more complex can contribute to errors and discrepancies between model predictions and observed data that are still not well understood. Often, calibrated values of the parameters in the ADR equations, when applied to the discretization of a system over large scales, are not easily comparable to values at small scales since they reflect adjustments to compensate for inadequacies in process representation due to model up-scaling.

iii. Soil organic matter effects

The impact of soil organic matter on U distribution in the vadose zone above the water table has not been thoroughly studied, so it is not included in our model. Also, our model does not account for the effects of manure, litter, humus, plant uptake, and fertilizers on U dynamics, currently thought to be insignificant. However, this could potentially affect U concentrations and its release into groundwater and should be examined more carefully.

iv. OTIS reactions

We assume that the U is highly soluble and mobile in streams due to strongly oxic conditions, so we did not include U chemical reactions within the stream water column. Only reactions with the stream bed were considered.

v. PESTPP-iES realizations

In our study, we utilize 500 realizations to calibrate the flow and solute transport models using PESTPP-iES. The use of additional realizations would likely enhance accuracy, especially for skewed frequency distributions, and in consideration of potential realization failures. However, this would typically necessitate the use of supercomputers or a larger array of machines. Due to resource and time constraints, we had to simplify.

vi. PESTPP sensitivity analysis

PESTPP offers a valuable tool for conducting sensitivity analysis (PESTPP-SEN). Given the large number of parameters in our model, it is an excellent tool for systematically evaluating the relative sensitivity of model predictions to the respective model parameters. However, due to time and budget constraints, the researcher explored sensitivity to model parameters manually instead.

vii. PESTPP-iES calibration routine

The MODFLOW and RT3D model packages were calibrated separately, leading to some limitations. Conducting these calibrations independently and sequentially neglects joint interactions between groundwater flow and contaminant transport, potentially leading to inconsistencies and less accurate predictions. Integrating both models in their coupled form using the PESTPP-iES ensemble method could enhance the calibration results. This approach could enhance the understanding of system interactions, leading to more reliable predictions and efficient use of computational resources.

4.3. References

Anderson, M. G., and Bates, P. D., 2001. Model validation: perspectives in hydrological science. In P. D. B. M. G. Anderson (Ed.), Model validation: perspectives in hydrological science. John Wiley andamp; Sons Ltd.

Anderson, M. P., Woessner, W. W., and Hunt, R. J., 2015. Applied groundwater modeling, 2nd Edition (2nd ed.), London. Academic Press. http://pubs.er.usgs.gov/publication/70160331

Bredehoeft, J. D., and Konikow, L. F., 1993. Ground-water models: Validate or invalidate. ground water, 31(2), 178–179. https://doi.org/10.1111/j.1745-6584.1993.tb01808.x

Bredehoeft, J. D., and Konikow, L. F., 2012. Ground-Water Models: Validate or invalidate. groundwater, 50(4), 493–495. https://doi.org/https://doi.org/10.1111/j.1745-6584.2012.00951.x

Böhlke, J. K., Smith, R. L., and Miller, D. N., 2006. Ammonium transport and reaction in contaminated groundwater: Application of isotope tracers and isotope fractionation studies. Water Resources Research, 42(5), 1–19. https://doi.org/10.1029/2005WR004349

Ceazan, M. L., Thurman, E. M., and Smith, R. L., 1989. Retardation of ammonium and potassium transport through a contaminated sand and gravel aquifer: The role of cation exchange. Environmental Science and Technology, 23(11), 1402–1408. https://doi.org/10.1021/es00069a012

DeSimone, L. A., and Howes, B. L., 1998. Nitrogen transport and transformations in a shallow aquifer receiving wastewater discharge: A mass balance approach. Water Resources Research, 34(2), 271–285. https://doi.org/10.1029/97WR03040

Doherty, J., and Hunt, R., 2010. Approaches to highly parameterized inversion: a guide to using PEST for groundwater-model calibration. U. S. Geological Survey Scientific Investigations Report 2010-5169, 70. http://pubs.usgs.gov/sir/2010/5169/

Gates, T. K., Cox, J. T., and Morse, K. H., 2018. Uncertainty in mass-balance estimates of regional irrigation-induced return flows and pollutant loads to a river. Journal of Hydrology: Regional Studies, 19(June), 193–210. https://doi.org/10.1016/j.ejrh.2018.09.004

Guimond, R. J., and Windham, S. T., 1975. Radioactivity distribution in phosphate products, by-products, effluents, and wastes. https://doi.org/10.2172/7151645

Hassan, A. E., 2004a. Validation of numerical ground water models used to guide decision making. Groundwater, 42(2), 277–290. https://doi.org/https://doi.org/10.1111/j.1745-6584.2004.tb02674.x

Hassan, A. E., 2004b. A methodology for validating numerical ground water models. groundwater, 42(3), 347–362. https://doi.org/https://doi.org/10.1111/j.1745-6584.2004.tb02683.x

Hill, M. C., and Tiedeman, C. R., 2007. Effective groundwater model calibration: With analysis of data, sensitivities, predictions, and uncertainty computer instructions for the exercises, using four U.S. Geological Survey computer programs: MODFLOW-2000 and its

Observation, Sensitivity, and Parameter-Estimation Processes; MFI2K; GW_Chart; and ModelViewer. http://water.usgs.gov/nrp/gwsoftware/MFI2K/MFI2K.html

Konikow, L. F., and Bredehoeft, J. D., 1992. Ground-water models cannot be validated. Advances in Water Resources, 15(1), 75–83. https://doi.org/10.1016/0309-1708(92)90033-X

N. Moriasi, D., N. Wilson, B., R. Douglas-Mankin, K., G. Arnold, J., and H. Gowda, P., 2012. Hydrologic and Water Quality Models: Use, Calibration, and Validation. Transactions of the ASABE, 55(4), 1241–1247. https://doi.org/https://doi.org/10.13031/2013.42265

Oreskes, N., Shrader-Frechette, K., and Belitz, K., 1994. In Models numerical and the confirmation of Earth Sciences. Science, 263(5147), 641–646.

Roessler, C. E., Smith, Z. A., Bolch, W. E., and Prince, R. J., 1979. Uranium and radium-226 in Florida phosphate materials. Health Physics, 37(3). https://journals.lww.com/health-physics/fulltext/1979/09000/uranium_and_radium_226_in_florida_phosphate.1.aspx

Tolson, B. A., and Shoemaker, C. A., 2007. Dynamically dimensioned search algorithm for computationally efficient watershed model calibration. Water Resources Research, 43(1). https://doi.org/https://doi.org/10.1029/2005WR004723

Van Breukelen, B. M., Griffioen, J., Röling, W. F. M., and Van Verseveld, H. W., 2004. Reactive transport modelling of biogeochemical processes and carbon isotope geochemistry inside a landfill leachate plume. Journal of Contaminant Hydrology, 70(3–4), 249–269. https://doi.org/10.1016/j.jconhyd.2003.09.003

Yen, H., Hoque, Y., Harmel, R. D., and Jeong, J., 2015. The impact of considering uncertainty in measured calibration/validation data during auto-calibration of hydrologic and water quality models. Stochastic Environmental Research and Risk Assessment, 29(7), 1891–1901. https://doi.org/10.1007/s00477-015-1047-z

Zielinski, R. A., Asher-Bolinder, S., Meier, A. L., Johnson, C. A., and Szabo, B. J., 1997. Natural or fertilizer-derived uranium in irrigation drainage: A case study in southeastern Colorado, U.S.A. Applied Geochemistry, 12(1), 9–21. https://doi.org/10.1016/S0883-2927(96)00050-9

CHAPTER 5: FUTURE DIRECTIONS

For future work, there are several recommendations for providing a better understanding of the LARV and similar areas with a view toward mitigating irrigation-induced pollution. These are:

1. Study the area that is immediately outside the domain of the DSR region of the LARV.

   Expanding the boundaries of the flow and reactive transport model beyond the northern and southern irrigated lands within the DSR would enhance the investigation of how geological formations and hydrologic conditions along tributary streams feeding the region influence the entering fluxes of U, Se, and NO_3. Improving the modeling of tributaries to accurately represent inputs from areas outside the irrigated valley will lead to less uncertainty in both flow dynamics and reactive transport analyses.

2. Evaluate more fully the effects of the riparian areas on U concentration.

   The impact of riparian corridors along the river and tributaries on U concentration should be more carefully studied. Riparian zones play a significant role in filtering and retaining pollutants, including U, before they reach water bodies. By assessing the riparian areas in more detail, including heterotrophic redox processes in the shallow vadose zone and plant uptake and volatilization, greater insights could be gained into their potential as natural buffers against pollution. This evaluation can inform land management strategies and conservation efforts aimed at preserving or restoring riparian zones to improve water quality and reduce U concentrations in aquatic ecosystems.

3. Include CO_3, HCO_3, and Ca chemistry in the RT3D model.

This involves directly examining how CO_3, HCO_3 anions in conjunction with the Ca cation interact with U throughout various environmental processes, such as dissolution, formation of complex ions, chemical precipitation, and sorption. Understanding the full cycle of these ions in the context of U can provide enhanced insights into its mobility, bioavailability, and potential for accumulation in different environmental compartments.

4. Evaluate the collective effectiveness of the BMPs in decreasing the contamination levels of U, Se, and NO_3 using the model developed here.

Five distinct BMPs are envisioned for application in the DSR with the aim of mitigating U, Se, and NO_3 groundwater concentrations, overall mass loading, and resulting stream concentrations. The considered BMPs encompass both water management and land management tools. Water management activities include: (1) reduced irrigation, (2) lease fallowing of agricultural land, and (3) sealing of irrigation canals. Land management tools consist of: (4) reducing fertilizer applications and (5) enhancing the riparian buffers adjacent to streams.

- Reduced irrigation entails improving irrigation practices to lower the amount of water applied to fields in excess of crop needs. This includes enhancing surface irrigation by properly grading the land surface and amending water application rates at the head of the field to reduce excess infiltration across the length of the field and surface runoff. It also could include shifting from surface irrigation to more efficient methods like sprinklers or drip irrigation. Reduced irrigation BMPs are simulated to have less irrigation water applied to fields by a specific fraction, which leads to lower the infiltration input to the UZF and reduces the calculated surface runoff from the field. The sprinkler method is more conservative since it can more

precisely apply smaller amounts of water over the field. A reduction in excess flows is expected to lower the dissolution and movement of solutes on the surface and subsurface. Consequently, there will be a decrease in the rate and quantity of solutes flowing back into streams, resulting in overall lower concentrations of solutes in the streams (Shultz et al. 2018b).

- Lease fallowing agreements allow farmers to fallow their irrigation fields and lease their water rights for a limited period (usually up to three years) to municipalities instead of transferring the water outside the agriculture domain, especially during a dry period. As with the reduced irrigation scenarios, the UZF input file will be modified to institute the removal of the applied irrigation water for fallowed fields, and ET will be changed to reflect the absence of crop demand. This is expected to diminish the mobilization and transfer of solute mass in return flows across the stream-aquifer system, resulting in decreased concentrations.
- Canal sealing could be used to decrease the rate of seepage from the earthen irrigation canals in the model domain. Polyacrylamide, or plant-derived polysaccharides like xanthan gum, has been suggested for use in agricultural contexts (Berninger et al., 2021, Lund et al 2023) and have been tested on irrigation canals in the LARV and in Pakistan (Lund et al 2021). At present, canals within the DSR are not sealed or lined, leading to a notable loss of conveyed water through seepage into groundwater. The RIV package input file, which simulated groundwater-canal interaction in the MODFLOW model (Morway et al 2013) was modified by Shultz et al (2018b) by the changing canal bed conductance to reflect several levels of canal seepage reduction during 40-year BMP simulations to

predict reduction of NO_3 and Se pollution in the LARV USR. A similar approach could be used with the model presented here to explore canal sealing impacts on U pollution. It is expected that the model will predict a similar decline in the movement and transfer of U mass across the stream-aquifer system of the DSR, resulting in decreased concentrations.

- In simulating a reduced fertilizer BMP, the amount of the N-fertilizer application to irrigated fields is to be lowered by altering the RT3D-OTIS input file. This is expected to lower simulated nitrification, thereby reducing the impact of excess NO_3 in dissolving U from shale and weathered shale and perhaps in inhibiting the chemical reduction of U(VI).
- Unlike Se, U is not known to be volatilized by plants. However, an enhanced riparian buffer strategy could increase the denitrification rate of NO_3 by extending the planted area of the riparian corridor and adding more organic carbon. This extension may facilitate the reduction of U(VI) and SeO_4 in riparian areas, thus potentially reducing the transfer of dissolved uranium in groundwater flows into the stream.

Shultz et al. (2018b) discovered an efficient combination of these classes of BMPs that resulted in reduced predicted Se and NO_3 levels in groundwater and in-stream concentrations in the USR. They found canal sealing along with reduced fertilizer application and improved riparian buffers most effective. A similar approach is proposed for analysis in the DSR using calibrated modeling of the BMPs to explore simulated concentrations of U, along with Se and NO_3, in comparison to baseline conditions.

5. Assess the general policies governing the implementation of the BMPs.

The efficacy of general policy interventions aimed at facilitating the adoption of BMPs needs to be evaluated in conjunction with a cost analysis. The predicted ability of interventions to effectively improve water and land management strategies must be considered in light of the preferences of irrigation farmers, water law and interstate compact requirements, financial implications, and other constraints. This investigation is crucial for informing the practicality of future interventions related to environmental conservation and pollution mitigation in valuable regions of irrigated agriculture like Colorado's LARV.

5.2 References

Berninger, T., Dietz, N., and González López, Ó., 2021. Water-soluble polymers in agriculture: xanthan gum as eco-friendly alternative to synthetics. Microbial Biotechnology, 14(5), 1881–1896. https://doi.org/https://doi.org/10.1111/1751-7915.13867

Lund, A. A. R., Martin, C. A., Gates, T. K., Scalia, J., and Babar, M. M. 2021. Field evaluation of a polymer sealant for canal seepage reduction. Agricultural Water Management, 106898. https://doi.org/10.1016/j.agwat.2021.106898

Lund, A. A. R. , Gates, T. K., and Scalia, J. 2023. Characterization and control of irrigation canal seepage losses: A review and perspective focused on field data. Agricultural Water Management, 289, 108516. https://doi.org/10.1016/j.agwat.2023.108516

Morway, E. D., Gates, T. K., and Niswonger, R. G., 2013. Appraising options to reduce shallow groundwater tables and enhance flow conditions over regional scales in an irrigated alluvial aquifer system. Journal of Hydrology, 495, 216–237. https://doi.org/10.1016/j.jhydrol.2013.04.047

Shultz, C. D., Gates, T. K., and Bailey, R. T., 2018b. Evaluating best management practices to lower selenium and nitrate in groundwater and streams in an irrigated river valley using a calibrated fate and reactive transport model. Journal of Hydrology, 566, 299–312. https://doi.org/10.1016/J.JHYDROL.2018.09.005

APPENDIX A

SUPPLEMENTARY DATA (CHAPTER 3)

Simulating multi-year nonpoint-source uranium pollution in an irrigated stream-aquifer system

Ibraheem A. Qurban[a,b], Timothy K. Gates[a,], Eric D. Morway[c], John T. Cox[d], Jeremy T. White[e], Ryan T. Bailey[a], Michael N. Fienen[f]

[a] *Dept. of Civil and Environmental Engineering, Colorado State University, Fort Collins, CO 80523, United States,*
[b] *Dept. of Civil and Environmental Engineering, King Abdulaziz University, Jeddah, Kingdom of Saudi Arabia,*
[c] *U.S. Geological Survey, Nevada Water Science Center, Carson City, NV 89701, United States,*
[d] *W.W. Wheeler and Associates, Denver, CO 80110, United States,*
[e] *INTERA Inc., Perth, Australia*
[f] *U.S. Geological Survey, Upper Midwest Water Science Center, Madison, WI 53726, United States*

** to whom correspondence should be addressed:*

Department of Civil and Environmental Engineering
Colorado State University
1372 Campus Delivery
Fort Collins, CO 80523
office: 970-491-5043
timothy.gates @colostate.edu

Journal of Hydrology

Redox chemical reactions in an irrigated stream-aquifer system

It is common for U to form soluble complexes with CO_3 which is often found at high concentrations in groundwater, at a neutral pH of 7, and with a 30 mM HCO_3 buffer. Complexes of CO_3 with U(VI), such as $(UO_2)_2CO_3(OH)_3^-$, $UO_2CO_3^0$, $UO_2(CO_3)_2^{2-}$, and $UO_2(CO_3)_3^{4-}$, are the most soluble in oxic environments (Duff et al. 1999, Fredrickson et al. 2000, Sani et al. 2002). Duff et al. (1999) explained the biologically mediated reaction of reducing soluble U(VI) to less soluble U(IV) through organic matter. Langmuir (1978) reports that high pH plays a significant role in facilitating U(VI) adsorption to sedimentary matrices. Also, CO_3 have a considerable impact on the U sorption (Gavrilescu et al., 2009). In addition, Ca and CO_3 are considered essential factors of U bioremediation in environmental waters (Wall and Krumholz, 2006). The injection of carbon electron donors near the subsurface has shown to be effective in reducing U(VI) concentrations and mobility and transferring it to immobile U(IV) in groundwater (Lovley et al. 1991, Williams et al. 2011, Newsome et al. 2014).

Equations and numerical models for reactive U transport in an unconfined aquifer system

The autotrophic reduction is facilitated by bacteria that derive energy from the oxidation of inorganic electron donors (such as ferrous iron Fe^{2+} and reduced sulfur S) (Korom, 1992). The mobilization of U occurs due to autotrophic oxidation reactions with minerals such as uraninite. These reactions produce soluble U species, which can then be transported through the environment. In the case of uraninite, which is a mineral containing U, autotrophic oxidation reactions can occur where certain microorganisms oxidize the uraninite, releasing soluble forms of U into the surrounding environment. This process contributes to the mobility and distribution of U in natural systems. Also, $O_2$and NO_3 can influence the fate and movement of Se by oxidizing residual Se present in marine Cretaceous shale. This Se exists in the form of $FeSe_2$ where Se

replaces sulfur (S) in pyrite (FeS2), as described by Bye and Lund (1982). Heterotrophic reduction is primarily observed in surface environments with more abundant organic matter. In contrast, autotrophic reduction has the potential to take place at various subsurface depths, provided there are suitable mineral electron donors available.

The oxidation reaction that changed the solid phase U(IV) to dissolved phase U(VI) is modeled by estimating the oxidation rate from the geogenic sources in the DSR due to the autotrophic reduction of DO and NO_3. Therefore, the following equation represents the autotrophic oxidation for O_2, NO_3, and U:

$$r_{f,O_2}^{auto} = \lambda_{O_2}^{auto} C_{O_2} \left(\frac{C_{O_2}}{K_{O_2} + C_{O_2}} \right) \tag{S1}$$

$$r_{f,NO_3}^{auto} = \lambda_{NO_3}^{auto} C_{NO_3} \left(\frac{C_{NO_3}}{K_{NO_3} + C_{NO_3}} \right) \left(\frac{I_{O_2}}{I_{O_2} + C_{O_2}} \right) \tag{S2}$$

$$r_{f,U_{(VI)}}^{auto} = Y_{U:O_2} \lambda_{O_2}^{auto} C_{O_2} \left(\frac{C_{O_2}}{K_{O_2} + C_{O_2}} \right) + Y_{U:NO_3} \lambda_{NO_3}^{auto} C_{NO_3} \left(\frac{C_{NO_3}}{K_{NO_3} + C_{NO_3}} \right) \left(\frac{I_{O_2}}{I_{O_2} + C_{O_2}} \right) \tag{S3}$$

Where:

r_f^{auto} = rate of autotrophic oxidation of O_2, NO_3, and U(VI) (M_f/L_f^3T)

λ^{auto} = first-order autotrophic reduction rate constant for O_2, NO_3, and U(VI) (1/T)

K_j = Monod half-saturation constant for species j (M_f/L_f^3)

$Y_{U:O_2}$ = mass ratio of U(VI) oxidized to DO reduced based on stoichiometry (M_f/ M_f)

$Y_{U:NO_3}$ = mass ratio of U(VI) oxidized to NO_3 reduced based on stoichiometry (M_f/ M_f)

The quantity of U released during these two reactions depends on the proportion of autotrophically-reduced O_2 or NO_3 that contributes to the generation of U(VI). Additionally, this

release is influenced by the stoichiometry of the chemical Eq. (1). This latter factor is considered because the autotrophic reduction of O_2 and NO_3 leads to the release of U from the shale. Referring to Eq. (1), the ratio $Y_{U:O_2}$ is determined as 94 (238 g/32 g) and for $Y_{U:NO_3}$ calculated as 42.5 (238 g/5.6 g). It is assumed in these equations that there is abundant and unrestricted availability of $FeSe_2$ in any shale material. All other species included in the model have been fully described by Bailey et al. (2013b). First-order kinetics is applied for decomposition, mineralization, and immobilization. Moreover, for all the UZF-RT3D chemical species used, first-order Monod terms are applied, as Bailey et al. (2013b) stated. Thus, the following equation represents the heterotrophic chemical reduction for all species:

$$r_{f,O_2}^{het} = \lambda_{O_2}^{het} C_{O_2} \left(\frac{C_{O_2}}{K_{O_2} + C_{O_2}} \right) \left(\frac{CO_{2,prod}}{K_{CO_2} + CO_{2,prod}} \right) E \tag{S4}$$

$$r_{f,NO_3}^{het} = \lambda_{NO_3}^{het} C_{NO_3} \left(\frac{C_{NO_3}}{K_{NO_3} + C_{NO_3}} \right) \left(\frac{CO_{2,prod}}{K_{CO_2} + CO_{2,prod}} \right) \left(\frac{I_{O_2}}{I_{O_2} + C_{O_2}} \right) E \tag{S5}$$

$$r_{f,U(VI)}^{het} = \lambda_{U}^{het} C_{U} \left(\frac{CO_{2,prod}}{K_{CO_2} + CO_{2,prod}} \right) \left(\frac{I_{O_2}}{I_{O_2} + C_{O_2}} \right) \left(\frac{I_{NO_3}}{I_{NO_3} + C_{NO_3}} \right) E \tag{S6}$$

Where:

r_f^{het} = rate of heterotrophic reduction for O_2, NO_3, and U(VI) (M_f/L_f^3T)

λ^{het} = first-order autotrophic reduction rate constant for O_2, NO_3, and U(VI) (1/T)

$CO_{2,prod}$ = the total mass of CO_2 during the organic matter decomposition

I_{O_2} and I_{NO_3} = inhabitation constant for O_2 and NO_3, respectively, (M_f/L_f^3). This implies that the concentration species effect reaches the higher-redox species.

E [-] = environmental reduction factor for soil moisture and soil temperature

The heterotrophic chemical reduction for all other chemical species has been described by Bailey et al. (2013b).

Several software models are commonly used for this purpose to solve ADR mass balance equations for multiple reactive chemical species in groundwater. MT3DMS is used for multi-species solute transport modeling. HydroGeoChem is a comprehensive software package designed to model groundwater flow, solute transport, and geochemical reactions. PHREEQC is a versatile software package for geochemical modeling; it can simulate complex reactive transport processes. FEFLOW is a finite element-based groundwater modeling software that supports multi-species solute transport modeling with reactive transport capabilities. These software models offer various capabilities for simulating groundwater flow and reactive transport processes, allowing users to accurately model complex scenarios involving multiple reactive chemical species. The UZF-RT3D model, utilizing the U module, was applied at the LARV. The grid employed finite difference methods, comprising one column and six layers. Each layer corresponded to a specific depth, comparing observed and simulated results.

Field Data:

Table S1. Number of groundwater and stream samples in the DSR per year for NO_3, Se, U, and TDS.

	Number of Samples							
	Groundwater				Streams			
Year	NO_3	Se	U	TDS	NO_3	Se	U	TDS
2003	42	218	-	86	14	46	-	16
2004	191	337	-	191	67	117	-	85
2005	141	288	49	142	46	97	-	46
2006	131	316	64	131	44	108	11	44
2007	173	264	-	174	73	109	-	75
2008	105	146	145	105	57	73	73	57
2009	107	109	109	107	54	54	54	54
2010	103	119	109	107	90	78	91	90
2011	28	28	28	28	57	57	57	57
2012	-	-	-	-	17	17	17	17
2013	-	-	-	-	-	-	-	-
2014	-	-	-	-	-	-	-	-
2015	30	30	24	30	3	3	3	3
2016	15	15	15	25	-	-	-	-
Total	1066	1870	543	1126	522	759	306	544

Table S2. Summary statistics for C_{NO_3}, C_{Se}, C_U, and C_{TDS} in groundwater samples gathered in the DSR and USR of the LARV.

	CDPHE standard for groundwater	Groundwater DSR			Groundwater USR		
		Average	Max	Overall 85th percentile	Average	Max	Overall 85th percentile
C_{NO_3} (mg/L)	10	3.9	86.4	6.4	4.8	66	8.46
C_{Se} (µg/L)	50	53.3	3760	58.9	76.8	1420	64.5
C_U (µg/L)	30	111.7	907	177	72	972	110.6
C_{TDS} (mg/L)	-	3357	13284	4661	2554	17420	3989

Table S3. Summary statistics for C_{NO_3}, C_{Se}, C_U, and C_{TDS} in stream samples gathered from the Arkansas River and from tributaries in the DSR and USR of the LARV.

	CDPHE standards for surface water	Arkansas River DSR				Arkansas River USR			
		N	Average	Max	Overall 85th percentile	*N*	Average	Max	Overall 85th percentile
C_{NO_3} (mg/L)	2	421	1.3	8.5	2	232	1.8	15.5	2.6
C_{Se} (µg/L)	4.6	603	12	93	17.3	233	9.6	53.2	13.9
C_U (µg/L)	30	256	61.8	252	91.3	205	19	197	29.8
C_{TDS} (mg/L)	-	439	2341	5384	3577	51	1100	3334	1993
		Arkansas River Tributaries DSR				Arkansas River Tributaries USR			
C_{NO_3} (mg/L)	2	101	1.4	5.4	2.3	38	2	4	2.9
C_{Se} (µg/L)	4.6	156	18.4	51.2	32.9	38	13.4	50.2	18
C_U (µg/L)	30	57	64.6	110	94.4	36	28	55.4	41.8

C_{TDS} (mg/L)	-	105	2731	5384	3577	12	2731	4666	3577

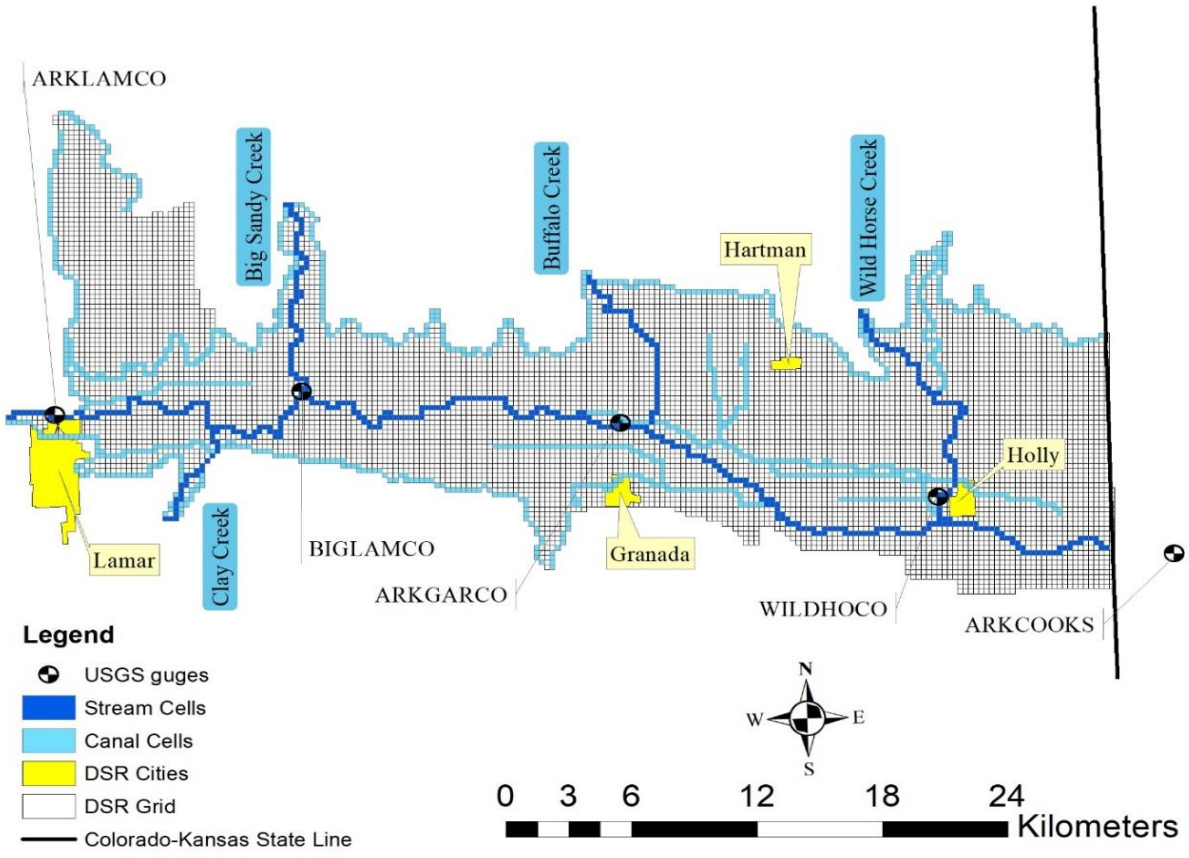

Figure S1. The finite-difference grid cells for MODFLOW, River network, tributaries, and canals.

The lower-efficiency surface irrigation systems have been replaced in many fields with higher-efficiency sprinkler and/or drip irrigation systems. The number of new irrigation systems, sprinklers, or drips, in the modeled study area doubled between 2008 to 2016, as seen in Fig. S2

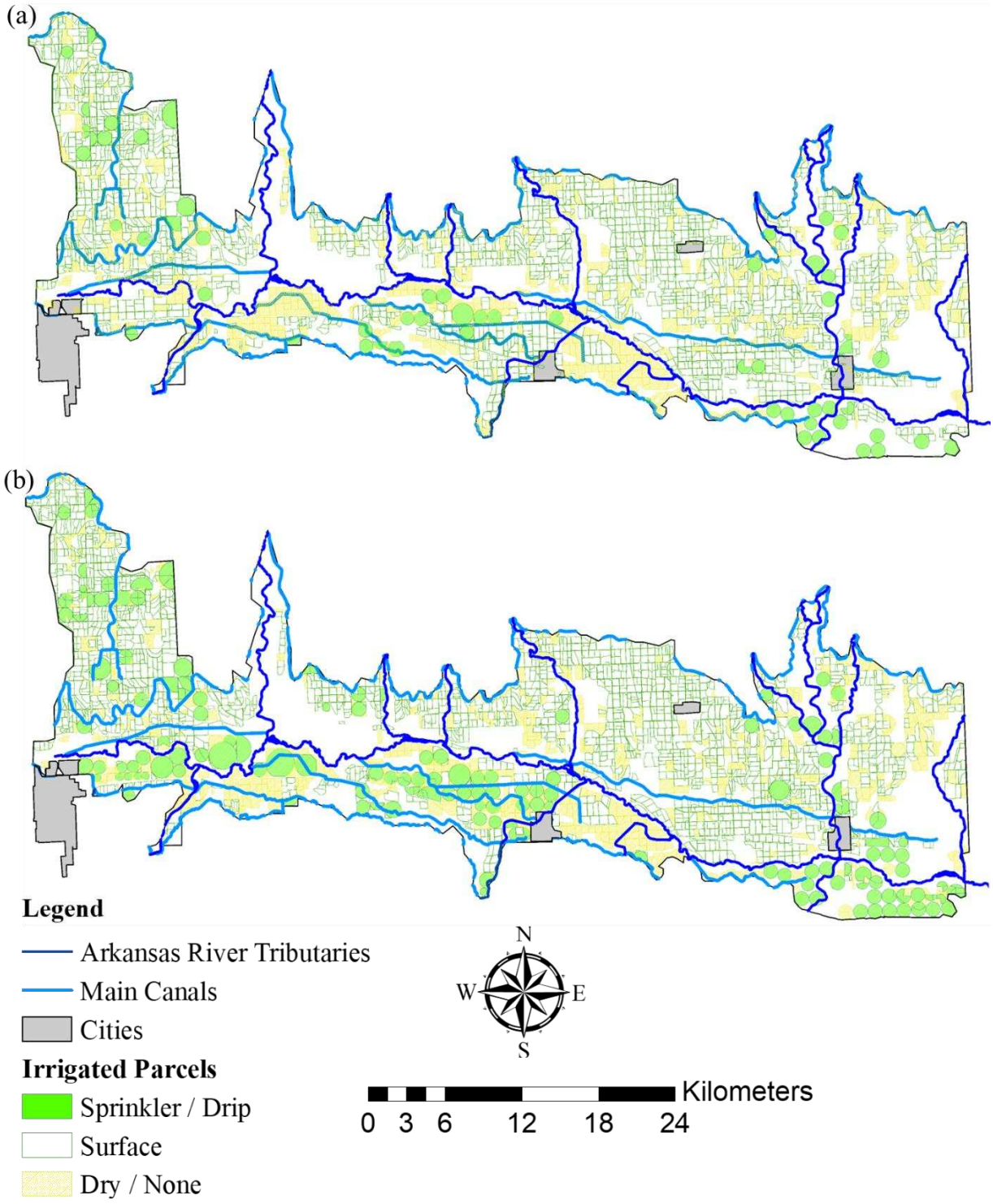

Figure S2. DSR irrigated parcel and irrigation technology, (a) 2008 and (b) 2016.

Numerical reactive transport model calibration/ PESTPP-iES

The weight that is used for RT3D-OTIS/PESTPP-iES is calcite differently than the weight in MODFLOW. The strategy for the weight is range from 0 to 1, with their total sum equal to 1. Each class corresponds to a fraction of these weights. The weight calculation process involved averaging the $w_{st_{unc_{i,j}}}$ across three main categories, multiplying them by an adjusting factor, resulting in $Adj_{w_{st_{unc_{i,j}}}}$ averages. These $Adj_{w_{st_{unc_{i,j}}}}$ were then multiplied by the $w_{st_{imp_{i,j}}}$, resulting $w_{st_{ij}}$. The $w_{st_{ij}}$ were summed across all combinations. Finally, the normalized wight is equal to $\frac{w_{st_{ij}}}{\sum_{i}^{N_{st}}\sum_{j}^{M_{st}} w_{st_{ij}}}$ to ensure commensurable units for each component in Eq. (19).

Flow Model Results

The automated PESTPP-iES provide final calibrated parameters of the MODFLOW-SFR, five parameters have been assigned to calibrate. Table S4 provides a range of each parameter. Since the SFR package is used in this model, the streambed conductivity and the groundwater return flow will be calibrated by PESTPP-iES.

Table S4. Final groundwater calibrated for the flow model parameters selected for the MODFLOW, as estimated by PESTPP-iES.

	Min	Average	Max
Kh lay 1 (m/week)	0.01	1528.6	1528.6
Kh lay 2 (m/week)	0.02	97.2	1496
Sy lay1	0.02	0.2	0.35
Sy lay2	0.03	0.2	0.35
Streambed K (m/week)	0.001	9.81	1000

PESTPP-iES provides insights into the uncertainty surrounding the MODFLOW-SFR model flow simulation within the DSR, in relation to uncertainties in estimating calibrated parameter values. In each iteration, the model is run with multi realizations of calibrated parameters, generating simulated flow values, including calibration targets and the objective function. Notably, during iteration 5 of the PESTPP-iES calibration run, the Base Realization yielded the minimum Φ_f value of 4.77E+09. Fig. S3 illustrates the parameter estimation uncertainty by representing prior and posterior frequency histograms of selected representative variables used as calibration targets. For instance, Fig. S3.a and b display prior and posterior distributions of simulated groundwater hydraulic head values at monitoring wells 359j and 328 for May 2016 and March 2015, respectively. These plots also include the calibration target values for the realization associated with the minimum Φ_f, along with observed field data for comparison. Similarly, Figs. S3.c and d show histograms for calibration targets related to total unaccounted for groundwater return flow to the Arkansas River within the DSR for October 2008 and December 2009. Additionally, Figs. S3.e and f present frequency histograms of simulated streamflow at

Granada and Coolidge for January 2007 and February 2014, respectively. The distribution spread of simulated values indicates the level of uncertainty, which notably decreases from the prior to the posterior, demonstrating how PESTPP-iES progressively refines estimated parameter values to achieve satisfactory matches with observed data across multiple targets, thus enhancing confidence in the calibration process.

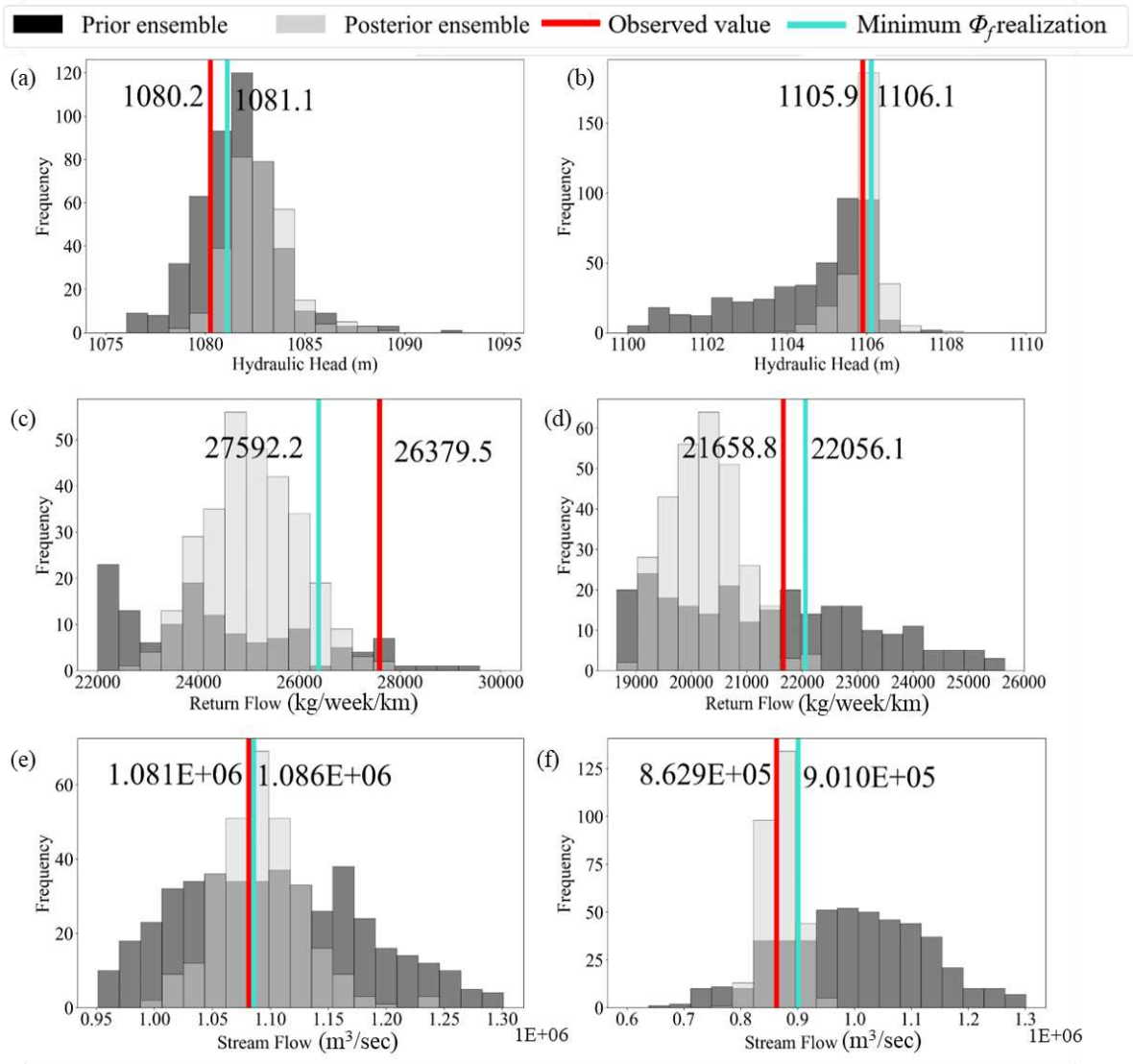

Figure S3. Prior and posterior frequency histograms of the ensemble of realizations of the values of the calibration MODFLOW-SFR target variables (a) groundwater hydraulic head well 359j, (b) groundwater hydraulic head well 328, (c) groundwater return flow October 2008, (d) groundwater return flow December 2009, (e) streamflow at Granada January 2007, and (f) streamflow at Coolidge February 2014.

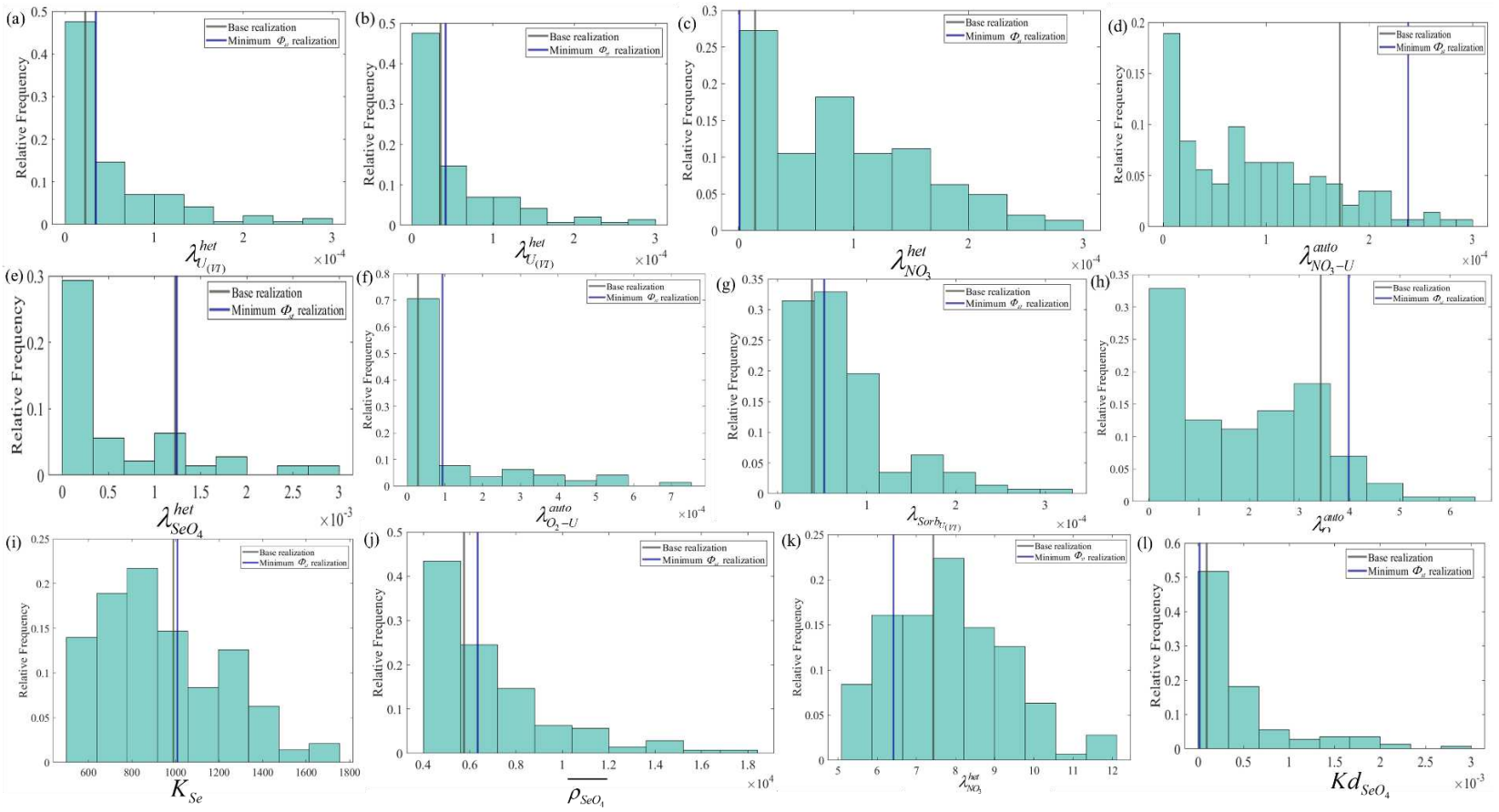

Figure S4. A comparison between the base realization and the minimum ϕ_{st} realization for random calibrated parameters over the entire region, showing the base realization aligns closely with the minimum ϕ_{st} realization. (a) riparian groundwater subregion in the south side of River segment 2, (b) non-riparian groundwater subregion 11, (c) riparian groundwater subregion in the south side of River segment 5a, (d) non-riparian groundwater subregion 1, (e) riparian groundwater subregion in the north side of River segment 4, (f) non-riparian groundwater subregion 8, (g) stream parameter over the entire River segment, (h) non-riparian groundwater subregion 1, (i) non-riparian groundwater subregion 10, (j) stream parameter in River segment 5, (k) non-riparian groundwater subregion 12, (l) stream parameter in River segment 3.

Fig. S5 illustrates the progression of uncertainty reduction for the solute transport model within the iES framework across six iterations for distinct targets. Specifically, it examines the convergence of uncertainty for C_U in groundwater sub-region 1 and C_U in river segments 2 and 6. Additionally, it analyzes the U mass loading on Apr-09. Fig. S5 displays all 500 realizations for each iteration that simulated the target. Each target is depicted with a distinct line plot, showcasing uncertainty evolution over the iterations. Initially, at iteration 0, the uncertainty for all targets is notably high, with considerable variability among the realizations. As the iterations progress, the uncertainty gradually diminishes, demonstrating the effectiveness of the iES approach in refining the model's predictions. Notably, the convergence pattern varies across targets, reflecting the unique characteristics of each simulation. The uncertainty decreases steadily across iterations for C_U in groundwater sub-region 1, indicating a consistent refinement in the model's understanding of this parameter. In contrast, C_U in river segments 2 and 6 exhibit a more fluctuating convergence pattern, likely influenced by the dynamic nature of river systems and their complex interactions with surrounding environments. The U mass loading on Apr-09 showcases a similar trend of uncertainty reduction, albeit with some variability, possibly due to factors such as temporal variations and the influence of external factors on U transport mechanisms. Overall, the figure demonstrates that observed data can influence model parameters and significantly narrow down the prior ensemble several order of magnitudes across various levels of uncertainty.

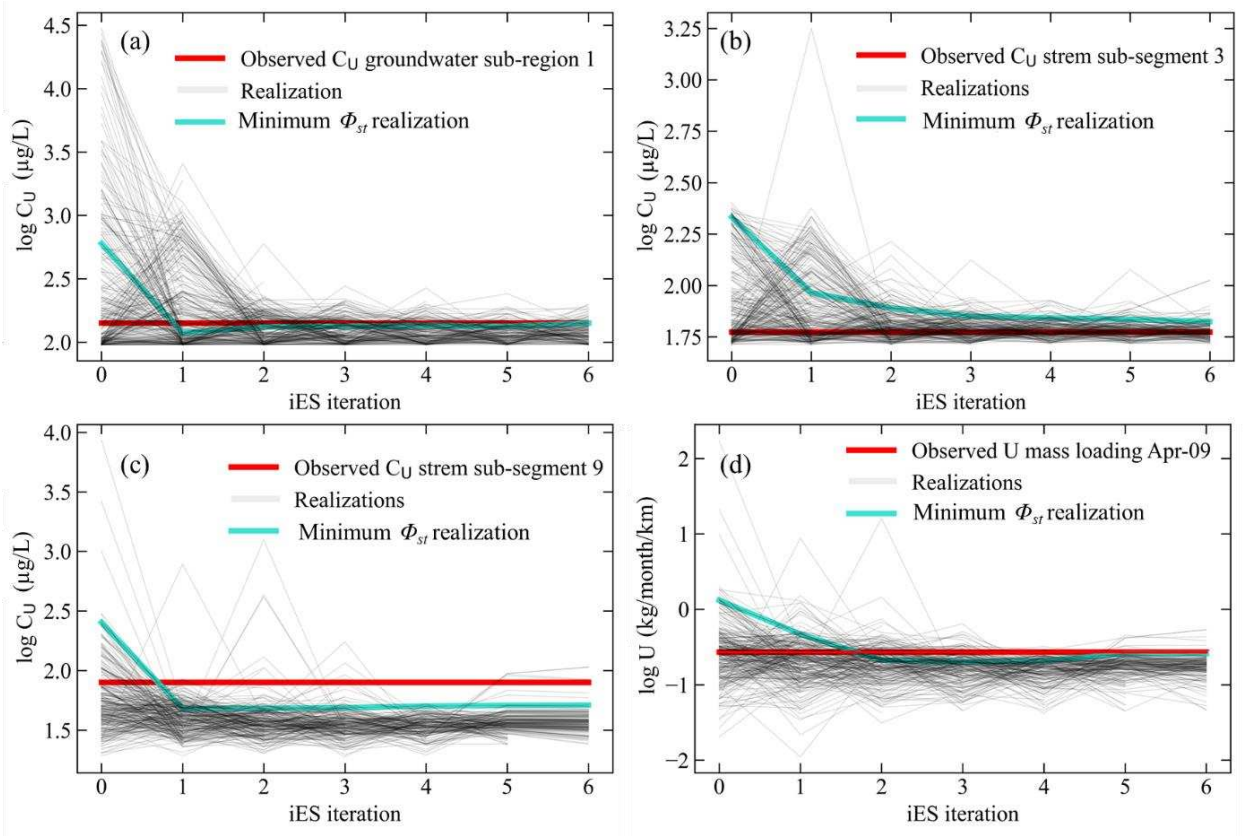

Figure S5. Simulated C_U concentrations for each iteration of PESTPP-iES over 500 realizations for (a) groundwater Sub-region 1, (b) river Segment 2, (c) river Segment 6, and (d) mass loading in April 2009. Showing the simulated and the observed values.

Table S5. Final groundwater calibrated chemical reaction parameters for the non-riparian areas selected for the RT3D aquifer, as estimated by PESTPP-iES.

Aquifer Sub-region	$\lambda_{O_2}^{auto}$ (1/day)	$\lambda_{U_{(VI)}}^{het}$ (1/day)	$\lambda_{O_2-U}^{auto}$ (1/day)	$\lambda_{NO_3-U}^{auto}$ (1/day)	$\lambda_{SeO_4}^{het}$ (1/day)	$\lambda_{SeO_3}^{het}$ (1/day)	$\lambda_{NO_3}^{auto}$ (1/day)	$\lambda_{NO_3}^{het}$ (1/day)	λ_{nit} (1/day)	K_{NO_3} (mg/L)	K_{Se} (mg/L)	$\lambda_{SeO_3}^{het(SeMet)}$ (1/day)
1	3.98E+00	1.46E-02	8.67E-07	2.10E-04	5.61E-01	6.00E-01	4.25E+00	9.21E-07	1.06E+00	7.70E+00	1.02E+03	4.38E-03
2	6.50E+00	9.27E-02	9.34E-05	5.56E-06	1.68E-05	1.03E-02	9.68E-02	3.16E-05	1.23E-01	6.65E+00	8.86E+02	2.93E-03
3	7.98E-04	2.13E-02	4.95E-05	1.28E-05	1.35E-04	9.01E-03	2.36E+00	3.53E+00	1.19E+00	1.12E+01	8.67E+02	4.90E-03
4	6.50E+00	1.03E-03	8.13E-07	1.16E-05	3.25E-03	1.31E-03	5.65E+00	6.70E-02	4.70E-01	8.55E+00	1.16E+03	4.12E-03
5	1.18E-03	1.74E-05	3.06E-07	1.87E-05	4.74E-07	7.30E-04	7.38E-02	5.30E-04	4.98E-01	5.97E+00	5.24E+02	7.37E-02
6	3.68E-07	2.54E-03	4.96E-06	1.69E-06	5.84E-01	2.46E-05	2.57E-02	6.50E+00	6.84E-01	6.36E+00	5.21E+02	6.69E-01

7	6.69E-05	2.01E-02	3.16E-07	5.80E-07	1.81E-01	1.51E-06	9.14E-04	3.19E-07	7.10E-01	5.60E+00	5.03E+02	1.79E+00
8	2.23E-04	9.95E-01	6.90E-05	2.36E-04	2.85E+00	6.00E+00	3.25E-03	3.03E+00	1.08E+00	7.56E+00	1.45E+03	8.72E-02
9	2.92E+00	9.95E-04	1.28E-04	2.69E-06	3.82E-05	6.50E+00	4.26E-01	3.59E-05	8.14E-01	5.05E+00	7.13E+02	1.29E-02
10	8.59E-03	4.94E-01	1.40E-03	3.04E-05	4.21E-06	1.67E-04	2.98E+00	2.85E-02	9.04E-01	5.00E+00	1.73E+03	1.10E-02
11	3.00E-07	1.96E-05	1.90E-04	3.03E-06	1.81E-04	2.91E-02	3.62E-04	3.08E+00	9.43E-01	8.60E+00	1.24E+03	3.86E-03
12	1.77E-05	4.97E-06	3.42E-05	3.57E-05	1.27E-05	3.47E-03	6.35E-07	1.13E+00	9.87E-01	6.42E+00	1.05E+03	5.79E-02
13	1.73E+00	2.57E-04	1.35E-04	1.31E-04	1.82E-04	2.11E-06	1.59E-03	2.44E-01	8.43E-01	8.40E+00	1.89E+03	3.30E-03
14	5.06E-02	4.06E-02	6.28E-07	2.34E-04	6.41E-03	1.87E-02	1.71E-03	2.06E-03	1.91E+00	1.41E+01	6.51E+02	6.34E-03

15	5.67E-05	4.50E-05	4.71E-06	4.91E-07	1.61E-05	3.97E-01	2.40E-03	1.37E-05	4.60E-01	7.44E+00	9.70E+02	4.66E-01

Table S6. Final groundwater calibrated chemical reaction parameters for the riparian areas selected for the RT3D aquifer, as estimated by PESTPP-iES.

Location	River Segment	$\lambda^{het}_{U_{(VI)}}$ (1/day) Riparian	$\lambda^{het}_{SeO_4}$ (1/day) Riparian	$\lambda^{het}_{SeO_3}$ (1/day) Riparian	$\lambda^{het}_{NO_3}$ (1/day) Riparian	λ_{nit} (1/day) Riparian	K_{NO_3} (mg/L) Riparian
North	1	2.01E+00	1.81E-04	7.94E-04	1.11E-05	1.88E+00	9.13E+00
South		5.61E-01	3.30E-09	7.79E-09	6.94E-08	6.50E-01	8.18E+00
North	2	3.75E-06	1.05E-08	3.00E-09	1.20E-05	8.85E-01	8.69E+00
South		1.07E-03	1.34E-07	1.08E-04	8.85E-08	1.72E+00	6.59E+00
North	3	6.00E+00	6.09E-09	4.65E-05	3.21E-01	5.02E-01	1.40E+01
South		1.24E-02	2.46E-01	2.47E-08	2.57E-07	6.00E-01	1.50E+01
North	4	6.00E+00	3.42E-09	3.07E-09	1.60E-04	4.69E-01	5.20E+00
South		3.25E-03	1.44E-06	1.41E-06	8.37E-05	1.71E+00	5.00E+00
North	5	6.00E+00	2.21E-07	1.78E-08	3.00E-09	6.22E-01	1.05E+01
South		1.05E-03	1.96E-04	1.75E-07	8.06E-06	7.20E-01	1.50E+01
North	5a	1.02E-08	3.06E-09	8.35E-09	2.48E-08	1.92E+00	1.10E+01
South		1.55E-02	8.99E-07	5.96E-06	5.08E-07	1.99E+00	1.50E+01
North	5b	1.89E-07	3.00E-09	3.00E-09	7.62E-08	6.16E-01	1.50E+01
South		2.58E+00	3.00E-09	4.65E-08	9.39E-09	1.44E+00	1.50E+01
North	5c	6.00E+00	1.15E-06	5.37E-07	4.95E-09	9.15E-01	1.40E+01
South		6.00E+00	8.09E-09	1.25E-06	6.07E-07	2.00E+00	1.50E+01
North	6	1.45E+00	3.54E+00	1.59E-03	4.11E-07	7.54E-01	1.50E+01
South		6.50E+00	4.59E-03	1.24E-08	5.59E-02	3.20E-01	5.00E+00
North	6b	6.00E+00	4.42E-02	2.28E+00	6.00E+00	4.85E-01	5.50E+00

South		6.00E+00	3.55E+00	2.71E-01	6.00E+00	6.59E-01	5.00E+00
East	Clay Creek	1.47E-08	1.58E-08	5.86E-04	1.79E-08	1.00E-01	8.10E+00
West		6.50E+00	3.02E-09	3.81E-08	1.79E-08	1.00E-01	1.35E+01
East	Big Sandy Creek	1.30E-08	3.84E-09	6.13E-08	1.72E-07	1.00E-01	5.05E+00
West		1.92E-08	3.00E-09	2.90E-08	4.60E-07	7.16E-01	1.39E+01
East	Buffalo Creel	1.46E-08	1.35E-08	3.61E-02	6.97E-09	1.68E+00	9.07E+00
West		3.47E-02	3.00E-09	1.26E-05	1.92E-08	1.00E-01	7.32E+00
East	Wild Horse Creek	3.00E-01	4.62E-09	8.74E-04	4.17E-01	1.32E+00	9.13E+00
West		3.00E-01	1.67E-07	8.79E-06	1.07E-07	3.61E-01	1.10E+01

Table S7. Final surface water calibrated chemical reaction parameters selected for the OTIS, as estimated by PESTPP-iES.

River Segment	$\overline{\rho_{U_{(VI)}}}$ (mg/L)	$\overline{\rho_{SeO_4}}$ (mg/L)	$\overline{\rho_{SeO_3}}$ (mg/L)	$Kd_{U_{(VI)}}$ (L/g)	Kd_{SeO_4} (L/g)	Kd_{SeO_3} (L/g)
1	4.28E+03	4.45E+03	5.66E+03	8.27E-03	3.11E-05	2.06E-02
2	4.03E+03	4.00E+03	1.16E+04	3.53E-03	2.38E-03	1.08E-06
3	4.70E+03	5.62E+03	6.71E+03	3.09E-03	7.17E-06	1.60E-05
4	4.00E+03	6.35E+03	8.07E+03	2.28E-03	9.35E-05	1.10E-04

5	4.32E+03	5.57E+03	6.11E+03	5.42E-03	4.91E-07	6.53E-03
Clay Creek	4.35E+03	4.77E+03	4.37E+03	3.47E-03	3.25E-04	8.67E-03
Big Sandy Creek	4.01E+03	4.65E+03	5.63E+03	4.33E-03	1.03E-04	4.90E-05
Buffalo Creek	5.79E+03	9.49E+03	7.39E+03	2.02E-03	3.88E-04	2.06E-02
Wild Horse Creek	4.02E+03	7.87E+03	4.64E+03	9.57E-03	2.52E-04	5.32E-07

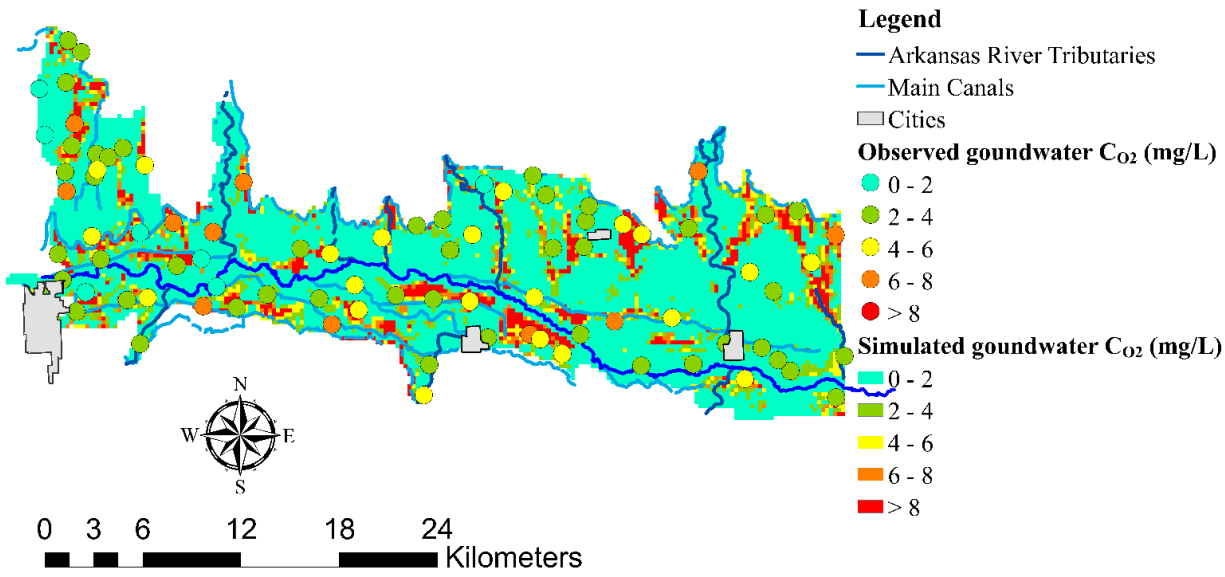

Figure S6. Average calibrated spatiotemporal groundwater concentrations of C_{O_2} compared with observed concentrations at different locations from 2003 - 2016.

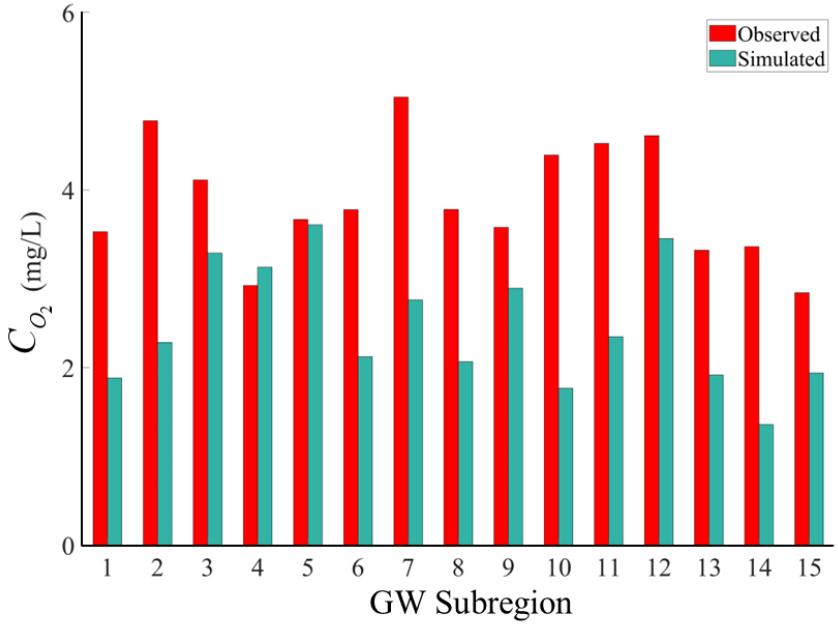

Figure S7. Average groundwater concentrations by the 15 sub-regions for observed and simulated values for the entire period for the C_{O_2}.

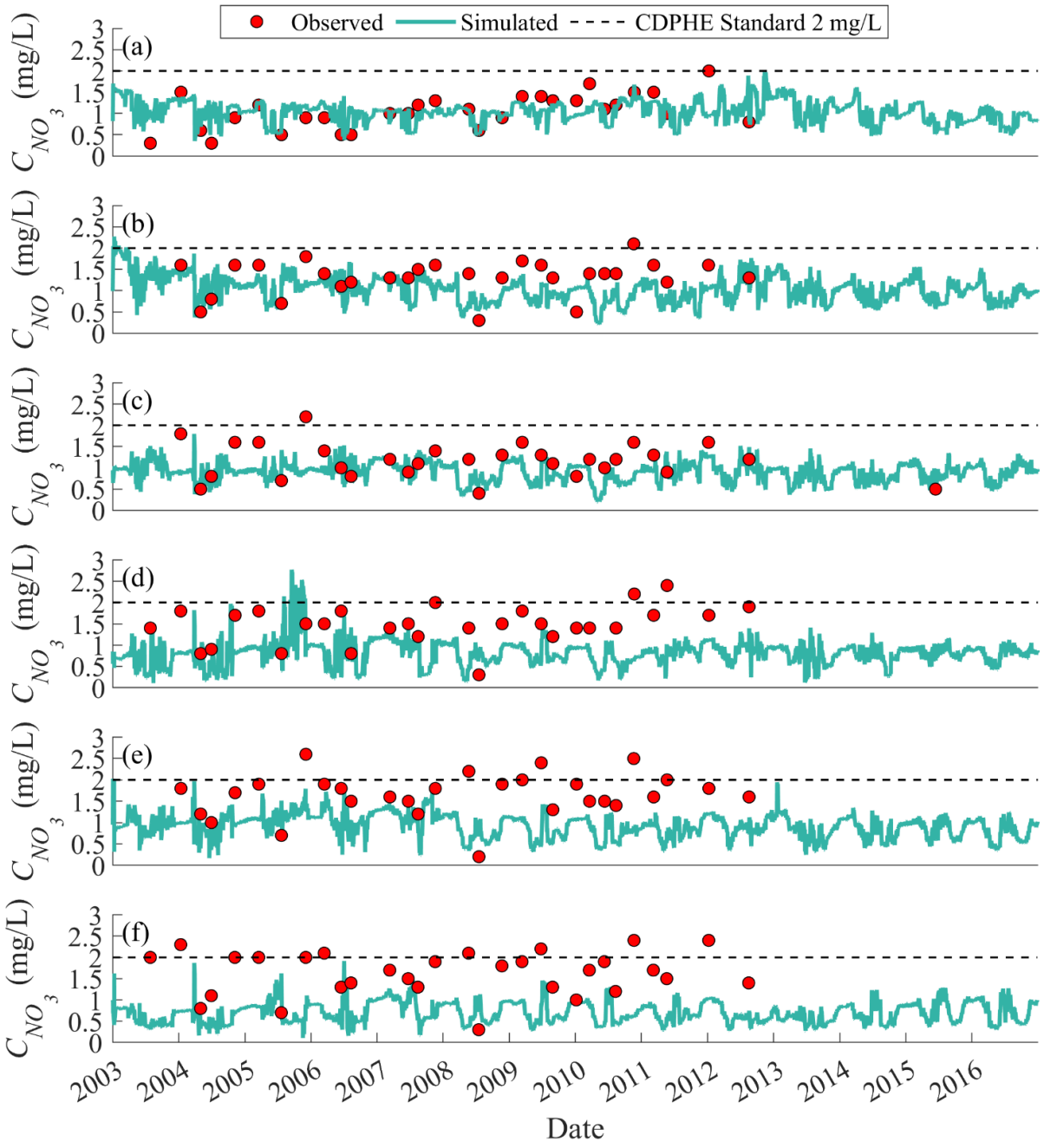

Figure S8. Simulated vs. observed river concentrations for C_{NO_3} (a) river segment 1, (b) river segment 2, (c) river segment 3, (d) river segment 4, (e) river segment 5, and (f) river segment 6 (ordered upstream to downstream) compared to CDPHE standard.

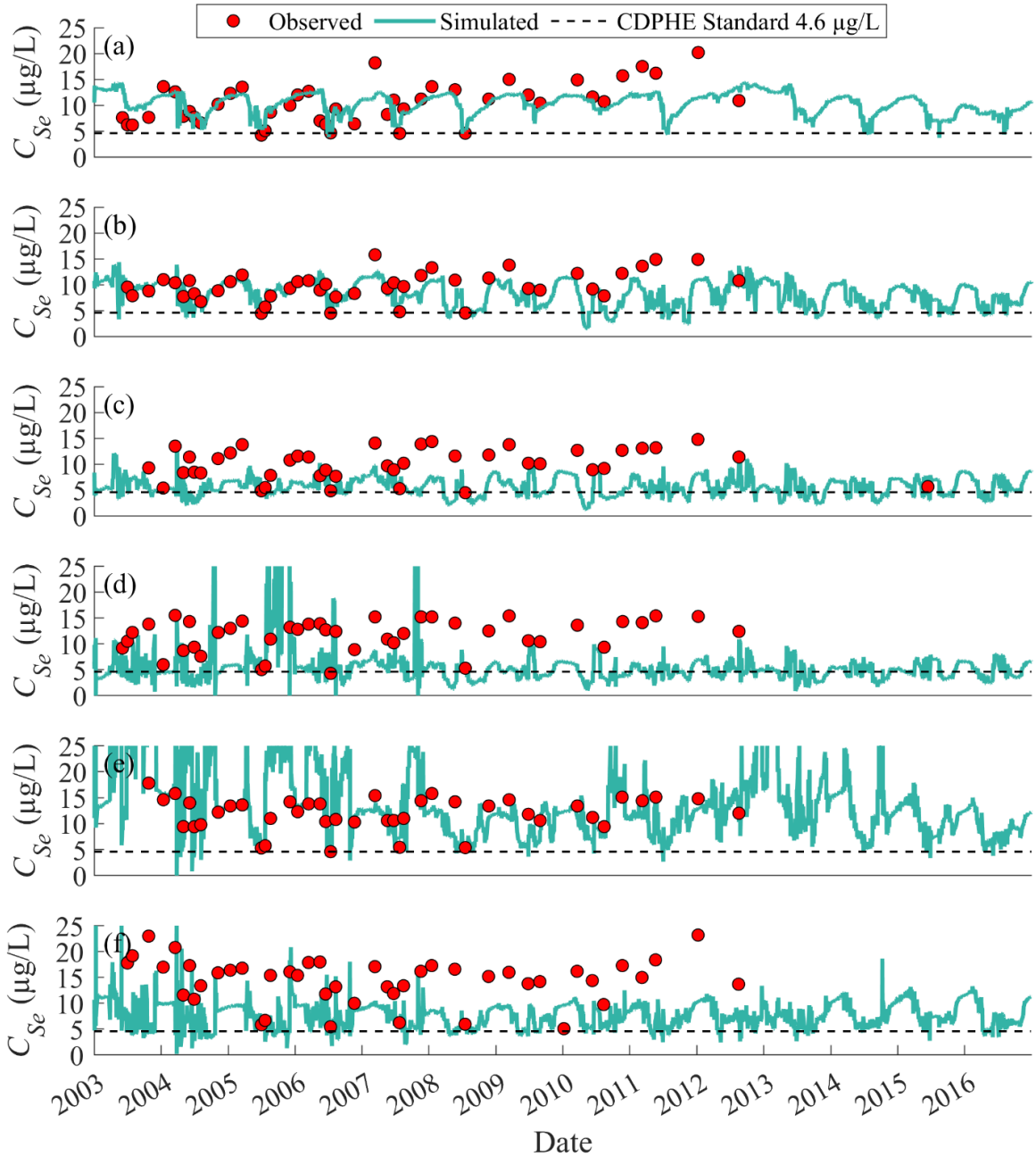

Figure S9. Simulated vs. observed river concentrations for C_{Se} (a) river segment 1, (b) river segment 2, (c) river segment 3, (d) river segment 4, (e) river segment 5, and (f) river segment 6 (ordered upstream to downstream) compared to CDPHE standard.

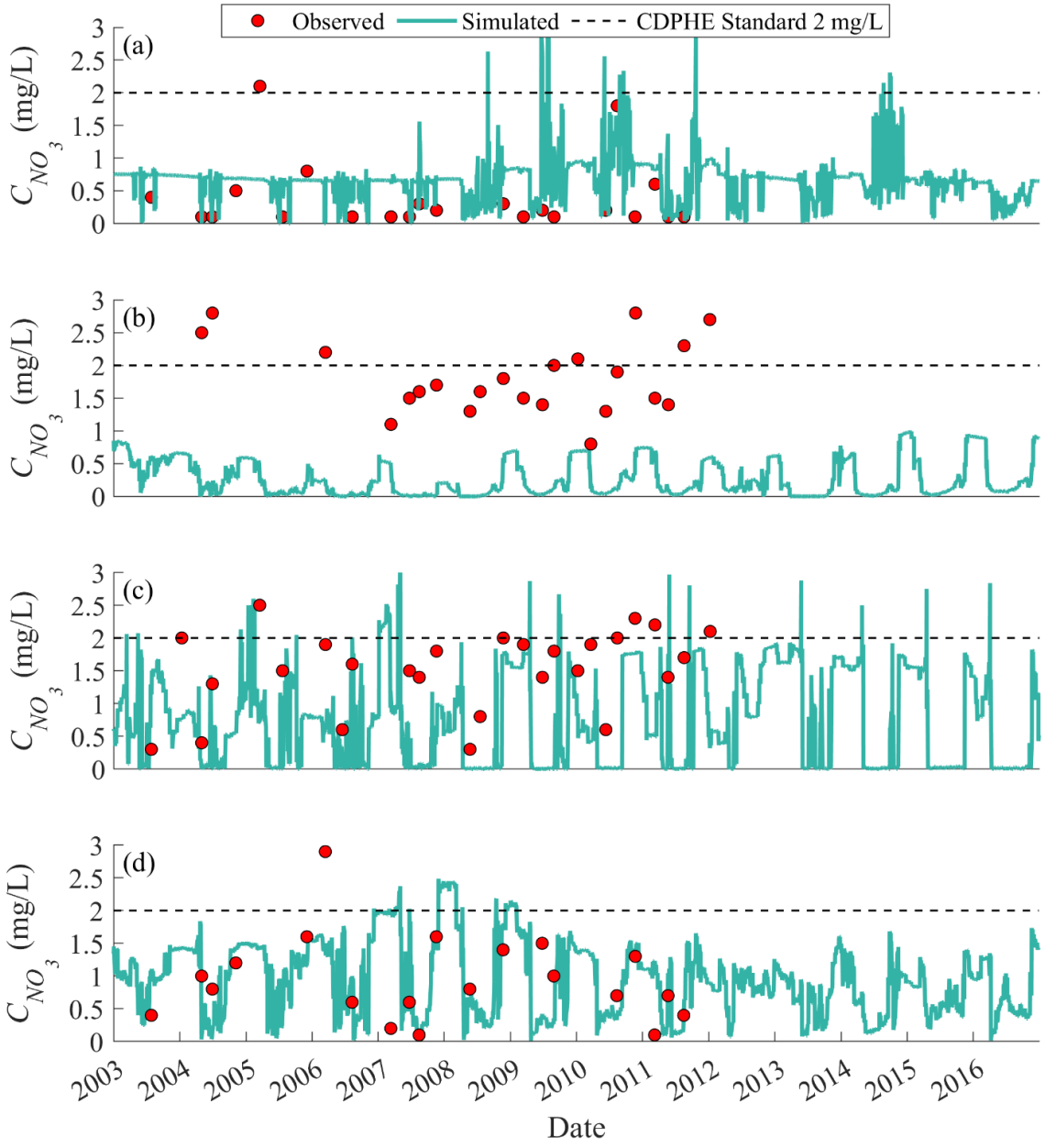

Figure S10. Simulated vs. observed river tributaries concentrations for C_{NO_3} (a) Clay Creek, (b) Big Sandy Creek, (c) Buffalo Creek, and (d) Wild Horse Creek (ordered upstream to downstream) compared to CDPHE standard.

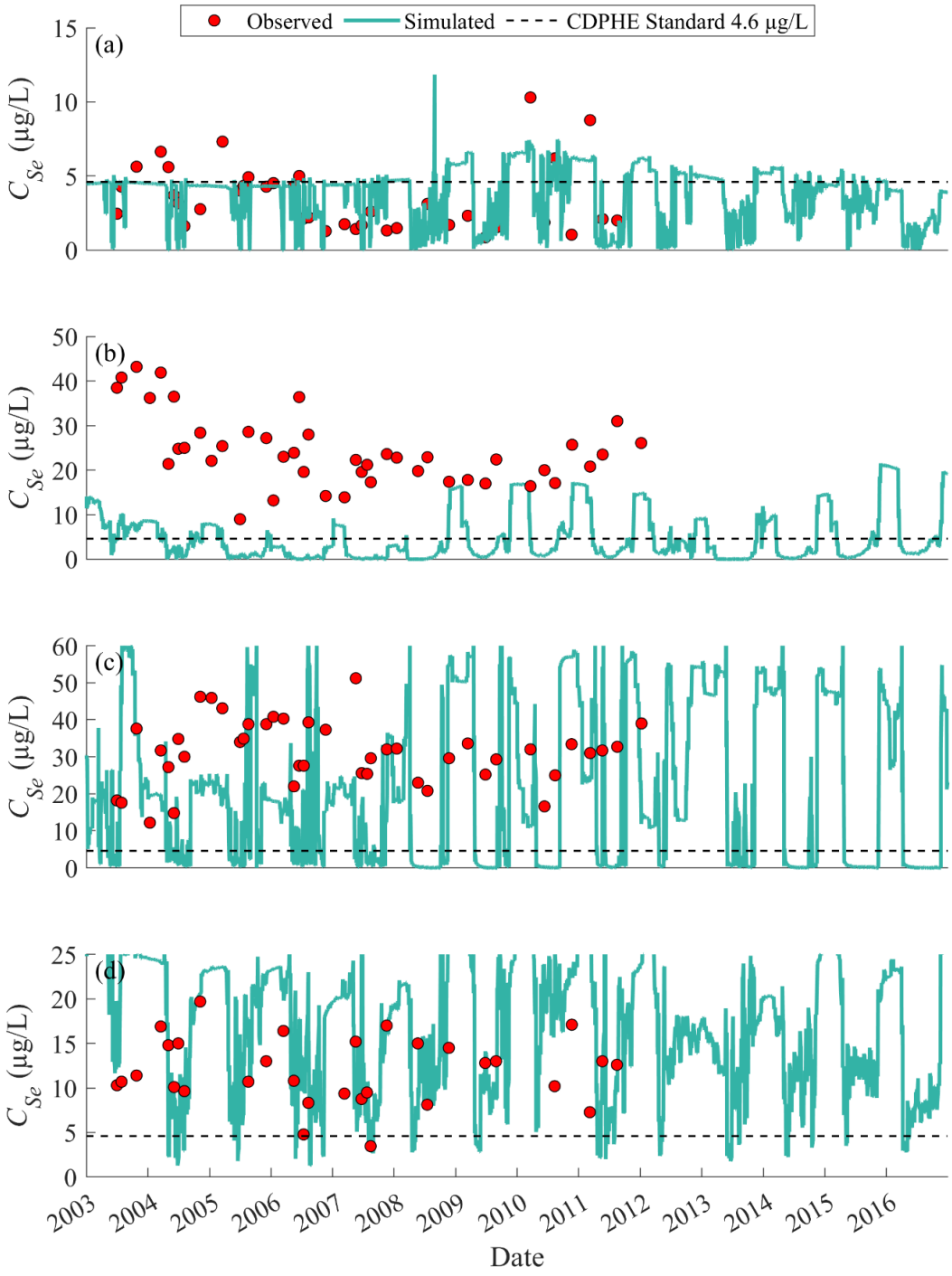

Figure S11. Simulated vs. observed river tributaries concentrations for C_{Se} (a) Clay Creek, (b) Big Sandy Creek, (c) Buffalo Creek, and (d) Wild Horse Creek (ordered upstream to downstream) compared to CDPHE standard.

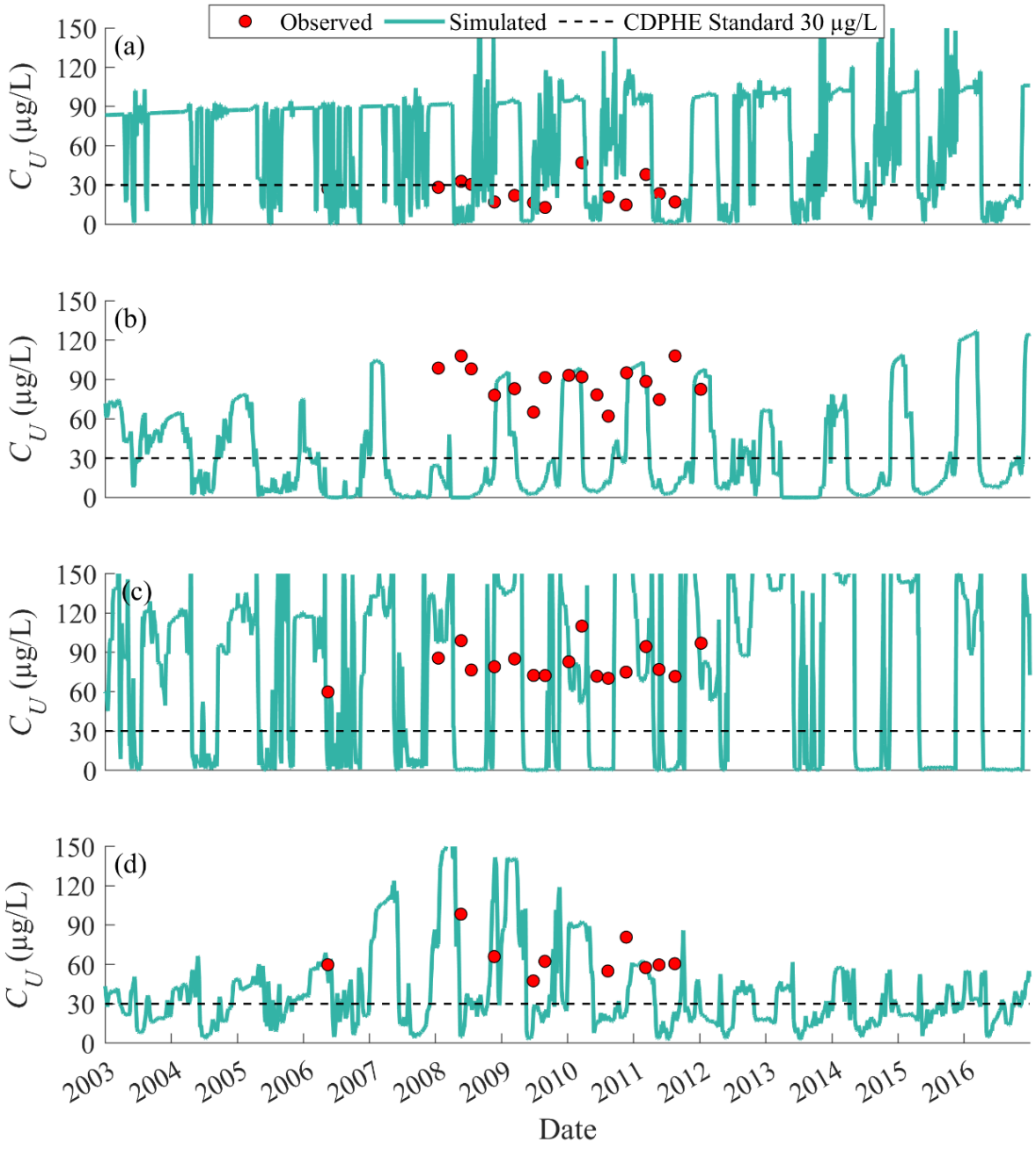

Figure S12. Simulated vs. observed river tributaries concentrations for C_U (a) Clay Creek, (b) Big Sandy Creek, (c) Buffalo Creek, and (d) Wild Horse Creek (ordered upstream to downstream) compared to CDPHE standard.

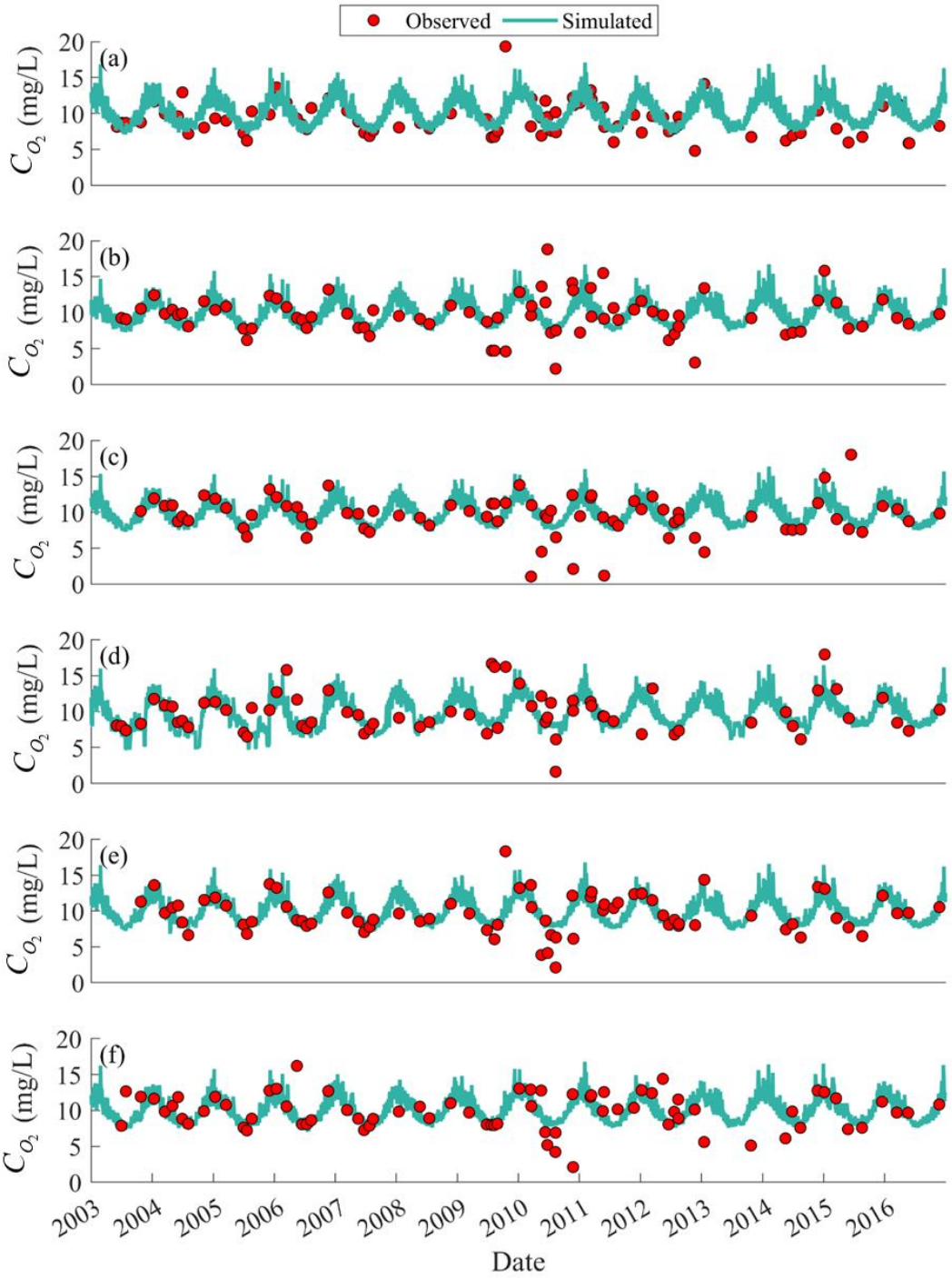

Figure S13. Simulated vs. observed river concentrations for C_{O_2} (a) river segment 1, (b) river segment 2, (c) river segment 3, (d) river segment 4, (e) river segment 5, and (f) river segment 6 (ordered upstream to downstream).

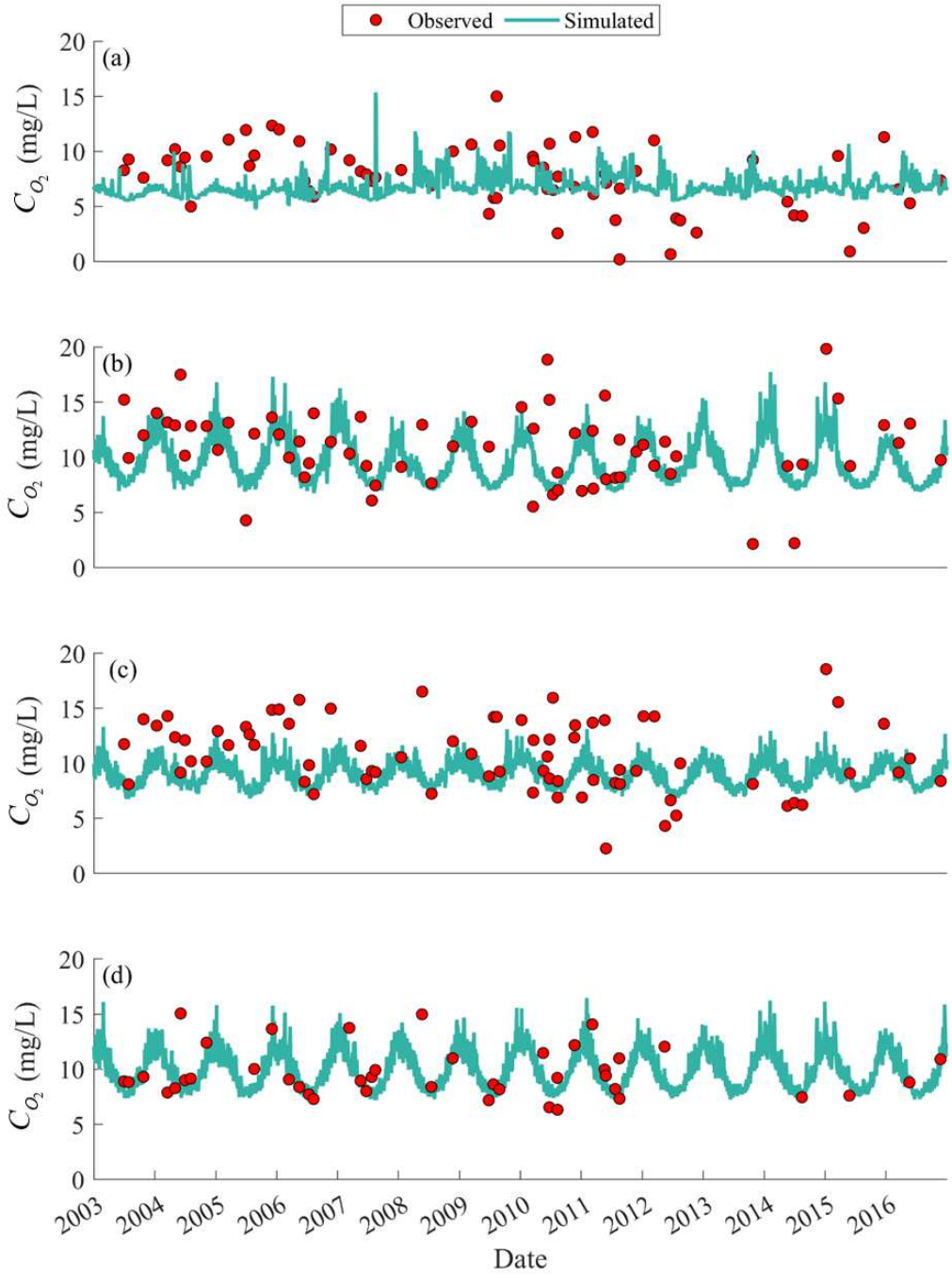

Figure S14. Simulated vs. observed river tributaries concentrations for C_{O_2} (a) Clay Creek, (b) Big Sandy Creek, (c) Buffalo Creek, and (d) Wild Horse Creek (ordered upstream to downstream) compared to CDPHE standard.

Appendix References

Bailey, R. T., Gates, T. K., and Halvorson, A. D., 2013b. Simulating variably-saturated reactive transport of selenium and nitrogen in agricultural groundwater systems. Journal of Contaminant Hydrology, 149, 27–45. https://doi.org/10.1016/j.jconhyd.2013.03.001

Bye, R., and Lund, W., 1982. Determination of selenium in pyrite by the atomic absorption-hydride generation technique. Fresenius' Zeitschrift Für Analytische Chemie, 313(3), 211–212. https://doi.org/10.1007/BF00488858

Davis, J. A., Meece, D. E., Kohler, M., and Curtis, G. P., 2004. Approaches to surface complexation modeling of Uranium(VI) adsorption on aquifer sediments. Geochimica et Cosmochimica Acta, 68(18), 3621–3641. https://doi.org/10.1016/j.gca.2004.03.003

Duff, M. C., Hunter, D. B., Bertsch, P. M., and Amrhein, C., 1999. Factors influencing uranium reduction and solubility in evaporation pond sediments. Biogeochemistry, 45(1), 95–114. https://doi.org/10.1023/A:1006185812588

Fredrickson, J. K., Zachara, J. M., Kennedy, D. W., Duff, M. C., Gorby, Y. A., Li, S. M. W., and Krupka, K. M., 2000. Reduction of U(VI) in goethite (α-FeOOH) suspensions by a dissimilatory metal-reducing bacterium. Geochimica et Cosmochimica Acta, 64(18), 3085–3098. https://doi.org/10.1016/S0016-7037(00)00397-5

Gavrilescu, M., Pavel, L. V., and Cretescu, I., 2009. Characterization and remediation of soils contaminated with uranium. Journal of Hazardous Materials, 163(2–3), 475–510. https://doi.org/10.1016/j.jhazmat.2008.07.103

Korom, S. F., 1992. Natural denitrification in the saturated zone: A review. Water Resources Research, 28(6), 1657–1668. https://doi.org/10.1029/92WR00252

Langmuir, D., 1978. Uranium solution-mineral equilibria at low temperatures with applications to sedimentary ore deposits. Geochimica et Cosmochimica Acta, 42(6 PART A), 547–569. https://doi.org/10.1016/0016-7037(78)90001-7

Lovley, D. R., Phillips, E. J. P., Gorby, Y. A., and Landa, E. R., 1991. Microbial reduction of uranium. Nature, 350(6317), 413–416. https://doi.org/10.1038/350413a0

Newsome, L., Morris, K., and Lloyd, J. R., 2014. The biogeochemistry and bioremediation of uranium and other priority radionuclides. In Chemical Geology (Vol. 363, pp. 164–184). Elsevier. https://doi.org/10.1016/j.chemgeo.2013.10.034

Sani, R., Peyton, B., Smith, W., Apel, W., and Petersen, J., 2002. Dissimilatory reduction of Cr(VI), Fe(III), and U(VI) by Cellulomonas isolates. Applied Microbiology and Biotechnology, 60(1–2), 192–199. https://doi.org/10.1007/s00253-002-1069-6

Wall, J. D., and Krumholz, L. R., 2006. Uranium reduction. Annual Review of Microbiology, 60(1), 149–166. https://doi.org/10.1146/annurev.micro.59.030804.121357

Williams, K. H., Long, P. E., Davis, J. A., Wilkins, M. J., N'Guessan, A. L., Steefel, C. I., Yang, L., Newcomer, D., Spane, F. A., Kerkhof, L. J., Mcguinness, L., Dayvault, R., and Lovley, D. R., 2011. Acetate availability and its influence on sustainable bioremediation of Uranium-contaminated groundwater. Geomicrobiology Journal, 28(5–6), 519–539. https://doi.org/10.1080/01490451.2010.520074